DISCHARGE OF BUOYANT FLUID JETS AND PARTICLE-LADEN JETS INTO STRATIFIED AMBIENT FLUID

by

Sunkyoung Annie Kim

B. A. Sc., Chungnam National University, Korea, 1994

M. A. Sc., Chungnam National University, Korea, 1996

A THESIS SUBMITTED IN PARTIAL FULFILLMENT OF
THE REQUIREMENTS FOR THE DEGREE OF

DOCTOR OF PHILOSOPHY

in

The Faculty of Graduate Studies
Department of Civil Engineering

We accept this thesis as conforming
to the required standard

THE UNIVERSITY OF BRITISH COLUMBIA

October 2001

In presenting this thesis in partial fulfilment of the requirements for an advanced degree at the University of British Columbia, I agree that the Library shall make it freely available for reference and study. I further agree that permission for extensive copying of this thesis for scholarly purposes may be granted by the head of my department or by his or her representatives. It is understood that copying or publication of this thesis for financial gain shall not be allowed without my written permission.

Department of Civil Engineering

The University of British Columbia
Vancouver, Canada

Date 26 Oct. 2001

Abstract

Extraction of petroleum from oil sands generates a vast quantity of fine tailings. A common form of tailings treatment involves discharging the tailings at an angle of minus a few degrees into a tailings pond. Tailings ponds generally have a two-layered structure involving an upper layer of clear water separated by a pycnocline from a lower layer of sludge. Discharge of fine tailings into such ponds raises concerns about the release of petroleum residuals into the upper layer and hence into the surrounding environment.

This study investigates the dynamics of fluid jets and particle-laden jets discharged downward at an angle of 3° into stratified ambient fluid. This in turn allows identification of the discharge conditions that minimize the release of undesirable substances into the upper layer of the pond. A series of laboratory experiments were conducted for round buoyant fluid jets and particle-laden jets, the latter consisting of buoyant interstitial fluid and varied particle concentration.

Important parameters affecting the behavior of fluid jets in two-layer systems were found to be the buoyancy flux, the magnitude of the density step, and the discharge distance to the pycnocline. These were combined into a dimensionless parameter, Ψ, which was then used to determine three flow regimes: the weak impingement, strong impingement and penetration regimes. Buoyant jets impinged weakly on the pycnocline and proceeded horizontally when $\Psi < 0.5$, the upper layer being undisturbed by the discharge. However, for $\Psi > 0.9$, buoyant jets penetrated to the water surface after discharge and spread above the pycnocline. During penetration, the entrained fluid from the lower layer was transported and mixed throughout the upper layer. For the transition regime, $0.5 < \Psi < 0.9$, buoyant jets caused significant mixing in the upper layer but no density change occurred at the surface.

The small discharge angle (-3°) was found to not significantly affect the behavior of buoyant jets relative to horizontal discharge. Backflows occurred along the pycnocline when the jet angle at the pycnocline was greater than 7° for the weak and strong impingement regimes. For the penetration regime $\Psi > 0.9$, some jet flow accumulated along the pycnocline and backflows also formed at the surface of the upper layer. Coanda bottom attachment occurred, independently of the ambient fluid conditions, when the dimensionless parameter $h/\ell_M > 0.22$.

The dimensionless maximum rise height and the top of the spreading layer were found to increase linearly with Ψ in the strong impingement regime but were constant in the weak impingement regime. Also, the spreading layer thickness increased with a dimensionless momentum term regardless of the presence of the density step.

Particle-laden jets with low particle concentration were found to behave like fluid jets, whereas those with high particle concentration behaved like negatively buoyant fluid. The particles were found to move with interstitial fluid and thus get transported to the upper layer during penetration. Also, grouping behavior of individual particles was observed. After the source momentum decays, the behavior of particle-laden jets was determined by a density difference ratio (R) and Ψ.

Four flow regimes were classified based on R and Ψ. When $0 < R < 1$, all particle-laden jets penetrated into the upper layer or strongly impinged on the pycnocline, depending on the magnitude of Ψ. However when $R < -2.0$, jets plunged to the bottom and propagated as a turbidity current regardless of Ψ. After significant settling, eventually the interstitial fluid rose but remained trapped under the pycnocline. When $-2.0 < R < 0$, jets initially plunged but after particle settling, formed an intermediate level gravity current.

The analysis of gross flow characteristics indicated that particles reduce the potential of buoyant interstitial fluid to rise or significantly penetrate into the upper layer.

Table of Contents

List of Figures

Chapter 1

Chapter 2

Chapter 3

Chapter 4

Chapter 5

Chapter 6

Appendix

List of Tables

Notation

The following symbols are used in this thesis:

A. Fluid jets

A	nozzle cross-sectional area
B	source buoyancy flux; $B = Qg'_o$
b	characteristic width of concentration at a radical position where $c/c_m = \exp(-1)$
b_u	characteristic width of velocity
b_2	experimental constant for a round plume ($b_2 = 0.35$, Fischer et al. 1979)
C_s	salt concentration
C_{25}	conductivity at 25 °C
c_m	maximum concentration
C_o	dye concentration at source
c_1	experimental constant of maximum rise height for fluid jets
c_2	experimental constant of top of the spreading layer for fluid jets
D	molecular diffusion coefficient, m^2/s
d	nozzle diameter
F_d	source densimetric Froude number; $F_d = u/\sqrt{g'_o d}$
G	circuit gain of a PME conductivity-temperature probe
g	gravitational acceleration
g'	modified gravitational acceleration
g'_m	modified gravitational acceleration at the centerline

g'_o modified acceleration based on the difference between jet and ambient fluid density; $g'_o = g(\rho_a - \rho_j)/\rho_a$

g'_a modified acceleration based on the difference between lower and upper layer density; $g'_a = g(\rho_2 - \rho_1)/\rho_2$

H total water depth above the nozzle

h discharge height above the bed

h_1 upper layer thickness in two-layer system

h_i proximity to the pycnocline from a discharge nozzle in a two-layer system

$h_{\frac{1}{2}I}$ half-thickness of density interface

$h_{\frac{1}{2}}$ half-thickness of spreading layer

J calibration constant of a PME probe

K calibration constant of a PME probe

L length of experimental tank

ℓ'_b length scale characterizing the relative importance of the buoyancy to ambient stratification ; $\ell'_b = B^{1/3}/N$

ℓ_M length scale characterizing the relative importance of the momentum and buoyancy of a buoyant jet; $\ell_M = M^{3/4}/\sqrt{B}$

ℓ_N length scale characterizing the relative importance of the momentum to ambient stratification; $\ell_N = M^{1/4}/\sqrt{N}$

ℓ_Q length scale characterizing the relative importance of the jet source geometry; $\ell_Q = M/\sqrt{B}$

M source momentum flux; $M = Qu$

M_o Molar concentration at 25 °C

M_v vertical momentum

m	specific momentum flux
m_h	horizontal momentum
m_v	momentum flux due to buoyancy for a plume
N	Brunt-Väisälä frequency buoyancy frequency; $N = \sqrt{\frac{-g\, d\rho}{\rho_o\, dz}}$
P_d	impingement height above the pycnocline
Q	source kinematic volume flux; $Q = \pi d^2 u/4$
r	radius of a jet
R_e	Reynolds number; $R = ud/\upsilon$
s	centerline displacement
t	time
T	water temperature (°C)
T_f	final spreading layer thickness
u	time-averaged jet velocity
$\overline{u}$	initial mean jet velocity
u_m	maximum time-averaged velocity
V_o	electrical voltage of a PME probe
X	volumetric concentration of particles
x	downstream distance
X_m	locations where maximum height of rise occurs
z	vertical distance from the jet centerline
Z_b	bottom of spreading layer
Z_m	maximum height of rise
Z_t	top of spreading layer
α	entrainment coefficient; $\alpha = 0.057 + 0.5 Fr^{-2} \sin\theta$
β	specific buoyancy flux

γ non-dimensional density of fluid jets; $\gamma = \rho_1 - \rho_i / \rho_2 - \rho_i$

μ volume flux at distance z

ν kinematic viscosity

θ discharge angle

θ_p jet angle at the pycnocline

ρ_j density of jet at the source

ρ_i density at the pycnocline

ρ_a density of the ambient fluid at discharge level

ρ_1 density of upper layer in a two-layer system

ρ_2 density of lower layer in a two-layer system

$\rho_w(T)$ density of fresh water at T °C

$\Delta\rho$ density difference between the ambient fluid and jet fluid at discharge level; $(\rho_a - \rho_j)$

$\Delta\rho_a$ density difference between the lower layer and the upper layer; $(\rho_2 - \rho_1)$

$\Delta\rho_s$ density increment due to NaCl

$\sigma(T)$ conductivity at T °C in Figure 3.14

$\sigma(ref)$ reference conductivity

ξ interface thickness $\xi = \sqrt{4\pi Dt}$

Ψ impingement-penetration parameter; $\Psi = \mathrm{B}^{2/5} / \mathrm{g}_a'^{3/5} \mathrm{h}_i$

B. Particle-laden jets

B_b initial bulk buoyancy flux; $B_b = Q\left(g\frac{\rho_a - \rho_b}{\rho_a}\right)$

B_f buoyancy flux of the interstitial fluid; $B_f = Q(1-X)\left(g\frac{\rho_a - \rho_f}{\rho_a}\right)$

($B_f = B$ in fluid jets)

B_p bulk density of a particle cloud

c_3 experimental constant of maximum rise height for particle-laden jets

c_4 experimental constant of top of the spreading layer for particle-laden jets

d_p particle diameter

E_R Relative error between measured dye concentration (C_M) and CORMIX1 prediction (C_c); $E_R = C_M - C_c / C_M$

R dimensionless density of particle-laden jets; $R = \rho_a - \rho_b / \rho_a - \rho_f$

R_c size of a particle cloud

R_h non-dimensional density of particle-laden fluid; $R_h = \rho_f - \rho_a / \rho_b - \rho_a$

w_s particle settling velocity; $w_s = \dfrac{g(\rho_P - \rho_a)d_p^2}{18\rho_a \nu}$

X volumetric particle concentration

z_c critical depth of the transition of a particle cloud

ρ_b bulk density of the particle-laden jet at the source

ρ_f density of the interstitial fluid of particle-laden jet at the source

ρ_p particle density

Acknowledgement

I would like to thank my primary supervisor Dr. Greg Lawrence for his invaluable intellectual guidance, patience and generosity, and my co-supervisor Dr. Loretta Li for her warm encouragement and sincere supervision. Without Dr. Lawrence and Dr. Li, my Ph.D. would not have been possible. I wish to also show my sincere appreciation to my thesis committee, Dr. Peter Ward, Dr. Susan Allen and Dr. Noboru Yonemitsu and the university examiner, Dr. Rob Millar for their kindness and valuable comments on my thesis.

I would also like to thank Kurt Nielson, Scott Jackson, Douglas Hudniuk, Douglas Smith and Herald Schempp of the Civil Engineering Hydraulic Laboratory, for their assistance in constructing the experimental facility, the data acquisition instrument and their constant help without any hesitation.

Special thanks go to my parents in Korea for their continued prayer and love, and Dr. Dongil Seo for his encouragement. Also, I wish to thank my classmates Violeta Martin and Tim Fisher for their constant help and friendship throughout the program.

Most of all, I would like to particularly express my gratitude to my husband, Charles Hyde, for his love, encouragement and his direct advice on my thesis. I also have to thank him for his sacrifice of his career in Australia to be with me over the past two years.

Chapter 1

Introduction

1.1 Background

The increase in production of petroleum extracted from oil sands has resulted in a vast quantity of oil sand tailings. As a result, the disposal of tailings has been one of the most sensitive environmental issues confronting the mining industry (Lawrence et al., 1991; Ward et al., 1994). Adequate discharge schemes and appropriate maintenance of fine tailings is essential for preventing environmental disasters. Sub-aqueous disposal is a common final treatment of oil sands tailings. This involves discharging the fine tailings into a pond through a pipeline. The end of discharge pipe usually follows the trend of the bottom slope of the tailings pond at an angle of minus a few degrees (Ward, 2001). The tailings are a slurry consisting mainly of water, fine sand, silt and clays, asphaltenes and residual bitumen, and unrecovered solvent (Petroleum Communication Foundation, 2000)

In practical applications, there are several structures of tailings pond such as a clear water layer with a linearly stratified sludge layer or a clear water layer with a uniform sludge layer. This study focuses on the two-layer structure consisting of a clear water layer and a homogeneous sludge layer. The tailings pond (see Figure 1.1) consists of an upper layer of clear water and a lower layer of sludge containing particulate substances from 10 % to about 50 % (Mackinnon, 1989). These two layers are separated by an intermediate thin layer called a pycnocline, where a dramatic density change occurs. The sludge layer is often divided into an immature sludge layer consisting mainly of fine silts and clays and a

mature sludge layer with coarse silts and fine sands (Mackinnon, 1989).

Generally, the water quality of the upper layer is important from both an environmental and industrial perspective. This is because the upper layer comes into direct contact with the surrounding environment and the upper layer is also recycled for industrial use (Petroleum Communication Foundation, 2000). Therefore, it is important to minimize the disturbance of the lower layer and pycnocline during the discharge in order to prevent undesirable substances from rising into the upper layer.

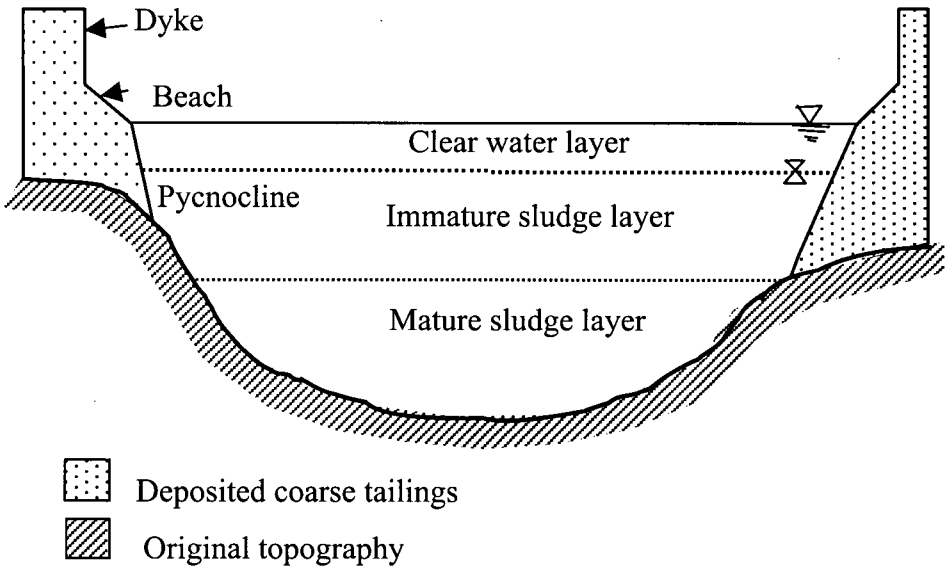

Figure 1.1 A sketch of a tailings pond (After MacKinnon, 1989):
Vertical scale is exaggerated.

There has been a great deal of research on the discharge of turbulent jets into homogeneous and linearly stratified receiving water (Abraham, 1965a, 1965b; Fan and Brooks, 1966, 1969; Hirst, 1972; List and Imberger, 1973; Wallace and Wright, 1984; Fischer et al., 1979; Lee and Jirka, 1981; Turner, 1973, 1986; Roberts, 1987; Sobey et al., 1988; Gu and Stefan, 1988a; Jirka and Doneker, 1991; Wood et al., 1993). Typically,

wastewater is discharged as a turbulent buoyant jet through a round nozzle or a diffuser into ambient fluid. The primary goal is to achieve high initial dilution of contaminated fluid adjacent to the discharge structure and thus to prevent a spreading layer of undiluted wastewater. Consequently, understanding the behavior of a buoyant jet and its mixing characteristics under a given discharge scheme and ambient fluid condition is essential prior to commencing wastewater disposal.

The dynamics of buoyant jets are controlled by three important factors: the discharge condition, geometrical factors and the receiving water condition. The discharge condition includes initial jet properties such as the volume and velocity of discharge and the density difference between the jet and the ambient fluid. The geometrical factors are associated with the source geometry configuration, the angles of the jet inclination, and proximity to the adjacent boundaries. Ambient conditions include the presence and type of density stratification, the cross-flowing current, and ambient turbulence (Fischer et al., 1979).

A turbulent buoyant jet initially has both source momentum and buoyancy. The initial momentum and geometry of discharge is the dominant factor affecting the entrainment and trajectory of a buoyant jet at the near field. However as the jet proceeds, its behavior is increasingly determined by the local buoyancy of the jet fluid and the ambient fluid condition (Fischer et al., 1979). In homogeneous ambient fluids, a jet grows linearly with distance and the total volume flux grows continuously with distance. Entrainment into the jet can come from the entire water depth. However, the stratification of the ambient fluid suppresses the vertical motion of jet fluid and thus the entrained flow is constrained vertically. As the jet velocity decays, the jet collapses vertically and then spreads laterally. Entrainment essentially ceases after collapse and the jet forms a horizontal spreading layer with a finite thickness (Manins, 1976; Brooks, 1980; Roberts, 1987; Wong and Wright, 1988). In contrast to the research on buoyant jets in homogeneous and linearly stratified ambient fluid, there has been surprisingly little research on buoyant jets in a two-layer system.

In many cases of industrial discharge such as fine tailings, the flow is not solely fluid but rather fluid associated with suspended particles. Hereafter, jets carrying particles are termed *particle-laden jets* and jets without particles are termed *fluid* jets. Most previous studies of jets and plumes have focused on fluid jets with little attention being paid to particle-laden fluid jets. The particle-laden flow behavior is more complicated due to 1) the particle sedimentation that occurs and 2) the buoyant jet processes due to the interstitial fluid. Depending on the particle concentration, the jet trajectory and flow characteristics of particle-laden jets can be significantly different from those of fluid jets.

It is important to comprehend not only the characteristics of turbulent fluid jets but also the fundamental mechanisms of particle/interstitial fluid interaction and its combined effect on the gross flow characteristics. However, most previous research associated with particles in flow has been focused on particle clouds without source momentum, and turbidity currents (Koh and Chang, 1973; Rahimipour and Wilkinson, 1992; Noh and Fernando, 1993; Ruggaber, 2000a, 2000b; Bonnecaze, 1993; Hallworth et al, 1996, 1998; Huppert et al., 1991, 1993, 1995; Hogg et al., 1999).

1.2 Objectives and Applications

To understand the behavior of fine tailings discharged into a tailings pond, it is necessary to understand the dynamics of particle-laden jets in two-layer systems. However, as mentioned in the previous section, little information is available on both buoyant jets in two-layer systems and particle-laden jets. Therefore, the present study examines 1) the dynamics of buoyant fluid jets and 2) the dynamics of particle-laden jets with buoyant interstitial fluid in two-layer system and linearly stratified ambient fluid. The specific objectives are:

- To understand the behavior of buoyant fluid jets of 3° downward discharge angle in two-layer systems

- To investigate the effect of particles on turbulent flow
- To identify important factors affecting the behavior of buoyant jets and particle-laden jets in two-layer systems
- To define the flow regimes and examine the gross behavior of both buoyant jets and particle-laden jets.

By achieving these objectives, this study provides a guide for the discharge of fine tailings so as to prevent upper layer disturbance and thus contamination of the pond surface.

The present study is also relevant to situations where the density interface (pycnocline or thermocline) should not be affected by the discharge flow such as hypolimnetic aeration in a stratified lake. Here aerated water is injected as a jet below a thermocline that is to be preserved. Another example is the discharge of warm water generated from a power plant into stratified receiving water. A third example is the dynamics of sediment-laden river plumes carrying nutrients into reservoirs.

1.3 Scope and Methodology

The objectives are achieved by a series of laboratory experiments for buoyant fluid jets and particle-laden jets. Dimensional analysis is also carried out and compared with the experimental results. The experimental results are also compared with previous research and CORMIX (Cornell Mixing Zone Expert System) predictions.

A physical discharge model was set up in a rectangular experimental tank and experiments with fluid jets and particle-laden jets were performed under various discharge schemes. Jets inclined downward at 3^{o} (5 % slope) are discharged into the stagnant two-layered ambient fluid, where the bottom bed is inclined at 5 % slope. This setup is a

simulation of a typical tailings pond and discharge angle. Linearly stratified fluid, two-layer stratified fluid and homogeneous ambient fluids are simulated, although the majority of experiments are conducted in a stagnant two-layer system. Jets are discharged only into the quiescent lower layer under a density step. The overview of the present study is summarized in Figure 1.2

1.4 Organization

Relevant previous studies on buoyant round fluid jets and particle-laden flows are reviewed in Chapter 2. Basic characteristics of jets, plumes and buoyant jets under various ambient conditions are discussed and the behavior of particle-laden flows such as particle clouds and turbidity currents are described. In Chapter 3, the experimental apparatus and instrumentation used in the laboratory experiments are presented and the experimental conditions, detailed experimental procedures, data acquisition and processing are presented.

Experimental results and discussion of fluid jets are presented in Chapter 4. The behavior of fluid jets in a two-layer system is described and dimensional analysis is conducted on the gross flow characteristics such as maximum rise height and horizontal spreading layer thickness. The important parameters are identified from the experimental results and asymptotic solutions are found. The results for buoyant jets in linearly stratified fluids are presented by means of the characteristic length scale technique and compared with previous investigations.

Chapter 5 presents the experimental results and dimensional analysis for particle-laden jets. The presentation and interpretation of experimental results follows the same format as in Chapter 4. The results are also compared with the predictions of CORMIX1 v3.2 and its suitability for particle-laden flow is examined.

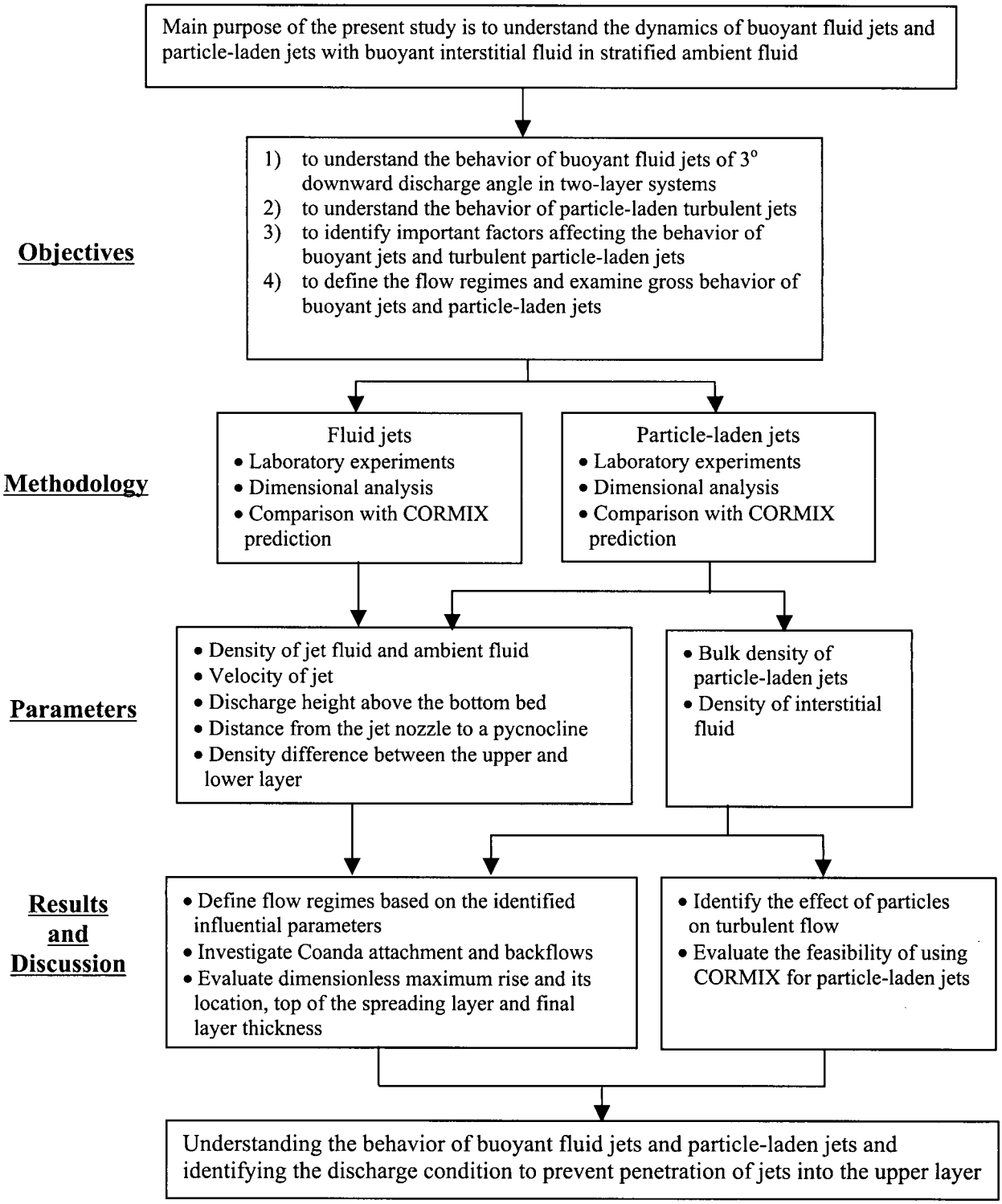

Figure 1.2 Overview of the present study

A comparison of the behavior of fluid jets and particle-laden jets is given in Chapter 6. Chapter 7 summarizes the main conclusions and the contributions of the present study. Recommendations for future research are also made.

The results and discussion of the behavior of buoyant jets in linearly stratified ambient fluid are presented in Appendix A. Appendix B contains the results relating to the behavior of particle-laden jets in linearly stratified fluid, while the comparison between the two types of jet is made in Appendix C. A overall experimental setup are sketched in Appendix D.

Chapter 2

Literature Review

2.1 Introduction

In order to predict the behavior of fine tailings discharged into a tailings pond it is essential to understand the characteristics of jets, plumes and buoyant jets and their behavior in various ambient conditions. In addition, it is necessary to understand the effect of particles on turbulent flow and gross behavior of particle-laden jets. As noted in Chapter1, however, there has been little research on buoyant jets in two-layer systems and particle-laden turbulent jets.

This chapter discusses the existing body of knowledge relating to the behavior of buoyant jets in homogeneous fluid and stratified ambient fluid. For particle-laden jets, past experimental studies on particle-laden flows such as particle clouds and turbidity currents are investigated.

2.2 Jets and plumes

2.2.1 Simple jets, plumes and buoyant jets

Discharges into ambient fluid are classified as jets, plumes and buoyant jets depending on the influence of the source momentum and buoyancy. A pure jet is discharge with initial momentum through a nozzle and two distinct regions are formed after discharge: the Zone of Flow Establishment (ZFE), and the Zone of Established Flow (ZEF). In the ZFE, the shear forces due to the interaction between the jet and ambient fluid do not affect the core of the jet. Thus the centerline velocity remains the same as the velocity at the jet nozzle.

This zone is often neglected because of its relatively short length (approximately six times the diameter of the jet nozzle) for a deeply submerged jet (Fischer et al., 1979). In the ZEF, the centerline velocity, temperature and density begin to decay due to the continuous entrainment of surrounding fluid. The time-averaged velocity and concentration profiles across a jet cross-section form Gaussian distributions (Fischer et al., 1979). A schematic diagram of the flow region is shown in Figure 2.1.

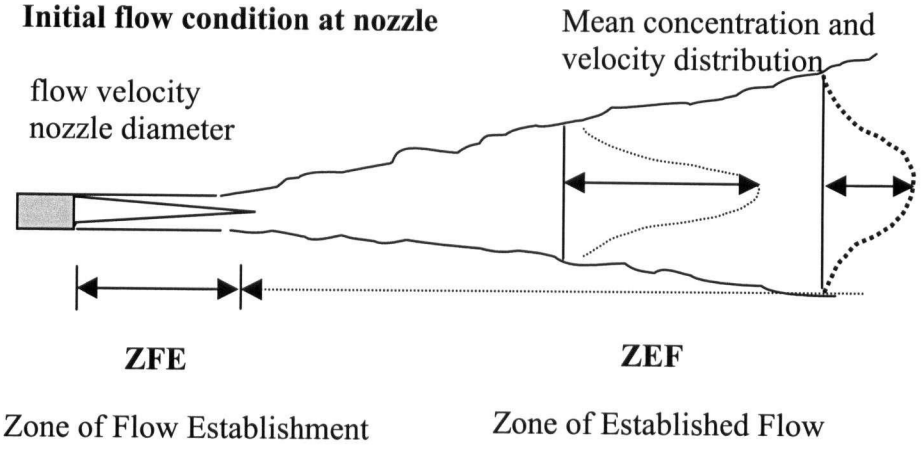

Figure. 2.1 A sketch of a jet geometry and flow regions

A plume is a discharge driven solely by the buoyancy due to the density difference between entering fluid and the ambient fluid. Thus, the local flow properties such as velocity and concentration are dependent on the initial buoyancy, the mass flux and the downstream distance.

Buoyant jets are typical of many environmental discharges having both initial momentum and buoyancy. Initially, a buoyant jet is dominated mostly by the source momentum and geometry, and after some distance the behavior is determined by the buoyancy and the ambient fluid condition. The centerline concentration decays after a short distance due to entrainment. Sufficiently far from the source all buoyant jets behave like plumes. If the

initial momentum of a jet is not in the direction of buoyancy, the jet trajectory becomes curved.

2.2.2 Theoretical background for buoyant jets

The dynamics of jets, plumes and buoyant jets have been well established. For a turbulent round buoyant jet, initial volume flux Q, momentum flux M and buoyancy flux B are given by Fischer et al. (1979):

$$Q = \frac{\pi}{4} d^2 \overline{u} \tag{2.1}$$

$$M = \frac{\pi}{4} d^2 \overline{u}^2 \tag{2.2}$$

where d : jet nozzle diameter

$\overline{u}$: initial mean jet velocity,

The initial density difference between a jet and the ambient fluid at the source can be represented by modified gravitational acceleration g'_o :

$$g'_o = \frac{\rho_a - \rho_j}{\rho_a} g \tag{2.3}$$

where

ρ_a : density of ambient fluid

ρ_j : density of jet

g : gravitational acceleration

Therefore, initial buoyancy flux B is given as

$$B = Qg'_o = \bar{u}A\left(\frac{\rho_a - \rho_j}{\rho_a}\right)g \tag{2.4}$$

where A : cross sectional area of a nozzle

If the density of the jet is close to that of the ambient fluid, the effect of the density difference is negligible on the inertia force, but it exerts a considerable effect on the buoyancy force. This Boussinesq approximation is generally valid when $\frac{\Delta\rho}{\rho_a} \leq 0.1$ (Baines and Hopfinger, 1984).

Table 2.1 shows the relevant parameters to the present study for round jets and plumes in homogeneous ambient fluid.

Table 2.1 Properties of turbulent round jet and pure plume (Fischer et al., 1979)

Parameter	**Round Jet**	**Round Plume**
Maximum time-averaged velocity (u_m)	$u_m \frac{Q}{M} = (7.0 \pm 0.1)\left(\frac{\ell_Q}{z}\right)$	$u_m = (4.7 \pm 0.2)B^{1/3}z^{-1/3}$
Momentum flux (m)	m = M (constant)	$m = b_2 B^{2/3} z^{4/3}$

where ℓ_Q : characteristic length ($\ell_Q = Q/\sqrt{M}$)

z : distance from source

b_2 : experimental constant $b_2 \approx 0.35$ (Fischer et al., 1979)

The gross buoyant jet behavior has been commonly described by integrating a set of ordinary differential equations of volume, momentum and buoyancy over the jet cross section. (Fan and Brooks, 1969; Hirst, 1972; List and Imberger, 1973; Wright and Wallace, 1979; Fischer et al., 1979; Lee and Jirka, 1981; Turner, 1986):

Volume flux $$\mu = \int_A u dA = 2\pi \int_o^\infty urdr \tag{2.5}$$

Momentum flux $$m = \int_A u^2 dA = 2\pi \int_o^\infty u^2 rdr \tag{2.6}$$

Buoyancy flux $$\beta = \int_A g \frac{\Delta\rho}{\rho} u dA = 2\pi \int_o^\infty ug' rdr \tag{2.7}$$

where A : the cross- sectional area of the jet

u : time averaged velocity in axial direction

μ : specific volume flux

m : specific momentum flux

β : specific buoyant flux

$\Delta\rho$: density difference between jet and ambient fluid

r : radius of a jet

g' : modified gravitational acceleration

The time-averaged profiles of velocity and passive tracer concentration are generally expressed as simple Gaussian distributions:

$$u(r,s) = u_m \exp\left[-\frac{r^2}{b_u^2}\right] \tag{2.8}$$

$$c(r,s) = c_m \exp\left[-\frac{r^2}{b^2}\right] \tag{2.9}$$

where b_u and b are the characteristic widths of the velocity and concentration (or density) profiles, respectively. The u_m and c_m represent the local centerline velocity and the concentration.

2.2.3 Entrainment

Entrainment, the ingestion of ambient fluid into a turbulent jet fluid, is the fundamental mechanism for dilution of discharged wastewater. As a jet leaves the source, shearing action between the jet and the ambient fluid develops and the neighboring fluid is accelerated. Entrainment primarily results from the engulfment of non-turbulent fluid by the large-scale eddies across the edge of a turbulent jet or plume (Fischer et al., 1979; Baines, 1975; Schneider, 1980; Lee and Jirka, 1981). The subsequent small-scale turbulence and diffusion is however, relatively insignificant to the overall mixing rate (Turner, 1986). For the final stage of external fluid ingestion into the turbulent flow, the viscous diffusion of vorticity plays an important role (Baines, 1975).

The classical entrainment hypothesis is that the mean inflow velocity of diluting fluid into a jet is proportional to the maximum local time-averaged velocity or the spatial-averaged velocity over the section of the turbulent flow (Rajaratnam, 1976; Fischer et al, 1979; Turner, 1986, Wright and Wallace, 1979). The inflow velocity at the edge of the flow is some fraction (α) of the maximum mean velocity (u_m) given as $\frac{d\mu}{dz} = 2\pi b_u \alpha u_m$, where α is the entrainment coefficient. For a horizontal discharge, $\alpha = 0.057$ (Wong, 1984).

2.2.4 Important parameters

2.2.4.1 Characteristic length scales

Characteristic length scales are often useful tools to express and interpret the gross behavior of flows. Also, the relative magnitude of the length scales is useful in identifying the dominant mechanisms under the prevailing jet and ambient conditions. Along with the important parameters for jet and ambient fluid, several useful characteristic length scales have been formed and used by many researchers (Fischer et al., 1979; Schneider, 1980; Roberts and Mathew, 1982, 1984; Wong, 1984; Lee and Cheung, 1986; Roberts, 1987; Sobey et al., 1988; Wong and Wright, 1988; Johnston and Volker, 1993; Johnston et al., 1994b; Jirka and Doneker, 1991; Jirka et al., 1996).

Geometric length scale

For a simple turbulent round jet, a characteristic length describing the relative importance of the source geometry, ℓ_Q can be formed (Fischer et al, 1979).

$$\ell_Q = \frac{Q}{\sqrt{M}} = \sqrt{A} \tag{2.10}$$

ℓ_Q characterizes the distance from the nozzle over which the source volume flux affects the flow field. If downstream distance is much greater than ℓ_Q (i.e. $z >> \ell_Q$), the influence of the initial volume flux is insignificant and the properties of the jet are independent of the source conditions.

Jet/plume transition scale

With distance buoyant jets undergo a transition from momentum-dominant to buoyancy-driven flow. This relationship associated with source momentum and buoyancy can be defined as

$$\ell_M = \frac{M^{3/4}}{B^{1/2}} \tag{2.11}$$

ℓ_M is a measurement of a characteristic distance at which the transition from jet-like behavior to plume-like occurs. If $z << \ell_M$, the momentum flux dominates and the flow behaves like a jet. For downstream distance greater than ℓ_M, the source momentum effect becomes negligible and the buoyant jet behaves like a plume over the entire trajectory.

Jet / linear stratification length scale

If the ambient fluid is linearly stratified and a jet is initially momentum-dominant, a characteristic length scale ℓ_N can be defined as

$$\ell_N = \frac{M^{1/4}}{N^{1/2}} \tag{2.12}$$

where N is a buoyancy frequency given as

$$N = \sqrt{\frac{-g}{\rho_o}\frac{d\rho}{dz}} \tag{2.13}$$

ℓ_N is a length scale characterizing the strength of the source momentum flux relative to the ambient linear stratification.

Plume/stratification length scale

If the source buoyancy is much stronger than the initial momentum, the momentum is ignored. A characteristic length ℓ'_b incorporating only buoyancy and ambient stratification

can be formed (Wright and Wallace, 1979; Lee and Cheung, 1986; Jirka and Doneker, 1991):

$$\ell'_b = \frac{B^{1/3}}{N} \tag{2.14}$$

ℓ'_b measures the distance at which a plume becomes strongly affected by the ambient stratification. In fact, ℓ'_b and ℓ_N are interdependent for a buoyant jet and its relationship can be expressed in the form of $\ell_M = \frac{\ell_N^3}{\ell_b'^2}$.

2.2.4.2 Dimensionless parameters

It is also useful to express the research results as familiar dimensionless parameters.

Reynolds Number

The Reynolds number defined below indicates whether the jet is laminar or turbulent.

$$R_e = \frac{\rho dv}{\mu} = \frac{ud}{\upsilon} \tag{2.15}$$

where ν is the kinematic viscosity of discharged fluid. In most cases, in nature, the flow generated by the discharge is turbulent. If the number exceeds 4,000 the flow is considered turbulent (Fischer, 1979).

Densimetric Froude Number

The densimetric Froude number is widely recognized as an influential parameter for buoyant jets. The Froude number relevant to the present study is a densimetric Froude number F_d:

$$F_d = \frac{u}{\sqrt{g'_o d}} \tag{2.16}$$

where g'_o is modified gravitational acceleration due to the density difference between the jet fluid at discharge level (ρ_j) and the ambient fluid (ρ_a).

2.2.5. Effect of source geometry

2.2.5.1 Discharge angle

The most significant difference between horizontal jets, downward inclined jets and vertical jets is difference in the direction of initial momentum and buoyancy. If the direction of initial momentum and buoyancy of a buoyant jet is different, the jet trajectory becomes curved when $z/\ell_M >> 1$ (McCorquodale et al., 1992). The flow spreads predominantly in the direction of the discharge due to the initial horizontal momentum, while the vertical momentum due to buoyancy is modified as it rises or sinks to the neutrally buoyant level. Thus the discharge angle significantly influences the dilution of inflow (Johnson et al., 1989). Hofer and Hutter (1981) suggested that the negative initial jet angles cause substantially larger undulations in the jet trajectory than positive angles.

2.2.5.2 Proximity to the adjacent horizontal bed

If a buoyant jet is discharged sufficiently close to the bed, the jet is deflected toward the floor for some distance. This phenomenon is called the *Coanda effect*. As a jet propagates along the bed, constant bottom friction reduces the horizontal momentum. Consequently, at some point the buoyancy force becomes dominant and the jet rises to its neutral buoyancy (Sharp and Vyas, 1977; Sobey et al., 1988; Johnson and Volker, 1993; Johnston et al., 1994a; Doneker and Jirka, 1991; Jirka and Doneker, 1991).

Sobey et al. (1988) suggested that proximity of the boundaries has a considerable influence on the near-field flow pattern. For $h/\ell_M < 0.1$, where h is discharge height above the bottom, initial jet development is predominantly influenced by Coanda attachment until buoyancy eventually prevails. They also indicated that the influence of the Reynolds number and densimetric Froude number on the Coanda bottom attachment to the bed is insignificant. Johnston and Volker (1993) also discovered that the jet path could be greatly influenced by the distance between discharge exit and the bed, and also the densimetric Froude number. When $h/\ell_M > 0.1$, the Coanda effect did not occur as observed by Sobey et al.(1988).

2.3 Dynamics of buoyant jets in various ambient conditions

2.3.1 Classification of ambient fluid

The receiving water conditions play a significant role in the dilution and trajectory of buoyant jets. As buoyant jets spread into the ambient water, the initial source characteristics weaken and the ambient fluid condition begins to influence the flow dynamics. In a homogeneous ambient fluid, a round horizontal jet exhibits an axisymmetric flow pattern and the entrainment of ambient fluid can occur from the entire water depth (Fischer et al, 1979; Abraham, 1965a; Fan and Brooks, 1969). However, in stratified ambient fluid the mixing and entrainment of jet fluid are constrained vertically due to the stratification.

Jirka and Doneker (1991) classified stratified ambient water into three categories based on the characteristics of the density stratification: linear stratification, two-layer stratification and two-layer stratification with a linearly stratified lower layer. The schematic diagrams of the ambient water conditions are shown in Figure 2.2. The two-layer system consists simply of a uniform upper layer (epilimnion) and a uniform lower layer

(hypoliminion). A two-layer system with a stratified lower layer may or may not be separated by a density jump (pycnocline) between the two layers.

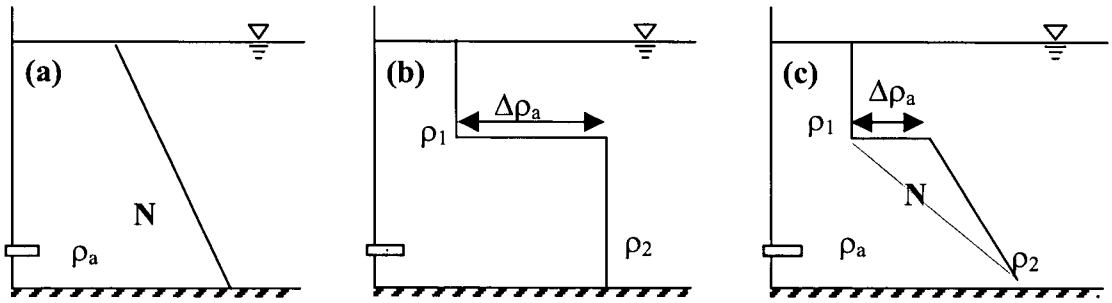

Figure 2.2 Schematic diagram for ambient fluid condition based on the density profile: (a) linearly stratified fluid, (b) two-layer system with a density step and (c) two-layer with a linearly stratified lower layer (Jirka and Doneker, 1991)

A tailings pond has a two-layer system with a linearly stratified lower layer or a two-layer system with a homogeneous lower layer. Thus this study focuses on the linearly stratified ambient fluid and two-layer system.

2.3.2 Stratified ambient fluid

2.3.2.1 Linearly stratified ambient fluid

The behavior of a jet in a linearly stratified ambient fluid is significantly different from its behavior in a homogeneous ambient fluid. In the immediate vicinity of the jet exit, the influence of stratification on the jet is rather insignificant and the width of the jet initially grows linearly with distance as in the case of an unstratified fluid (Roberts, 1987; Wong and Wright, 1988). However, at some distance the jet entrains ambient fluid selectively from a finite thickness, collapses vertically and proceeds as a horizontal density current (Maxworthy, 1973; Manins, 1976; Brooks, 1980; Roberts and Mathews, 1984; Roberts, 1987).

2.3.2.2 Two-layer system

A jet trajectory in a two-layer system is different from that in homogeneous system or linearly stratified fluid due to the presence of a layer of rapid density change. When discharged into the lower layer, a buoyant jet rises to the pycnocline, which inhibits the vertical transport of energy and mass and diverts it horizontally. Entrainment across the density step is determined by the characteristics of the turbulence within the flow at impingement on and at a density interface (Baines, 1975). In addition, entrainment is affected not by the density of ambient fluid but only by the presence of a density step across the pycnocline.

The proximity between a discharge exit and the density step is a critical factor affecting vertical movement of the flow (Schneider, 1980). The spreading layer thickness decreases as the ratio of half thickness of interface depth ($h_{\frac{1}{2}I}$) to half thickness of spreading layer ($h_{\frac{1}{2}}$) increases. Also, at approximately $h_{\frac{1}{2}I}/h_{\frac{1}{2}}=1$, mixing at the front of the flow ceases (Britter and Simpson, 1981).

If the density step $\Delta\rho_a$ is large, the jet trajectory and mixing become trapped under the pycnocline and the role of upper layer becomes insignificant (Schneider, 1980). In such cases, the lower layer of the two-layer system can be regarded as shallow homogeneous ambient fluid. Sobey et al. (1988) indicated that in shallow water, both proximity to an upper boundary (h_i) and bottom (h) significantly influence the jet path. The flow patterns occurring in an initially stagnant ambient fluid are illustrated in Figure 2.3. If the free surface parameter $h_i/\ell_M > 0.05$ and bed parameter $h/\ell_M < 0.1$, then a buoyant jet initially experiences Coanda attachment to the bottom and then rises (Figure 2.3(a)). On the other hand, if $h_i/\ell_M < 0.05$ and $h/\ell_M < 0.1$, then a buoyant jet is confined in the shallow ambient fluid and no rising to the surface occurs (Figure 2.3(c)).

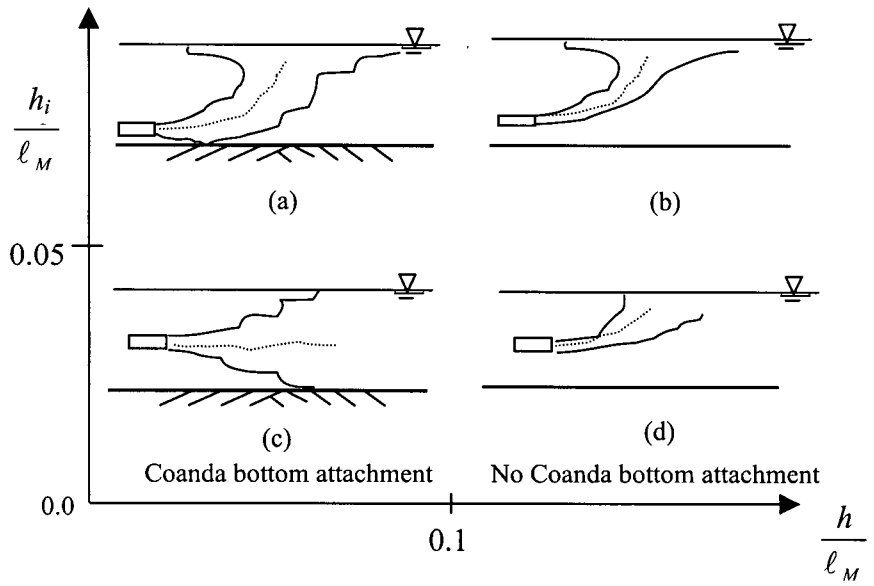

Figure 2.3 Flow patterns in shallow and deep ambient fluid (a) a buoyant jet with initial Coanda attachment and transition to surface jet, (b) buoyant jet and transition to surface jet without bottom attachment, (c) confined jet and (d) surface jet (After Sobey et al., 1988)

Jirka and Doneker (1991) suggested that if $\ell_M / h_i \leq 1$, the flow is dominated by buoyancy after a short distance and has no interaction with the water surface. If $\ell_M / h_i \geq 1$, the flow is dominated by momentum in relation to h_i and the surface interaction for a horizontal discharge depends on the discharge angle.

Balasubramanian and Jain (1978) found that when a jet with high momentum and low buoyancy is injected in shallow water conditions, the energy input into the receiving water may be so strong that a unstable flow can be formed due to insufficient buoyancy. Consequently, this results in recirculation near the jet discharge leading re-entrainment of partially diluted fluid into the discharge. However, rising buoyant jets with low F_d submerged in a deep receiving water entrain only ambient fluid but not the partially diluted jet fluid. Re-entrainment of partially diluted fluid occurs if $H/h < 0.36F_d$ where H is total water depth and h is the distance between discharge and the bottom boundary.

2.4 Previous experimental studies

There has been little research on buoyant jets in two-layer system. Table 2.2 summarizes previous experimental studies of horizontal buoyant jets in two-layered stagnant ambient fluid and experiments of Coanda attachment in homogeneous shallow water.

Table 2.2 Summary of the previous experimental studies on horizontal buoyant jets in two-layer systems and homogeneous shallow ambient fluid

Investigators	Conditions		Parameters and measurement techniques
	Ambient fluid	Density relations	
Schneider (1980)	two-layer system	$\rho_j = \rho_a$ discharge into the lower layer	entrainment flux across the interface (shadow graph), a single-electrode resistivity probe and a thermistor
Roberts and Mathew (1984)	two-layer system with a linearly stratified lower layer	$\rho_j = \rho_a$ discharge into the lower layer	spreading level, collapsed layer thickness and volume flux, entrainment location and thickness; density profile using a two-wire conductivity probe photographs of dye streaks
Sharp and Vyas (1977)	Homogeneous shallow ambient fluid	$\rho_j < \rho_a$	velocity profile using hydrogen bubble generator
Balasubramanian and Jain (1978)	Homogeneous shallow water	$\rho_j < \rho_a$	density profile by thermistors, velocity distribution using a orifice meter
Sobey et al.(1988)	Homogenous shallow water with two boundaries: the bed and free surface	$\rho_j = \rho_a$	thermistor probes
Johnston and Volker (1993)	Shallow water with two boundaries: the bed and the free surface	$\rho_j = \rho_a$	jet trajectory, temperature profile and velocity distribution laser doppler velocimeter, thermistors, planimeter
Johnston et al. (1994b)	Shallow water with two boundaries: the bed and the free surface	$\rho_j < \rho_a$	jet trajectory, temperature profile and velocity distribution in horizontal and vertical direction thermistor probes

ρ_j, ρ_a : density of jet fluid and ambient fluid

2.5 Behavior of particle-laden flow

2.5.1 Particle clouds without source momentum

The sedimentation of particles from a turbulent jet is a complicated process. The particles in the jet flow constantly settle due to gravity but the turbulence of the jet maintains the particles in suspension. Therefore, prior to analyzing the complex dynamics of a particle-laden jet, it is useful to understand the fundamental behavior of a cloud of dense particles released without initial momentum in the ambient fluid.

Koh and Chang (1973) categorized the gross behavior of dredged particulate material discharged into open water through a barge into three regimes: convective descent, dynamic collapse and passive diffusion regime illustrated in Figure 2.4.

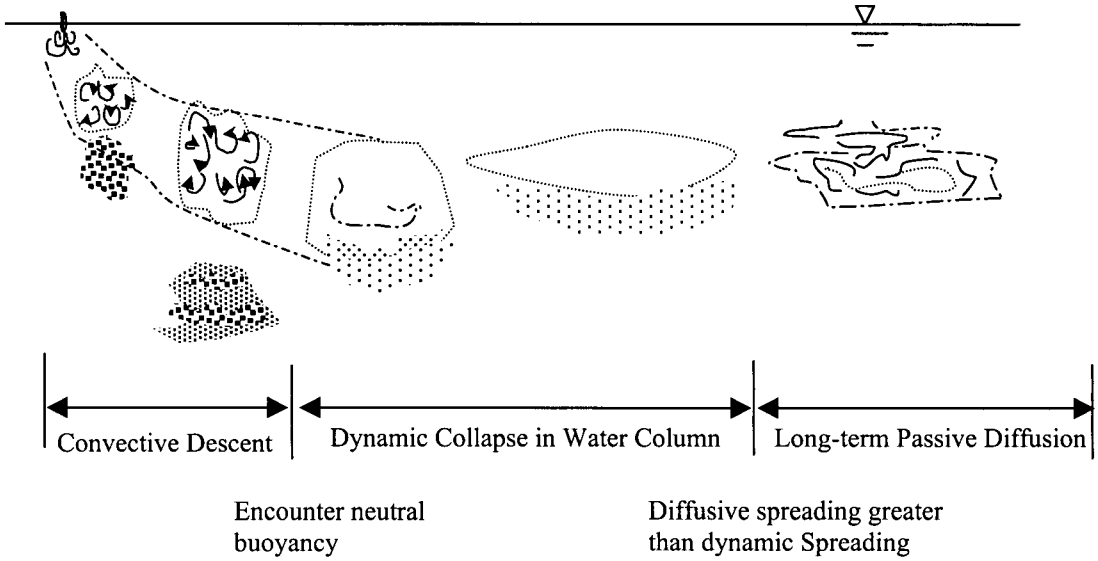

Figure 2.4 Behavior of a particle cloud (After Ruggaber, 2000a)

- Convective descent: the released dense particulate moves downward due to its negative buoyancy and creates a particle cloud in the water column.

- Dynamic collapse: depending on the local buoyancy of the particle cloud, the cloud may reach the bottom of the water basin or approach its neutral buoyancy level in the water column. When the vertical motion of the cloud ceases, it collapses and spreads horizontally.

- Passive diffusion: after the dynamic spreading due to initial mixing in the vertical and horizontal directions, the particle cloud moves with the ambient fluid.

The convective descent phase in a homogeneous ambient fluid has been intensively investigated while the dynamic collapse and passive diffusion regimes have been little studied. The convective descent phase includes initial acceleration, cloud and dispersive (particle-settling) regimes.

- Initial acceleration: the released particle-laden fluid accelerates due to initial buoyancy. Shear force due to the density and velocity difference at the boundary causes entrainment of ambient fluid and the cloud expands. Typically, a particle cloud enters the second phase of motion when its travel distance approaches 1 - 3 initial cloud diameters (Baines and Hopfinger, 1984).

- Cloud (thermal): during this phase the size of the cloud continues to increase with time, however its velocity decreases with the rapid entrainment of less dense ambient fluid caused by large eddies. A conspicuous internal circulation in the cloud occurs (Rahimipour and Wilkinson, 1992). The spherical vortex is formed as the cloud descends. The particle cloud becomes flattened and forms a mushroom-shape structure due to the induced internal circulation (Ruggaber, 2000a). The mixture of fluid and particle clouds descends as a swarm of individual particles and

gradual separation between particles and parent fluid occurs (Noh and Fernando, 1993). In addition, as the particle cloud descends, re-entrainment of the particles suspended in the ambient fluid into the cloud can occur at the edge of the cloud (Carey and Sigurdsson, 1988; Ruggaber, 2000b)

- Dispersive (particle-settling): in this regime, the particle cloud decelerates toward the settling velocity of individual particles. Thus, internal circulation is suppressed and becomes insufficient to keep the particles in suspension. Consequently, active settling of particles occurs although the cloud continues to expand at a lower velocity (Rahimipour and Wilkinson, 1992; Ruggaber, 2000a). The descending velocity of the cloud is dependent either on the individual particle settling velocity or the motion of the cloud (Noh and Fernando, 1993).

2.5.2 Characteristics of particles in flow

2.5.2.1 Particle settling

The Stokes' free settling velocity of an individual spherical particle, w_s is expressed as

$$w_s = \frac{g(\rho_P - \rho_a)d_p^2}{18\rho_a \nu} \tag{2.17}$$

where ρ_P and ρ_a are the density of the particle and ambient fluid and d_P is an equivalent particle diameter and ν is its kinematic viscosity. Strictly speaking, the Stoke's velocity is valid only for spherical particles of $d_P < 60\mu m$. The important factors affecting the particle settling velocity include the particle size, density, shape and roughness. Dietrich (1982) found that for large particles, particle roughness and shape are both influential, but the latter has more effect on the particle settling behavior. For small size particles, smooth

surface of particles result in a large reduction in settling velocity. For example, particles with pointed ends settle faster than those with flat ends (Ilic et al., 1992)

Rahimipour and Wilkinson (1992) indicated that the behavior of particles within a cloud and the cloud itself is determined by the relative magnitude of the individual particle settling velocity (w_s) to the internal circulation velocity defined as $\sqrt{B_p / \rho_a R_c^2}$, where B_p is bulk density of a particle cloud and R_c the size of the cloud. On release all particles are incorporated into the cloud and remain until the cloud velocity approaches the particle settling velocity (Ruggaber, 2000a, 2000b)

2.5.2.2 Effect of particle size and concentration

Particles with smaller settling velocity than the flow velocity initially move with fluid. However, significant separation of particles occurs as the settling velocity approaches the flow velocity (Hinze, 1972). The movement of particles is due primarily to large eddies, which promote the formation of a group of particles, resulting in large-scale fluctuations of concentration within the flow (Hinze, 1972). Also, particles with small size at large viscosity tend to move together with the fluid as a particle cloud (Noh and Fernando, 1993). The presence of small amounts of fine particles in a coarse-grained current enhances flow velocity because the fine particles remain suspended and maintain an excess current density for a longer time (Gladstone et al., 1998).

The concentration of particles is another influential factor on particle-laden flows. In a very low concentration, the effect of presence of particles is insignificant and thus the main flow pattern of the fluid remains unchanged (Owen, 1969). Kana and Hanatty (1960) found that particles with volume concentration less than 2.5 % have no significant impact on the diffusion rate unless the slip velocity between particles and the fluid is large. At high concentrations, however, particles tend to be less mobile than at low concentrations.

Individual particles collide with each other and behave as a group. The grouping behavior of particles can significantly modify the flow pattern (Hinze, 1972; Kada and Hanratty, 1960). Moreover, at very high concentration the interaction of the particles can cause turbulent motion to halt (Hallworth and Huppert, 1998).

If particle concentration is high but w_s is small, a flow plunges as a particle cloud. For low concentration but large w_s, the particles sink as individual particles leaving interstitial fluid (Noh and Fernando, 1993).

2.5.2.3 Density and buoyancy

If the density of the interstitial fluid is less than that of the ambient fluid, the behavior of the particle-laden fluid is determined by its initial bulk density. Turner and Huppert (1992) proposed a stability parameter (R_h), which is a ratio of the density difference between the interstitial and ambient density to the difference between the bulk density of the suspension and the ambient density.

$$R_h = \frac{\rho_f - \rho_a}{\rho_b - \rho_a} \tag{2.18}$$

where ρ_f, ρ_a and ρ_b represent the density of interstitial fluid, ambient fluid and the bulk density of suspension.

A two-phase jet such as a particle-laden jet can be characterized by two buoyancy fluxes; initial bulk buoyancy flux (B_b) and the buoyancy flux of the interstitial fluid (B_f) (Carey and Sigurdsson, 1988). The initial density of a particle-laden jet is a function of particle concentration and the density of the interstitial fluid.

$$B_b = Q\left(g\frac{\rho_a - \rho_b}{\rho_a}\right)$$

$$B_f = Q(1-X)\left(g\frac{\rho_a - \rho_f}{\rho_a}\right) \tag{2.19}$$

where X is the volumetric concentration of particles.

2.5.3 Gravity current

A gravity current is driven by the density difference between inflow and the ambient fluid. The density difference can be attributed to dissolved or suspended material or temperature difference. A turbidity current is one type of gravity current due to suspended particles such as mud and silt in its interstitial fluid (Simpson, 1982). In general, three types of gravity currents occur in nature: surface overflow, underflow and intermediate flow. If the entering fluid is denser than the ambient fluid, the current plunges and then forms an underflow. If the entering fluid is lighter than the ambient fluid, it forms a gravity current at the surface of the ambient water body (i.e. surface overflow). In addition, a current with an intermediate density forms an intermediate level intrusion at the level of neutral buoyancy (Fischer et al., 1979; Simpson, 1982).

2.5.3.1 Particle-laden flow with reversing buoyancy

If the bulk density of particle-laden flow exceeds that of the ambient fluid, the flow plunges down to the bed and forms an underflow regardless of the interstitial fluid density. As the flow propagates, the suspended particles settle out and the flow decelerates rapidly. Consequently, the buoyancy reverses due to sedimentation. This type of flow is called a turbidity current with reversing buoyancy. The remaining interstitial fluid rises through the upper surface of the flow while the particles descend continuously (Huppert et al., 1991;

Sparks et al., 1993; Hürzerler, 1994; Rooij et al., 1999; Hogg et al., 1999; Hallworth and Huppert, 1998).

While the detraining interstitial fluid ascends, it carries fine particles into the overlying ambient fluid (Fischer and Smith, 1983; Carey and Sigurdsson, 1988; Rooij et al., 1999). Particle re-entrainment occurs at the edge of a particle-laden flow, causing denser margins than the ambient fluid. This convective instability enhances the sedimentation (Carey and Sigurdsson, 1988). After the particles settle out, the entrainment of ambient fluid into the intrusion becomes the dominant mechanism (Rooij et al., 1999). However, the spreading rate of the particle-laden flow decreases continuously due to the detrainment. The flow eventually lifts off from the bed and develops a surface overflow downstream (Hürzeler et al., 1996).

2.5.4 Experimental conditions of previous studies

Table 2.3 summarizes the experiment conditions of particle-laden flow from previous investigations.

Table 2.3 Experimental conditions of previous studies on particle-laden flow

Researchers	Type, Size (μm) Density (kg/m^3) of particles	Measurement	Conditions
Hallworth et al (1998)	Silicon carbide 9, 17, 23, 37, 53 1,019-1,957 kg/m^3	Position of flowfront, sediment distribution on the floor	Lock exchange A homogeneous ambient fluid
Carey and Sigurdsson (1988)	Silicon carbide 7 – 120 1,000-1,060 kg/m^3	Density, particle concentration profiles	Buoyant plume of fresh water and solid particles in a salt ambient fluid
Green (1987)	Taconite tailings < 10 specific gravity 2.07		Lock-release, a mixture of warm water and taconite tailings into a cold clear ambient fluid,
Hogg et al. (1999)	Silicon carbide 23 μm 3,217 kg/m^3	Lift-off distance	Interstitial fluid: methanol + fresh water ambient fluid, Lock-release
Hürzeler et al. (1994)	Silica flour 28.59 μm 2,650 kg/m^3	Vertical density structure, spreading velocity	Lock-release, freshwater + particles propagating into saline ambient water
Sparks et al. (1993)	Alumina particles 66.5 μm, 3,985 kg/m^3	Lift-off distance tracking of the current front	Interstitial fluid: Methanol & fresh water Ambient fluid: fresh & saline water, fixed volume of dense jet with/without particles by lock-release technique
Popper et al. (1974)	Oil droplets < 50 (μm)	Velocity distribution of oil droplets	Oil particles in air jet
Goldschmidt et al. (1972)	Nitrogen gas bubble and oil droplets 343, 527, 780 and 970 (μm)	N2 gas bubble concentration and velocity profile	Water jet with N2 gas bubbles in homogeneous ambient air
Rooij et al. (1999)	Silicon carbide 23, 37(μm), 3,217 kg/m^3	Spreading velocity of saline and particle laden flow, bottom sediment distribution	Saline fluid and particle-laden flow releasing along the density step in two-layer system

2.6 CORMIX (Cornell Mixing Zone Expert System)

The mixing model CORMIX v3.2 was used to compare with the experimental results for fluid jets and particle-laden jets in two-layer systems. The suitability of the model for particle-laden jets is also examined.

2.6.1 CORMIX v3.2

CORMIX is a dimensionless length scale-based model developed by Cornell University for the US EPA. The program can be used for the analysis, prediction and design of discharge into an aqueous environment (Jirka et al., 1996). CORMIX consists of three integrated submodels: CORMIX1, CORMIX2 and CORMIX3. CORMIX 1 is a model used for positively and negatively buoyant submerged single port discharges. CORMIX 2 is used for submerged multiport diffuser discharges and CORMIX 3 for buoyant surface discharges. The models can simulate steady and unsteady ambient fluid with various density stratification types (Jirka et al., 1996).

The core of CORMIX is a flow classification, which provides a generic qualitative description of the discharge flow in the given ambient fluid condition. The CORMIX model classifies the discharge configuration with regard to discharge conditions and ambient conditions into a generic flow classification by means of length scale analysis. An example of the schematic diagram of a flow classification is shown in Figure 2.5 for buoyant jets. Once the flow classification has been performed, a sequence of hydrodynamic simulation submodels are executed to predict the jet trajectory, dilution characteristics, position and width of the plume (Jirka et al., 1996).

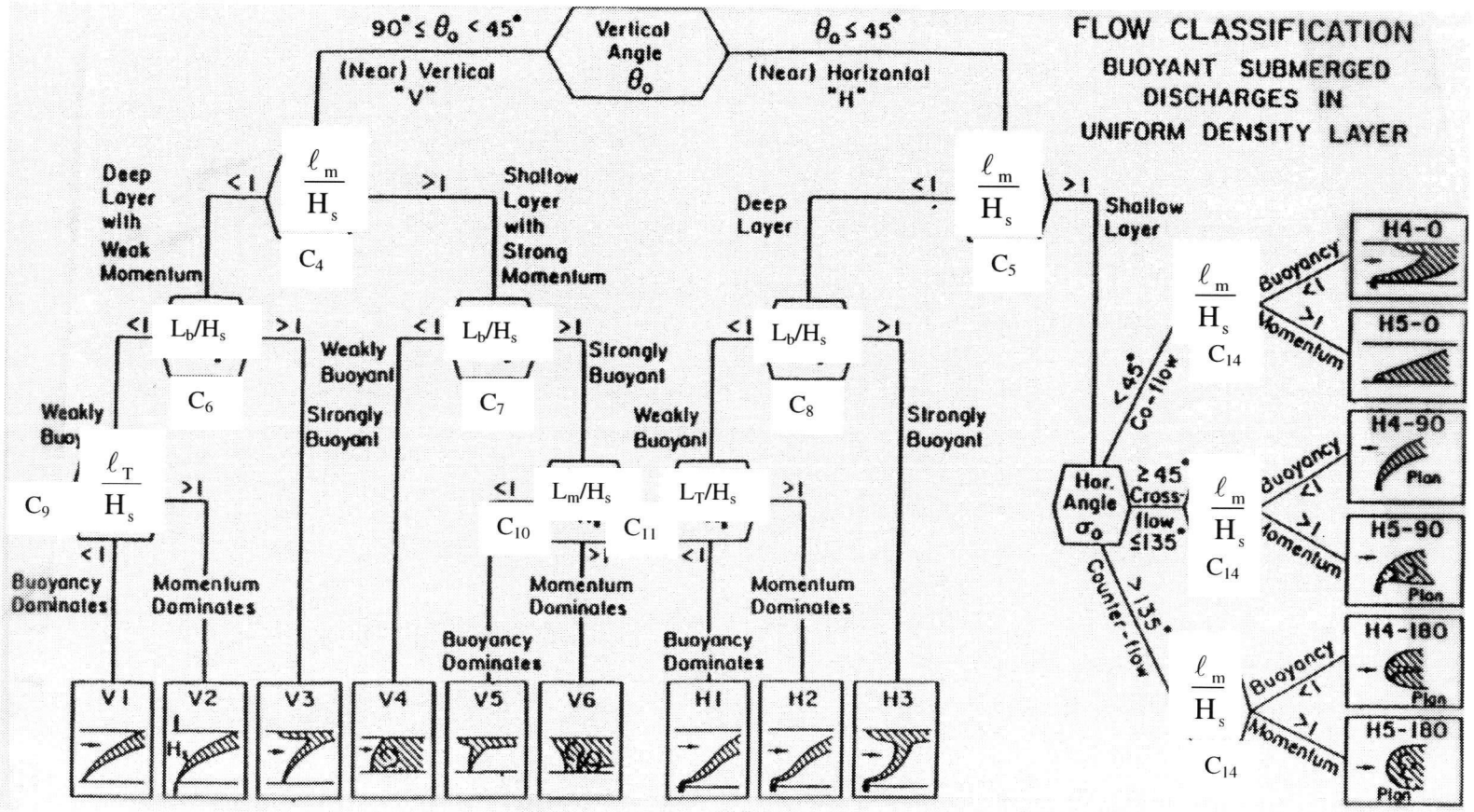

Figure 2.5 CORMIX1 Flow classification for buoyant submerged discharge in uniform density layer (Jirka et al., 1996)

2.7 Summary

There have been numerous investigations into problems of turbulent buoyant jets discharged into homogeneous and linearly stratified ambient fluids. However, only a limited number of studies on the dynamics of jets in two-layer systems have been published. Moreover, most of research was conducted on fluid jets and little information on particle-laden jets are available. Although in the 1970's a small number of studies on the trajectory of individual particles in an air jet were conducted, the particle concentration was low and thus the effect of particles on the jet behavior was insignificant. In addition, most studies on the flows associated with particles have been on behavior of particle clouds without source momentum such as ocean dumping of dredged material or turbidity current proceeds along the bottom bed.

Figure 2.6 shows a summary of the scope of the present study in relation to the range of possible related studies.

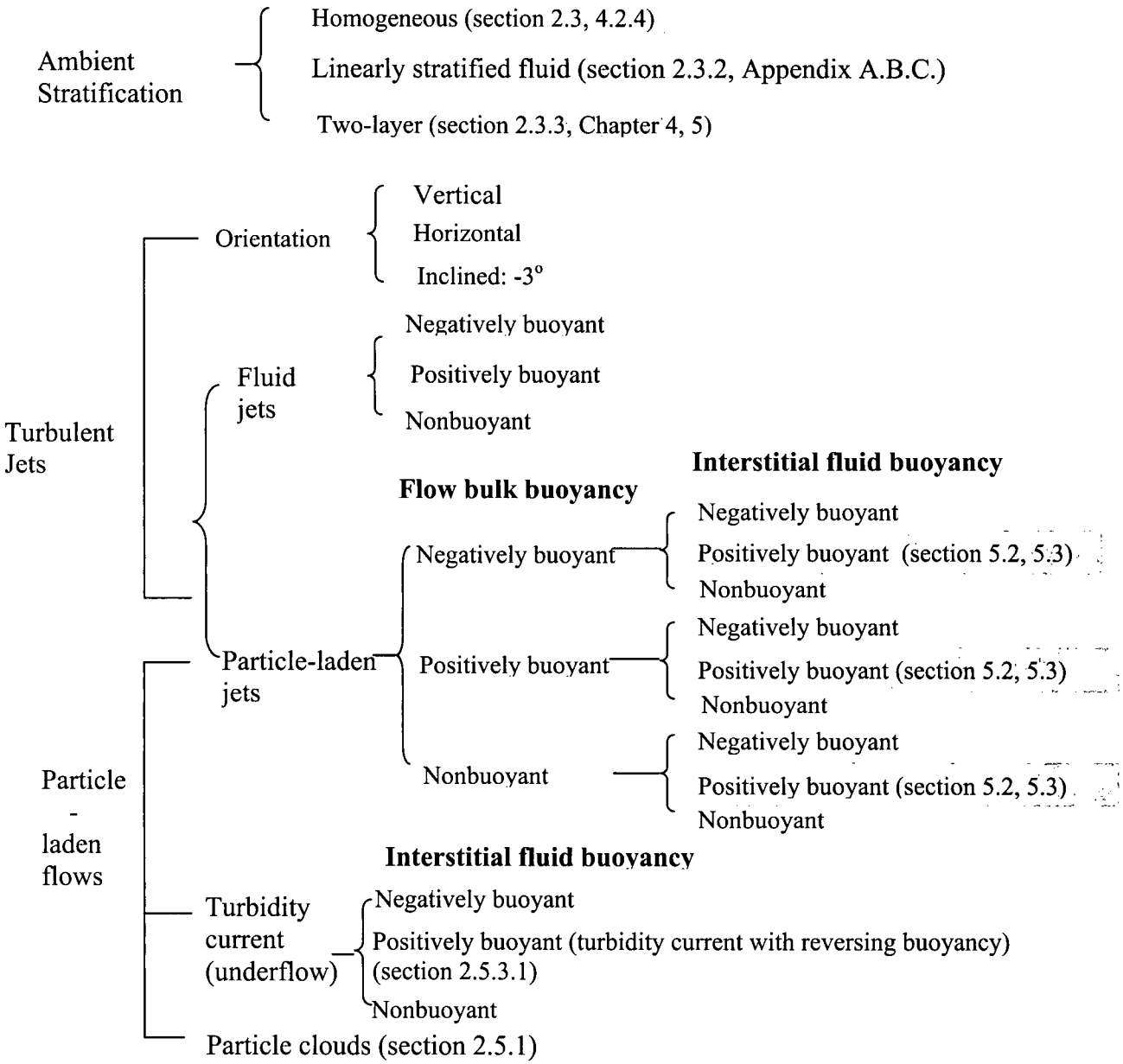

Figure 2.6 Summary of the scope of the present study in relation to the range of possible related studies (Area of this study)

Chapter 3

Experimentation

3.1 Introduction

The present study investigates the behavior of turbulent fluid jets and particle-laden jets in stagnant receiving water. Buoyant round fluid jets and particle-laden jets with buoyant interstitial fluid were injected under various discharge conditions and three different ambient fluid conditions: two-layer system, linearly stratified fluid and homogeneous fluid. All jets were discharged at 3^{o} downward inclination, parallel to the bottom bed.

In two-layer systems, the interstitial fluid was kept highly buoyant relative to the lower layer for all experiments so as to simulate the worst possible tailings disposal scenario, where the buoyant jets penetrate into the upper layer. In addition, the bulk density of particle-laden jets, primarily determined by particle concentration, varied across experimental conditions.

3.2 Experimental apparatus

3.2.1 Physical set-up

All experiments were performed in the Civil Engineering Hydraulics Laboratory at the University of British Columbia. A photograph and a sketch of the experimental setup is shown in Figure 3.1 and Appendix D. Also, the individual components of the apparatus are discussed in the following subsections.

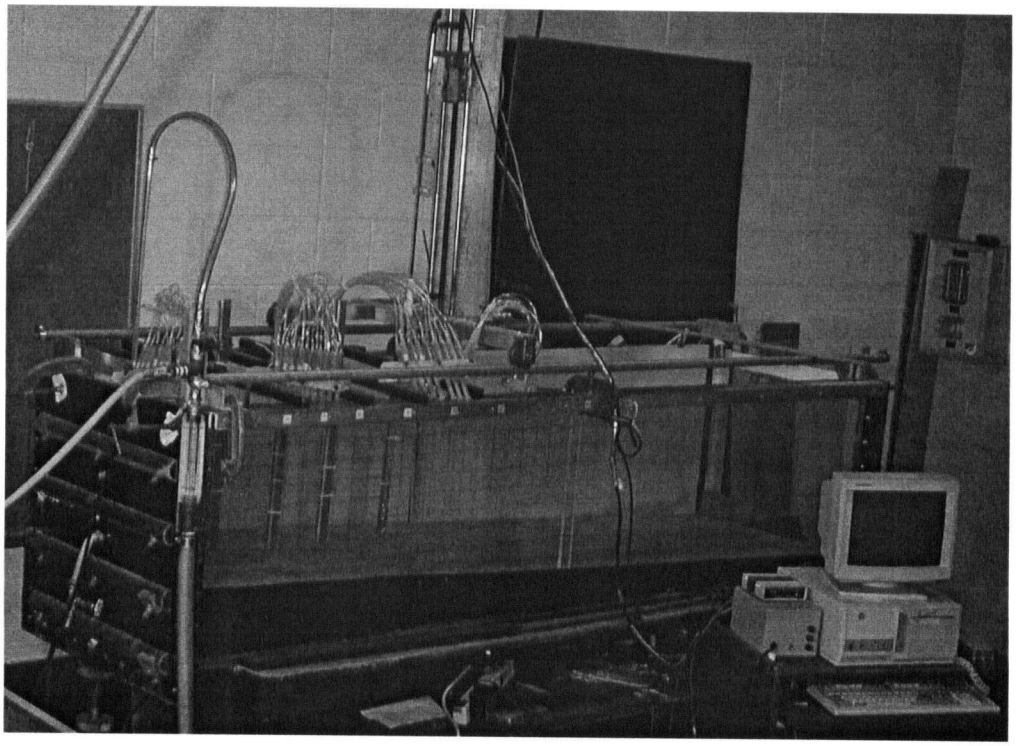

Figure 3.1 Experimental facility

3.2.1.1 Main experimental tank

All the experiments were conducted in a main tank 2.4 m long, 0.6 m high and 0.6 m wide in a hydraulics laboratory. The tank was constructed with transparent Plexiglas vertical sidewalls with the bottom of the bed at 5 % slope. Drainage of the main tank was accomplished through a 2.54 cm diameter pipe at the bottom. Figure 3.2 shows a schematic diagram of the main experimental tank.

The tank was equipped with sampling racks and trolley. Two rails at the top of the tank allowed a trolley to be moved along the length of the tank. A computer controlled traversing mechanism was mounted on the trolley, which carries a conductivity and

temperature probe connected to a 486 PC. The traversing mechanism moved vertically by the signals from the computer while horizontal direction control was achieved manually. Four stainless steel sampling racks were installed along the tank (x = 10, 30, 45 and 75 cm). Each rack holds 16 sampling tubes spaced at 2 - 4 cm intervals. Each sampling tube was connected to a 10 mL syringes for sample collection.

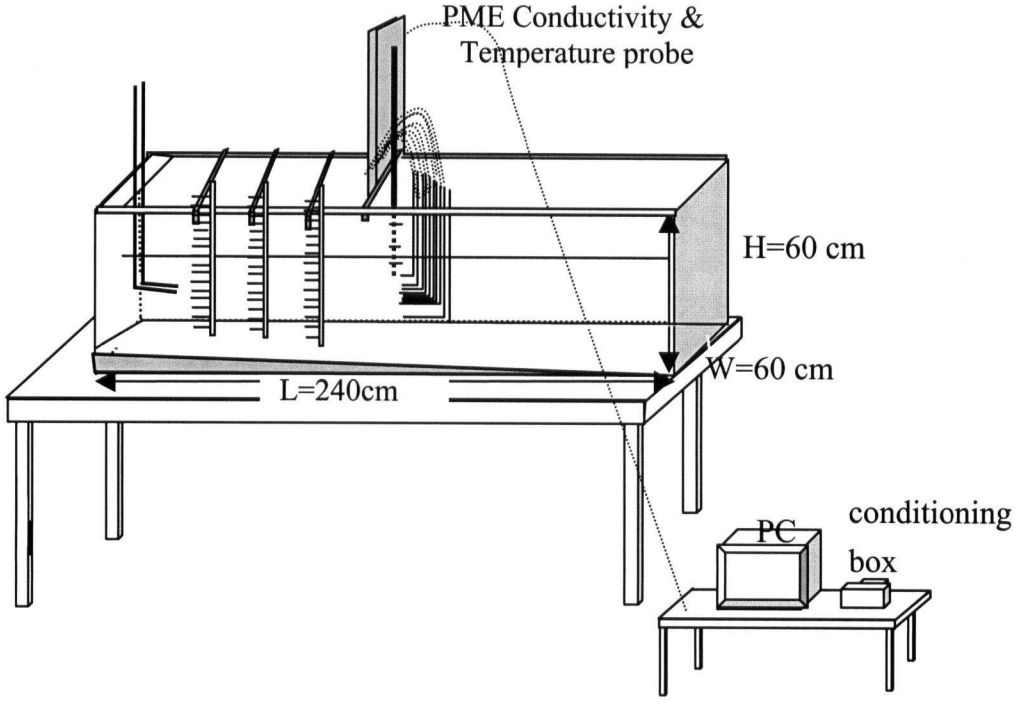

Figure 3.2 A sketch of the main experimental tank

At x = 75 cm, 10 copper sampling tubes passing through ten holes with inner diameter of 3.1 mm were fixed at the rear of the trolley. Each sampling tube was fixed with a tube holder to enable adjustment of the vertical position. The top of the tubes were connected to 7016 Masterflex tubes which were in turn connected to an I/P7553-70 Masterflex pump with a maximum capacity of 600 rpm. The transparency of the hose facilitated monitoring of the fluid and particle motion in the tubes. These tubes were bent at right angles and faced upstream on a line perpendicular to and passing though the jet axis.

3.2.1.2 Jet discharge system

The discharge system, shown in Figure 3.3, consisted of a mixing tank, a flowmeter, a flow control valve, a pump and a discharge nozzle. A mixing tank with a 90 L storage capacity was used to supply completely mixed jet fluid. The tank was equipped with a motor, kept at rotation rate of 60 rpm connected to an arm sufficiently large to provide complete mixing. The mixing tank was connected to the main tank by a pipe. The pump used was a Jet Pump Motor by Dayton Electric MFG Co with a maximum capacity of 56 J, 60 Hz and 3450 rpm. The flow rate was controlled by an inlet valve attached to the main tank and monitored with a flowmeter. The flowmeter used was a ColeParmer P03248-56 by KING, with operating range 6.3 - 63 mL/s. This range of flow rate ensured the jet was fully turbulent at all times for the discharge pipe size used. An assistant valve was installed in order to remove the residual fluid, gas or particles accumulated in the pipe and the pump prior to commencing experiments.

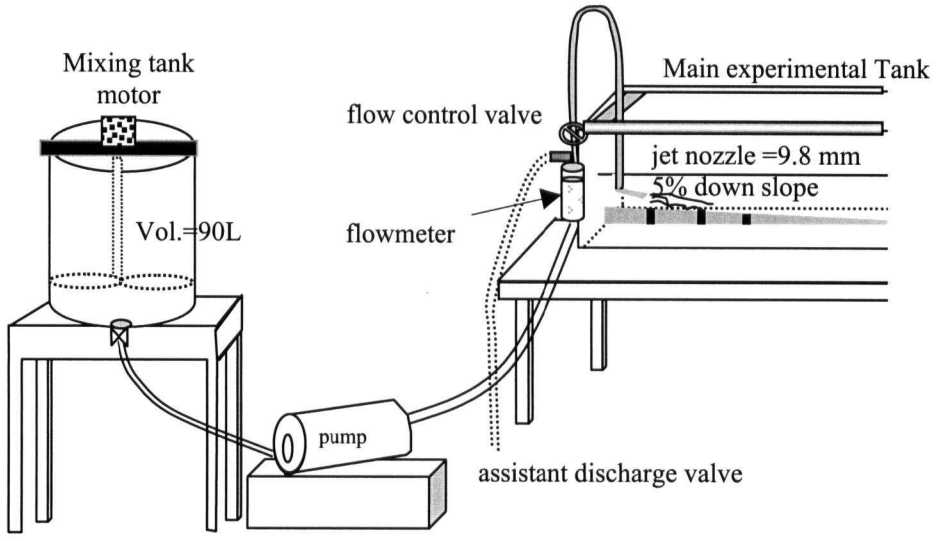

Figure 3.3 A sketch of discharge system

A vertically adjustable discharge nozzle with a 9.8 mm inner diameter was set up 10 cm from the center of the tank wall. The distance between the nozzle tip and the wall was determined to ensure sufficient mixing area downstream and avoidance of the turbulence due to the back wall. An elbow with 3° angle parallel to the bed slope was attached to the end of the nozzle.

3.2.1.3 Ambient fluid stratification system

Two reservoir tanks with capacity of 500 L were situated approximately 3 m above the ground to achieve sufficient hydraulic head. The filling speed was controlled by a valve attached to the tank (Figure 3.4). A 2.54 cm diameter pipe was used to supply the prepared reservoir fluid to the main tank through a floating spreader. A valve attached to the tank was used to control the filling speed of the main tank. One reservoir tank stored fresh water and the other saline water. These were used to create linearly stratified and two-layer stratified ambient fluid. A motor and two 300 W submersible heaters with thermostat were set up in the tank ensuring constant water temperature and complete mixing.

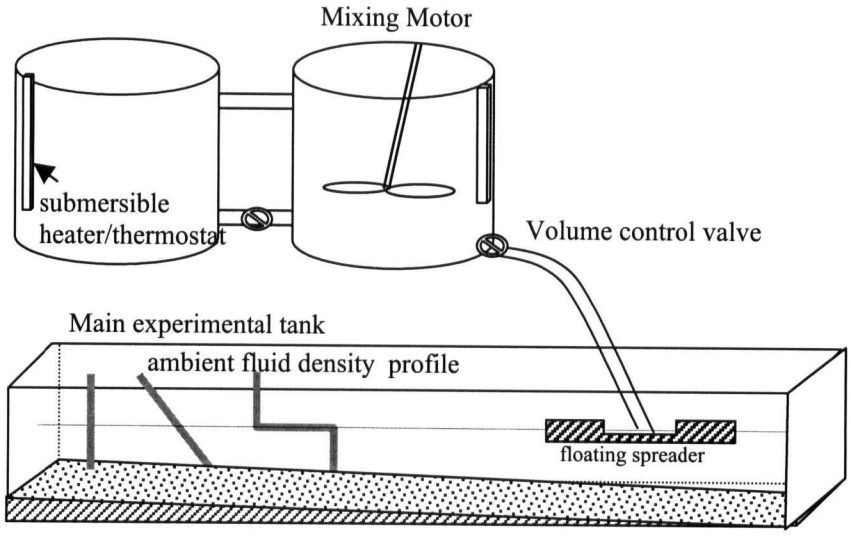

Figure 3.4 Ambient fluid stratification system

3.2.2 Instrumentation

3.2.2.1 PME conductivity and temperature probe

Conductivity and temperature measurements were performed using a Model 125 Microscale Conductivity Temperature Instrument manufactured by Precision Measurement Engineering (PME) shown in Figure 3.5. The probe consists of a conductivity and temperature sensor on a 0.63 cm diameter stainless steel shaft mounted onto a long stainless steel waterproof housing that contains an electronic preamplifier (PME, 1999). The sensor provides two analog voltage outputs that are functions of the solution electrical conductivity and temperature respectively. The sensors are connected to a probe controller which performs amplification and control functions. The controller was connected to an A/D board PC-LPM-16 by National instruments in an IBM 486 PC.

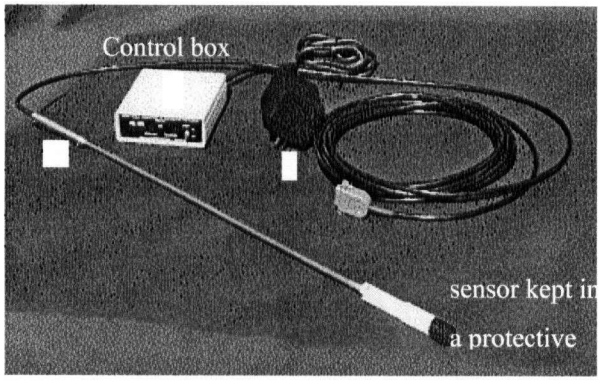

Figure 3.5 PME conductivity and temperature probe

This A/D board was used to convert analog voltages received from the conductivity sensor to machine-readable digital data. It can accept up to 16 channels of analog single ended signals. The range of stable linear conductivity is between 5 mS/cm and 800 mS/cm where the accuracy within this range is ± 1 %. The temperature can be measured from –10 up to 100 °C. A data acquisition program was designed to sample probe measurements at approximately 35 Hz and the measured values were recorded in a data file for later analysis.

3.2.2.2 Calibration of a PME probe

Conversion of conductivity and temperature probe electrical readings requires that the probe be calibrated with known conductivity. It was necessary to calibrate the probe prior to each experiment since the probe holds an 8-hour calibration stability. Initially, calibration was conducted by measuring the voltage both from a highest known possible conductivity and the lowest temperature expected during experiments. This procedure was important in that it ensured the measurements do not go out of the detection range. Once the gain setting was complete, it was necessary to check that the calibrated probe provides linearity between the measured conductivity and the voltage output. This was achieved by testing a series of solutions of the conductivity suggested in CRC Handbook of Physics and Chemistry (Weast, 1985).

The standard solutions for calibration were prepared by addition of a known mass of laboratory grade Sodium Chloride (NaCl) to a 250 ml volumetric flask with distilled water at room temperature at 20 °C using Table 3.1. A 1.032 mol/L NaCl solution was used for the highest conductivity. The calibration curves were obtained to confirm that the conductivity measurement shows linearity.

Table 3.1 *NaCl* standard solution for calibration (After Weast, 1985)

Molar Concentration (g mol/L)	Density (D_4^{20})*	Specific electrical conductance @ 20 °C (mmho/cm, mS/cm)
0.051	1.0004	5
0.172	1.0053	9.8
0.276	1.0096	24.6
0.47	1.0175	39.9
0.613	1.0232	50.7
0.739	1.0282	59.9
1.032	1.0398	80.0

* density ratio at 4°C and 20°C

Measured conductivity and temperature were converted into salinity and eventually fluid density using the procedure described in section 3.5.2.

3.2.2.3 Anton Paar density meter

The bulk density of the particle-laden jets was measured using an Anton Paar DMA5000 (Figure 3.6). The Anton-Paar density meter vibrates a 1mL sample in a U-shaped tube and measures the frequency of oscillation. The U-tube continuously oscillates at the characteristic frequency by a magneto-electrical excitation system. The measured period of oscillation of the sample tube is converted into density and displayed on the meter. The uncertainty of measurement is 10^{-1} to 10^{-3} kg/m^3 (Anton-Paar, 2000).

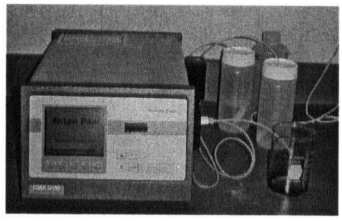

Figure 3.6 Anton Paar DMA 5000 density meter

3.2.2.4 MACH Spectrophotometer

Dye concentration was measured using a MACH spectrophotometer. It passes a beam of broadly polychromatic radiation through the sample and measures the intensity of power of radiation as a function of wavelength. A wavelength of 520 nm was used.

Figure 3.7 MACH spectrophotometer

3.2.3 Material

3.2.3.1 Jet and ambient fluid

Density modification of the jet fluid and the ambient fluid was obtained by adding fine granulated sodium chloride from the Canadian Salt Company Limited. The salt was added to water in all experiments in order to ensure the conductivity is within the linear range of the conductivity probe. Thus, the minimum conductivity of fluid was maintained at 5 mS/cm. Rhodamine dye was added to the jet fluid to provide a qualitative indication of the extent of dilution by the mixing process in the flow. The dye was sufficiently diluted to avoid a density change.

The particle-laden jet consists of particles and interstitial fluid. The mixing tank was filled with water and Rhodamine dye, while sodium chloride was added to yield the minimum conductivity of 5 mS/cm. The fluid was heated to 30°C to achieve high buoyancy. The particle suspension was sustained by continuously stirring at a fast speed to avoid settling and accumulation of the particles in the tank. Completely-mixed jet fluid was pumped at a constant flow rate through a flowmeter into the main experimental tank.

3.2.3.2 Particles

The particles used for particle-laden jets were spherical glass beads with a density of 2,450 kg/m^3 manufactured by Canasphere Industries Limited, Alberta. The glass beads were used because they have narrow particle size distributions and exhibit uniform behavior and settling velocity. Also, these glass beads have no conductivity and are non-cohesive in saline solution. The particle settling velocity is determined primarily by the size, shape and specific gravity of particles in accordance with Stoke's Law. Therefore, it was necessary to investigate the feasibility of using glass beads as a substitute for fine tailings from Shell tailings pond in terms of the particle size distribution and shape.

Particle size distribution

The particle size distribution of glass beads was obtained by a Sedigraph 5100 Particle Size Analysis System. The Sedigraph 5100 determines particle size by the gravity-induced travel rates of different size particles in a liquid with known properties. Settling velocity is measured using a finely collimated beam of x-rays passing through the sample cell to a detector. The particle size is calculated based on Stoke's Law. 0.05% Calgon was used as a dispersant for the particles, which has a density of 0.9941 g/mL and a viscosity of 0.724 g/mL. The analysis showed that approximately 92% of the particles ranged between 30-60 μm and the mean diameter were 38.72 μm. The detailed particle size distribution is given in Figure 3.8. The mean settling velocity calculated using Stoke's law was 1.14 mm/s at 20 °C.

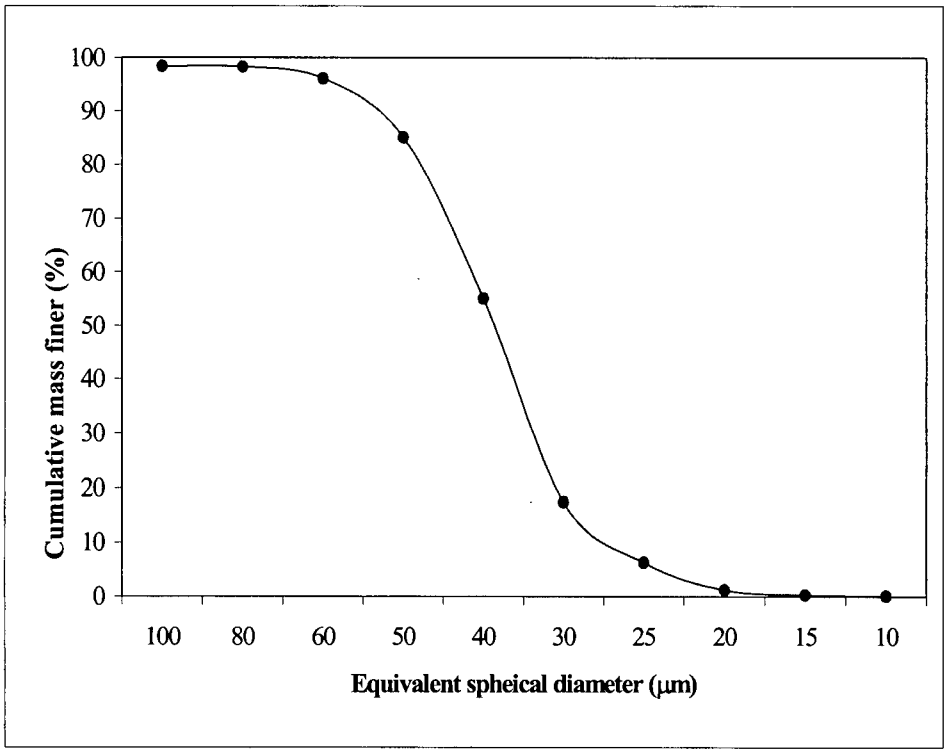

Figure 3.8 Particle size distribution of glass beads

Particle shape

The shape of the particles is a critical factor for the particle size determination since Stoke's law is valid only for spherical shaped particles. Fine tailings taken from a tailings pond in Alberta was used as reference particles. However, measuring the fine tailings particle size was not possible due to equipment restrictions and the nature of the fine tailings. Namely, fine tailings contain bitumen, which exerts a strong viscosity, and they tend to attach to the instrument wall and testing tube. It was also difficult because the shape and size of tailings are easily modified by a small disturbance.

As an alternative, photographs of tailings were taken and compared. The shape of both glass particles and fine tailings were observed by a Nikon Microflux EFM (semi-automatic photomicrograph attachment) and photographs were taken. Figure 3.9(a)(b)(c) show the shape of fine tailings, the mixture of glass beads and fine tailings and the glass beads respectively. Glass beads show fairly uniform round shape whereas fine tailings are more angular or amorphous. Despite this constraint, fine tailings are roughly spherical and of similar enough size to glass beads that the latter approximately simulate the fine tailings.

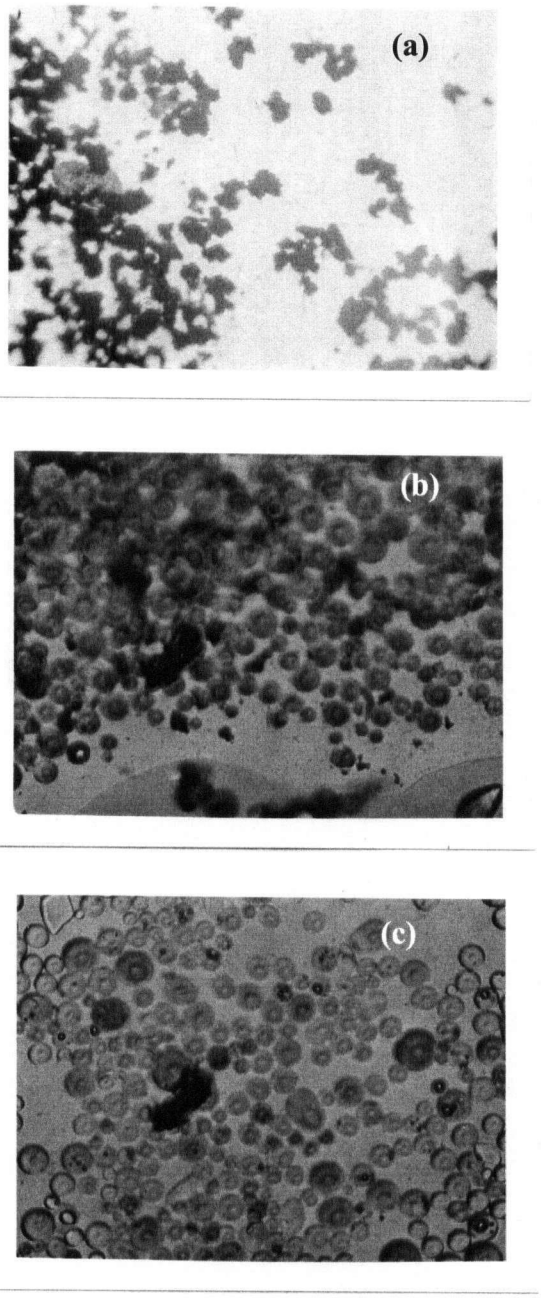

Figure 3.9 Shape of particles (a) fine tailings, (b) mixture of fine tailings and glass beads and (c) glass beads

3.3 Experimental conditions

All experiments were conducted with Reynolds number greater than 5,000, ensuring fully turbulent jets. The experimental conditions for fluid jets and particle-laden jets are shown in Figure 3.10 and 3.11 respectively.

3.3.1 Fluid jet

A total of 59 experiments were conducted for fluid jets: 32 experiments for a two-layer system, 14 for a linearly stratified ambient fluid, and 13 for homogeneous ambient fluid. Experiments in homogeneous fluid were studied only to examine Coanda bottom attachment. The individual experimental conditions of fluid jets are given in detail in Tables 3.2, 3.3 and 3.4. The details of the results in the tables will be discussed in Chapter 4.

Two-layer system

- Densimetric Froude number (F_d): 8.1 - 52.9
- Density difference between two layers ($\rho_2 - \rho_1$): 2.9 – 25.6 kg/m^3
- Discharge height above the bed (h): 5 – 19.5 cm
- Distance to the density jump (h_i): 3.5 - 18 cm
- Total water depth at the discharge location (H): 34 cm

Linear stratification

- Densimetric Froude Number (F_d): 8.7 - 55.5
- Buoyancy frequency (N): 0.58 - 0.78 s^{-1}
- Discharge height above the bed (h): 2 - 15 cm

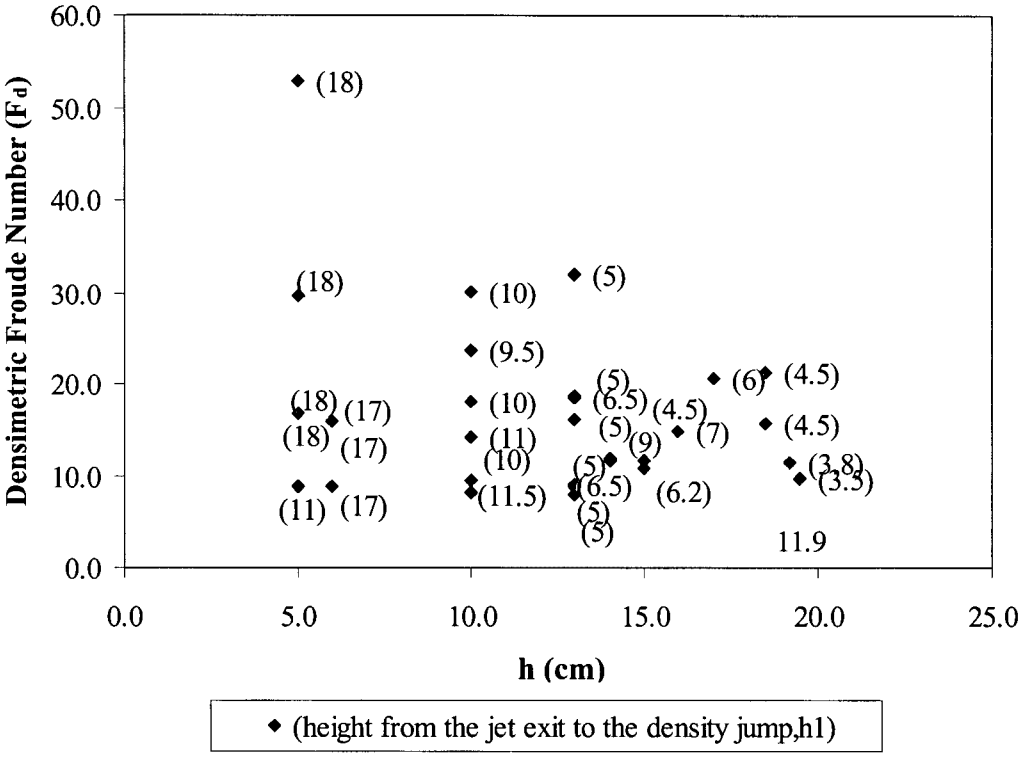

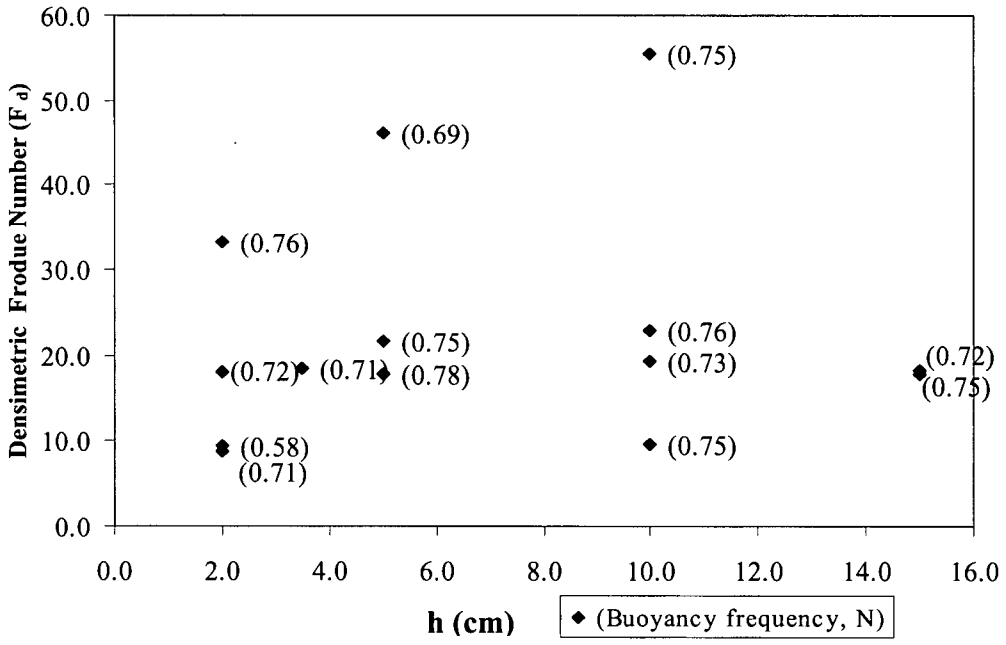

Figure 3.10 Experimental conditions for fluid jets: (a) two-layer systems and (b) linearly stratified fluid

Table 3.2 Experimental conditions for fluid jets in two-layer systems

EXP#	ρ_j (σ_t)	ρ_1 (σ_t)	ρ_2 (σ_t)	h (cm)	h_i (cm)	h_1 (cm)	Q (cm^3/s)	M (cm^4/s^2)	B (cm^4/s^3)	F_d	L_M (cm)	h/L_M	h_i/L_M	Ψ	Backflow	Regime	Figure
A6	19.14	0.64	21.79	5	18	16	63.0	5262	160	53.0	48.9	0.10	0.37	0.07	No	I	
A18	14.55	1.67	21.90	6	17	17	31.5	1315	222	15.9	14.7	0.41	1.16	0.09	Yes	I	
A17	-0.84	1.44	22.31	6	17	17	31.5	1315	699	9.0	8.3	0.73	2.06	0.13	Yes	I	
A4	0.04	2.89	26.02	5	18	16	63.0	5262	1563	16.9	15.6	0.32	1.15	0.16	Yes	I	
A19	0.28	1.71	7.35	6	17	17	31.5	1315	217	16.1	14.8	0.40	1.15	0.18	Yes	I	4.1(a) 4.2
A5	-0.05	1.71	8.22	5	18	16	63.0	5262	507	29.8	27.5	0.18	0.66	0.22	Yes	I	
A21	-0.16	1.45	20.56	10	10	24	31.5	1315	627	9.5	8.7	1.15	1.15	0.23	Yes	I	
A23	-0.31	1.26	21.76	10	10	24	63.0	5262	1334	18.3	16.9	0.59	0.59	0.30	Yes	I	
A22	-0.35	1.14	6.96	10	9.5	24.5	47.3	2960	336	23.7	21.9	0.46	0.43	0.38	No	I	
A34	-1.89	3.49	20.90	13	6.5	27.5	31.5	1315	689	9.0	8.3	1.56	0.78	0.39	Yes	I	
A24	-0.48	1.78	7.54	10	10	24	63.0	5262	491	30.2	27.9	0.36	0.36	0.42	No	I	4.8 (a)
A72	-1.00	2.12	13.00	16	7	27	41.0	2223	562	14.9	13.7	1.17	0.51	0.44	Yes	I	
A36	-0.48	6.35	31.91	13	6.5	27.5	63.0	5262	1938	15.2	14.0	0.93	0.46	0.47	Yes	I	
A37	-2.01	3.02	20.49	13	5	29	31.5	1315	681	9.1	8.4	1.55	0.60	0.50	Yes	I	4.3 (a)
A40	-0.24	18.39	22.88	5	11	23	31.5	1315	698	9.0	8.3	0.60	1.33	0.52	Yes	II	4.8 (b)
A52	1.02	16.83	24.31	10	9	25	50.4	3368	1123	14.3	13.2	0.76	0.68	0.57	Yes	II	
A51	0.75	20.94	28.32	10	8	26	31.5	1315	828	8.2	7.6	1.32	1.05	0.57	Yes	II	4.3 (b)
A39	-1.07	16.85	23.90	5	10	24	63.0	5262	1506	17.3	15.9	0.31	0.63	0.59	Yes	II	
A71	-0.92	15.51	21.20	14	9	25	41.0	2223	889	11.9	10.9	1.29	0.83	0.61	Yes	II	4.1(b)
A73	5.39	1.99	5.39	17	6	28	35.3	1650	186	20.6	19	0.9	0.32	0.66	No	II	
A77	-0.77	2.13	13.20	19.2	3.8	30.2	31.5	1315	432	11.5	10.5	1.83	0.36	0.72	No	II	
A41	0.44	4.30	7.50	13	6	28	31.5	1315	216	16.1	14.9	0.88	0.40	0.72	No	II	
A76	-1.14	4.60	18.45	19.5	3.5	30.5	31.5	1315	605	9.7	8.9	2.20	0.39	0.78	No	II	
A38	-1.47	10.93	19.29	13	6.3	27.7	63.0	5262	1257	18.9	17.4	0.75	0.36	0.79	No	II	
A75	7.33	1.13	5.13	18.5	4.5	29.5	31.5	1315	203	15.8	15.3	1.21	0.29	0.82	No	II	
A74	5.4	2.25	5.86	18.5	4.5	29.5	36.5	1770	193	21.3	19.6	0.94	0.23	0.86	No	II	
A42	7.1	4.3	7.5	13	6.5	27.5	63	5262	435	32.1	29.6	0.44	0.22	0.88	No	II	
A70	-2.99	17.30	20.20	14	9	25	41.0	2223	933	11.6	10.6	1.32	0.85	0.93	Penetration	III	4.1(c)
A49	-2.75	18.47	23.22	15	6.2	27.8	41.0	2223	1018	11.0	10.1	1.48	0.61	1.04	Penetration	III	
A35	-0.48	18.93	22.91	13	5.5	28.5	31.5	1315	706	8.9	8.2	1.58	0.67	1.12	Penetration	III	
A33	-5.93	18.61	22.70	13	5.2	28.8	31.5	1315	864	8.1	7.4	1.75	0.70	1.27	Penetration	III	4.4
A50	-0.13	18.59	22.45	15	4.5	29.5	41.0	2223	886	11.8	10.9	1.38	0.41	1.53	Penetration	III	

Regime I: Weak Impingement, Regime II: Strong Impingement, Regime III: Penetration

Table 3.3 Experimental conditions for fluid jets in homogeneous ambient fluid

EXP#	$\rho_\alpha - \rho_j$ (kg/m^3)	h (cm)	Q (cm^3/s)	V (cm/s)	M (cm^4/s^2)	B (cm^4/s^3)	F_d	L_M (cm)	h/L_M	Reynolds No	Figure
A43	5.61	5.0	63.0	83.5	5261.9	346.3	36.0	33.2	0.15	8185	
A44	5.61	8.0	63.0	83.5	5261.9	346.3	36.0	33.2	0.24	8185	
A45	6.50	6.5	63.0	83.5	5261.9	401.2	33.4	30.8	0.21	8185	4.1
A46	7.67	4.5	63.0	83.5	5261.9	473.2	30.8	28.4	0.16	8185	
A47	6.76	15.0	63.0	83.5	5261.9	417.0	32.8	30.3	0.50	8185	6.1(a)
A48	20.01	15.0	63.0	83.5	5261.9	1234.2	19.1	17.6	0.85	8185	
A61	4.66	5.2	31.5	41.8	1315.5	146.8	19.7	18.0	0.29	4093	
A62	5.16	3.5	31.5	41.8	1315.5	162.4	18.8	17.1	0.20	4093	
A63	8.50	3.5	37.8	50.1	1894.3	321.4	17.5	16.0	0.22	4911	
A64	9.33	2.7	37.8	50.1	1894.3	352.5	16.7	15.3	0.18	4911	
A65	5.37	5.5	63.0	83.5	5261.9	338.5	36.8	33.6	0.16	8185	
A66	8.50	3.3	37.8	50.1	1894.3	321.2	17.5	16.0	0.21	4911	
A67	8.18	3.0	34.7	45.9	1591.7	283.5	16.4	15.0	0.20	4502	

Table 3.4 Experimental conditions for fluid jets in linearly stratified ambient fluid

EXP#	$\rho_2 - \rho_j$ (kg/m^3)	h (cm)	Q (cm^3/s)	V (cm/s)	M (cm^4/s^2)	B (cm^4/s^3)	N (s^{-1})	F_d	h/L_M	L'_b (cm)	Figure
A1	6.7	5	63.0	83.5	5261.9	210.3	0.69	46.2	0.12	8.67	
A2	19.0	5	63.0	83.5	5261.9	960.9	0.75	21.6	0.25	13.10	
A3	25.0	5	63.0	83.5	5261.9	1407.7	0.78	17.8	0.30	14.39	
A8	9.4	10	63.0	83.5	5261.9	145.5	0.75	55.5	0.20	7.04	
A9	9.9	2	63.0	83.5	5261.9	408.4	0.76	33.1	0.07	9.74	
A10	25.7	2	63.0	83.5	5261.9	1400.1	0.72	17.9	0.12	15.52	
A11	25.7	10	63.0	83.5	5261.9	1207.4	0.73	19.3	0.56	14.67	
A12	27.8	10	31.5	41.8	1315.5	596.8	0.75	9.7	1.12	11.19	4.20
A13	11.8	10	31.5	41.8	1315.5	106.9	0.76	22.9	0.47	6.26	A.1 (a)
A14	8.3	3.5	31.5	41.8	1315.5	166.5	0.71	18.4	0.21	7.72	
A15	21.3	2	31.5	41.8	1315.5	623.1	0.58	9.5	0.23	14.76	
A16	26.2	2	31.5	41.8	1315.5	733.6	0.71	8.7	0.25	12.66	
A53	23.1	15	63.0	83.5	5261.9	1427.3	0.75	17.7	0.92	15.00	A.1 (b)
A54	22.0	15	63.0	83.5	5261.9	1357.4	0.72	18.2	0.89	15.40	

3.3.2 Particle-laden jets

A total of 30 experiments were conducted for particle-laden jets: 20 for a two-layer system and 8 for a linear stratification. In addition, 2 experiments were conducted in homogeneous ambient fluid to observe the difference between fluid jets and particle-laden jets in the absence of the effect of the ambient fluid condition in Chapter 6. The following is a summary of the experimental conditions and the individual details are given in Tables 3.5 and 3.6.

- Densimetric Froude number (F_d): 6.6 – 32.8
- Dimensionless density ratio (R): -18.2 - 0.63
- Total water depth (H): 34 cm
- Discharge height above the bed (h): 15 cm
- Distance to the pycnocline (h_i): 3.5 - 6.8 cm

3.4 Experimental procedures

3.4.1 Preparation

Prior to conducting the main experiments, all the individual instruments were carefully tested to avoid experimental errors due to instrumental instability. The jet fluid was prepared and a small amount of well-mixed fluid was released to remove the residual fluid and particles from the pipe prior to initiation of the experiment.

3.4.1.1 Stratification of ambient fluid

The reservoir tanks were filled with tap water and salt was added. The stirrer in the

reservoir tank was operated at 120 rpm, ensuring a complete mixing of ambient fluid. Two submersible heaters were set at room temperature. After ensuring the desired water temperature was reached, the fluid was gradually discharged through a pipe into the experimental tank.

The two-layer density stratified fluid was achieved by slowly releasing the upper reservoir fluid through a floating spreader placed on the top of the dense lower layer. The spreader floated freely on the water surface as the tank was being filled. The water temperature was maintained constant in order to avoid the double diffusive effects between two layers. This technique has been used by some researchers as an effective method to minimize turbulent mixing at the interface during filling (Maxworthy, 1973; Wong, 1984).

The filling rate is a critical factor in creating a sharp interface. Rapid filling can cause turbulent mixing at the density interface. On the other hand, slow filling rate ensures no turbulence but if the filling is too slow molecular diffusion becomes important. The interface thickness (ξ) can be estimated as (Fischer et al., 1979)

$$\xi = \sqrt{4\pi D t} \tag{3.1}$$

where D: molecular diffusion, m^2/s

$D = 1.39\,(1 + 0.029\,(\theta_T - 20)) \times 10^{-9}$ (Schmidt, 1997)

θ_T: water temperature, °C

t: time (s)

The filling time for the present experiment was set at 5 hours which was determined through preliminary tests. Using (3.1), the interface thickness increment due to molecular diffusion at 20 °C for 5 hours was estimated at 1.8 cm. After filling, the ambient fluid was allowed to stand for approximately 10 minutes to allow any turbulence to subside.

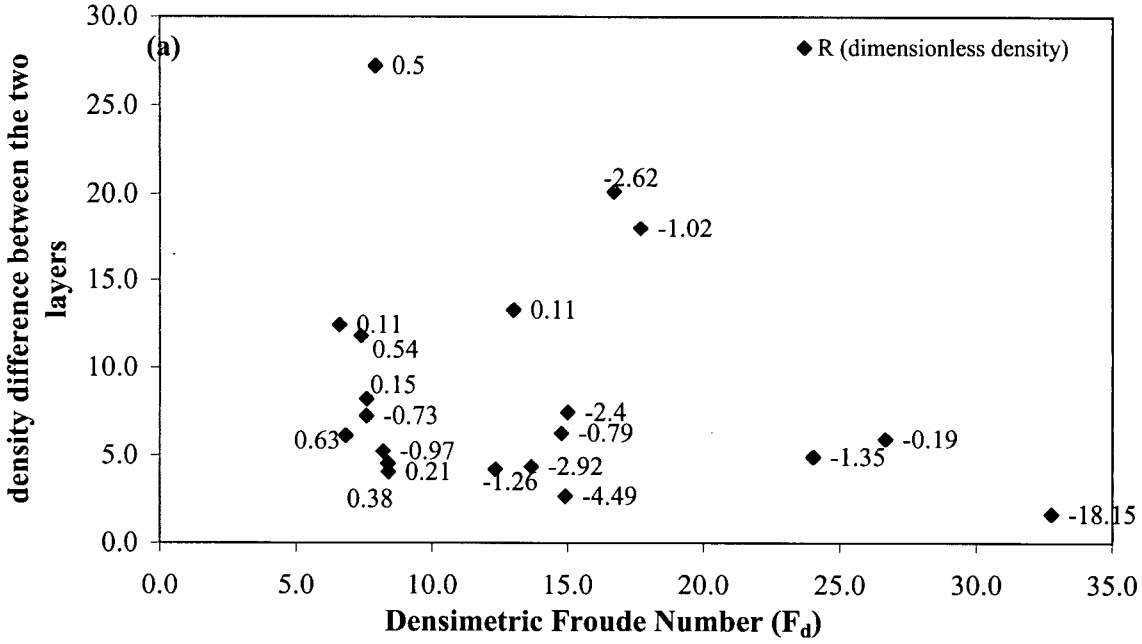

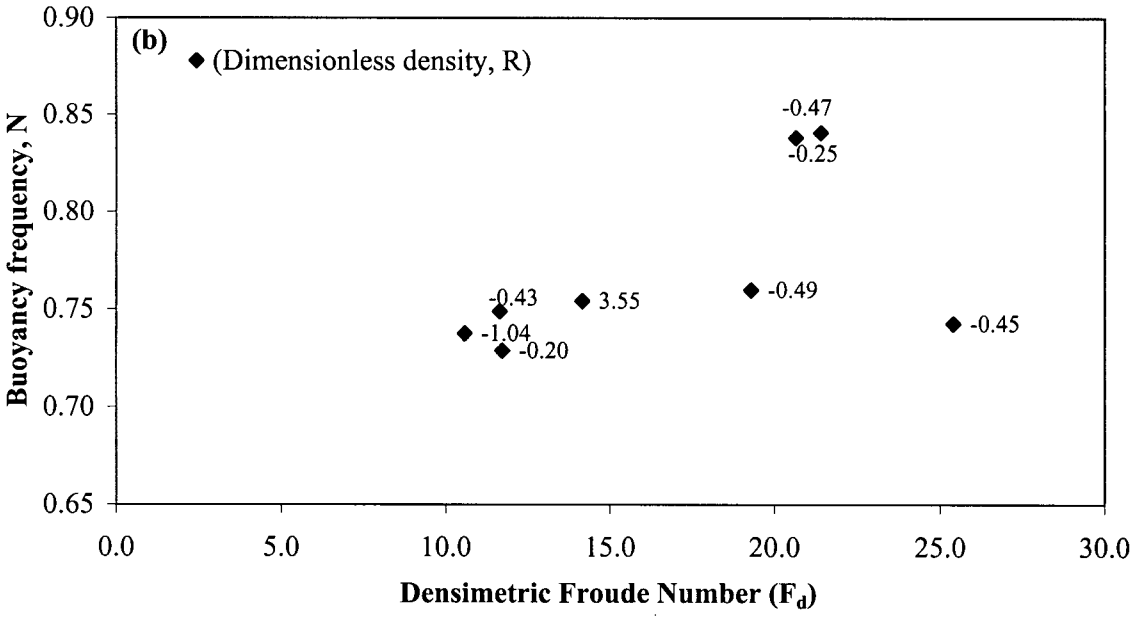

Figure 3.11 Experimental conditions of particle-laden jets (a) two-layer systems and (b) linearly stratified ambient fluids

Table 3.5 Experimental condition for particles-laden jets in two-layer systems

EXP#	$\rho_a-\rho_b$ (kg/m^3)	$\rho_2-\rho_1$ (kg/m^3)	h	h_i (cm)	Co	Q (cm^3/s)	M (cm^4/s^2)	B_b (cm^4/s^3)	B (cm^4/s^3)	F_d	L_M (cm)	R	Ψ	Flow Regime	Figure
P5	14.33	27.2	15	6.5	1.60	31.5	1315.5	436.3	893.0	7.9	7.3	0.50	0.33	I	
P6	-21.42	18.0	15	6.5	1.87	59.9	4748.8	-1207.4	1228.0	17.7	16.3	-1.02	0.48	WP	
P7	-122.78	1.6	15	6.5	1.89	63.0	5261.9	-6713.8	417.8	32.8	30.2	-18.15	1.30	SP	
P8	-9.54	4.9	15	6.5	1.55	47.3	2959.8	-434.7	327.4	24.0	22.2	-1.35	0.61	WP	
P9	-1.74	5.9	15	6.5	2.73	59.9	4748.8	-101.2	540.2	26.7	24.6	-0.19	0.67	WP	
P10	-61.43	20.1	15	6.5	2.59	59.9	4748.8	-3325.1	1375.0	16.7	15.4	-2.62	0.47	SP	
P16	-12.17	4.2	15	6.5	2.77	28.4	1065.5	-332.1	268.3	12.3	11.4	-1.26	0.62	WP	
P17	-28.34	4.3	15	6.5	2.97	31.5	1315.5	-845.2	300.1	13.7	12.6	-2.92	0.64	SP	
P18	-29.59	2.6	15	6.5	2.68	28.4	1065.5	-795.2	183.5	14.9	13.8	-4.49	0.70	SP	
P19	17.91	11.8	15	6.5	3.03	31.5	1315.5	545.6	1022.7	7.4	6.8	0.54	0.58	I	
P20	24.56	6.1	15	4.5	3.19	31.5	1315.5	749.6	1200.8	6.8	6.3	0.63	1.32	P	5.1(a)
P21	4.84	8.2	15	6.5	3.17	31.5	1315.5	146.0	970.4	7.6	7.0	0.15	0.70	I	
P22	-23.02	7.2	15	6.5	3.14	31.5	1315.5	-675.4	971.3	7.6	7.0	-0.73	0.76	WP	5.1(c), 5.4 (c)
P23	-77.00	7.4	15	6.5	3.17	63.0	5261.9	-4296.9	1988.6	15.0	13.9	-2.40	0.99	SP	5.1(d), 5.4 (d)
P24	4.91	13.3	15	6.5	3.01	63.0	5261.9	292.7	2647.2	13.0	12.0	0.11	0.79	I	5.1(b), 5.4(b)
P25	4.48	12.5	15	6.5	3.12	31.5	1315.5	133.6	1285.3	6.6	6.1	0.11	0.61	I	
P57	5.34	4.0	15	4.7	3.02	31.5	1315.5	161.8	793.4	8.4	7.8	0.21	1.37	P	5.3(a), 5.4(a)
P58	-26.25	5.2	15	6.5	3.15	31.5	1315.5	-770.9	833.6	8.2	7.6	-0.97	0.86	WP	5.3(b)
P59	9.83	4.5	15	3.5	3.06	31.5	1315.5	299.4	797.5	8.4	7.7	0.38	1.72	P	
P60	-18.92	6.3	15	6.8	3.38	53.6	3801.7	-952.8	1260.8	14.8	13.6	-0.79	0.87	WP	

Flow Regime: P: Penetration, I: Impingement, WP: Weak Plunging, SP: Strong Plunging

Table 3.6 Experimental condition for particles-laden jets in linearly stratified ambient fluids

EXP #	$\rho_a-\rho_b$ (kg/m^3)	R	Co	Q (cm^3/s)	V (cm/s)	M (cm^4/s^2)	B (cm^4/s^3)	F_d	L_N (cm)	$L_{b'}$ (cm)	L_M (cm)	N (s^{-1})
P1	3.68	0.28	1.469	37.8	50.1	1894.3	483.01	14.2	7.60	10.41	24.7	0.75
P2	-15.57	-0.96	1.888	31.5	41.8	1315.5	500.79	10.6	7.01	10.77	10.1	0.74
P3	-20.04	-2.20	1.391	56.7	75.2	4262.1	506.54	25.4	9.38	10.74	16.0	0.74
P4	-32.28	-2.04	1.742	56.7	75.2	4262.1	877.80	19.3	9.27	12.60	12.8	0.76
P11	-33.63	-2.12	2.221	63.0	83.5	5261.9	978.80	21.4	9.29	11.81	13.9	0.84
P12	-67.66	-3.98	2.959	63.0	83.5	5261.9	1051.13	20.7	9.30	12.13	9.9	0.84
P13	-31.05	-2.33	3.167	31.5	41.8	1315.5	413.06	11.6	6.96	9.95	7.2	0.75
P14	-67.06	-5.09	3.128	31.5	41.8	1315.5	407.52	11.7	7.05	10.17	5.0	0.73

Linear stratification was accomplished in a similar manner to the two-layer system. However, the left tank was filled with freshwater and right one with saline water. The dense saline water being discharged from the tank was constantly recharged by freshwater from the left tank by the hydraulic pressure gradient. The motor continuously mixed the freshwater and saline water vigorously. By this process, the density of mixed fluid linearly decreases as the tank fills.

3.4.1.2 Calibration of the PME probe and flow visualization

While the experimental tank was being filled, the conductivity probe was calibrated according to the procedure described in section 3.5.2. A Panasonic HS video camera was set up in front of the main tank to take flow images.

3.4.2 Measurement and sampling

Prior to jet discharge, some of the jet fluid was discarded through an assistant discharge pipe to remove residual fluid. After completing ambient fluid preparation, the density profile was taken with a calibrated conductivity-temperature probe. The experiments during discharge were implemented simply by turning on the jet pumping system and setting the flow control valve to obtain the required flow rate.

3.4.2.1 Fluid jet

The measurement locations were chosen based on the characteristics of jets obtained from preliminary observation. Measurement of the density profile was conducted at i) three points near jet discharge (x = 10, 20 and 30 cm from the jet nozzle), ii) transitional points (x = 45, 60 and 75 cm, and iii) locations considered relatively far from the discharge (x = 90, 105 and 120 cm). Conductivity profiles were taken prior to the discharge, during and after injection of the jet. Due to the constraints on the dimension of the main tank, the

profiles were obtained before the front of the spreading flow reached the other end of tank wall.

The traversing speed of the PME probe was set at 50 mm/s to obtain an instantaneous density profile. After each measurement, the trolley was quickly moved to the next location. The measurement time, position, conductivity and temperature voltage output were saved in a text file and loaded into a Matlab file for further analysis. Using the equations described in section 3.5.2, the readings were converted into parameters such as salinity and density.

3.4.2.2 Particle-laden jet

The density of interstitial fluid was estimated using a PME probe while the bulk density was measured using the DM5000 Anton-Paar. The samples of particle-laden jets were taken at four locations along the tank: x = 10, 30, 45 and 75 cm. To alleviate the loss of particles during the sampling procedure, the collected samples were rapidly transferred from the syringes into glass bottles manufactured for spectrophotometer use. Blank samples were also taken from the ambient fluid prior to the discharge. The samples were collected during discharge and the lids placed on immediately after filling and then dated and kept at room temperature for later analysis.

At x = 75, the samples were initially drawn by a pump sampler. The samples were taken directly into 15 mL mass cylinders through sampling tubes with 3 mm inner diameter. 10 samples were taken at a pump speed of 300 rpm, which was determined to be the optimum speed based on preliminary tests of different pumping speeds. It ensures no disturbance of the ambient fluid due to fast withdrawal and also prevents particles from settling in the tube due to slow sampling speed.

3.5 Data acquisition and processing

3.5.1 Data acquisition

3.5.1.1 Dye concentration measurement

The particle-laden samples were centrifuged until all particles completely settled to the bottom of the bottle. The complete separation of particles and interstitial fluid prevents the fine suspended particles from interfering with light penetration. The bottles were carefully placed in the spectrophotometer cell slot without disturbance. Since red Rhodamine G6 was used to color the interstitial fluid, the wavelength used was 520 nm, which absorbs red-pink.

3.5.1.2 Suspended particle concentration

After completing the dye concentration measurement, the samples were filtered using a vacuum filtering system through a glass fiber filter (G6). Figure 3.12 shows the vacuum filtering system. The filtered particle samples were dried at 103 – 105 °C for over an hour. Then the weight was measured using a four digit electric balance, Mettler AC 100, with accuracy of ± 0.0001g. The particle weight was calculated by subtracting the pre-measured precise filter weight from the total weight.

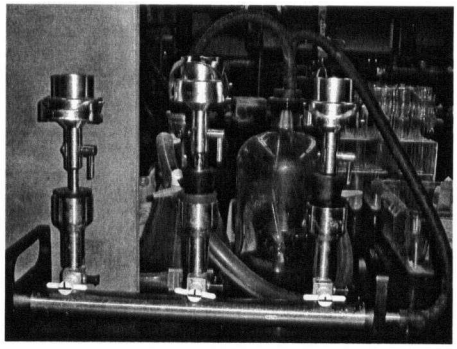

Figure 3.12 Vacuum filter system

3.5.1.3 Bulk density

The bulk density of particle-laden jet was measured using the Anton Parr DM5000 described in section 3.2.2. The bulk density of the particle-laden jets was rather difficult to measure with high accuracy and consistency because the measurement was highly sensitive to particle settling in the inner tube of the Anton-Paar. In particular, at high concentrations, the measured density difference was relatively large and thus 10 samples were taken from two location: the mixing tank and the discharge nozzle. Individual density was calculated and averaged.

3.5.1.4 Density profile

The density profiles of fluid jets and interstitial fluid of particle-laden jets were taken using a PME conductivity and temperature probe before and after discharge. Vertical and horizontal profiles were obtained. Other parameters were obtained by both visual measurement and the density profile analysis. The measurement parameters such as the final spreading layer thickness, the maximum rise height and the location were obtained by video images taken along the jet trajectory against a 5 cm grid on the tank wall. In each experiment, 20 video images were captured using a frame grabber and averaged. The flow images were obtained only before the head of flow reached the downstream wall. The experimental parameters and measurement methods employed are summarized in Table 3.7.

Table 3.7 Summary of experimental parameters and measurement techniques

Parameters	Measurement Technique
Density profile	Measurement of density profile using a PME micro-scale conductivity and temperature probe
Bulk density and interstitial fluid density of particle-laden fluid	Measurement of bulk density using Anton-Paar DMA 4500/5000 density meter and interstitial fluid density using PME probe

Maximum rise height (Z_m) and the location (X_m), impingement height above the pycnocline (P_d), spreading layer thickness(T_f) top and bottom of the spreading layer (Z_t, Z_b)	Flow visualization: video image capturing using a Panasonic video camera Density profile analysis
Dye concentration	Centrifuge the samples Measure the dye concentration using a MACH spectrophotometer
Suspended particles	Centrifuge samples and filtrate using a vacuum filtering system, Drying the filter and particles Measure the weight using a electric balance Mettler 100

The definition sketch of parameters is given in Figure 3.13. The symbols h_i, h_1, and h are the distance to the pycnocline, the upper layer thickness and discharge height above the bed respectively.

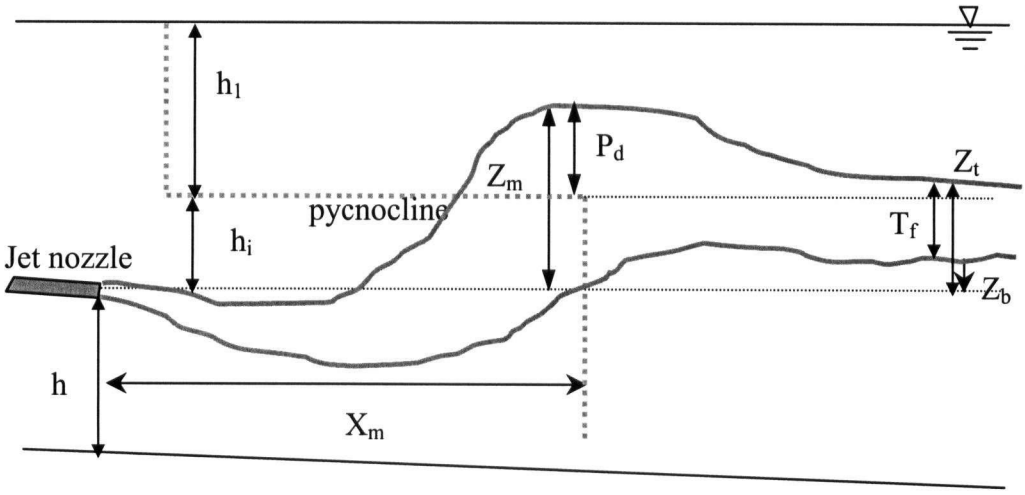

Figure 3.13 Definition sketch of parameters

3.5.2 Density data processing

3.5.2.1 Fluid density estimation

The density estimation procedure is divided into three stages: conversion of electrical voltage into conductivity and temperature, conductivity into salinity; and salinity/temperature into density. It is essential to obtain temperature and conductivity data simultaneously since conductivity significantly varies with temperature. The first step in the processing of density data is to extract the electric voltage output from a data file format. A simple calculation program was designed to estimate the density from the raw data file using the Matlab program.

The density of sodium chloride (NaCl) is a function of the NaCl concentration and solution temperature. The density of NaCl solution is estimated as the sum of fresh water density at temperature (T) and the concentration increase due to NaCl (ΔC_s) at that temperature. The equations Head (1983) suggested were used for the density calculation and the schematic procedure of density estimation is shown in Figure 3.14. The procedure is divided into two steps: calibration and data conversion from raw experimental data.

STEP I

Conductivity probe calibration consists of three stages: gain set-up, calibration data acquisition and numerical analysis. From measured conductivity and temperature base electrical voltages (V_{Coff} and V_{Toff}), the circuit gain G is determined using the following equations.

$$V_o(\sigma_{ref}) = G \cdot \sigma_{ref} + V_{coff} \tag{3.2}$$

$$\ln(V(T) - V_{Toff}) = K + J/T \tag{3.3}$$

where K and J are constants that can be obtained with two reference temperature data points. These coefficients are case-specific and have to be determined for each experiment.

STEP II

Once G, V_{Toff} and V_{Coff} are determined, the probe can be used to measure the electrical conductivity and temperature of solutions. The density calculation from temperature-compensated conductivity and temperature consists of two processes: pure water density calculation at temperature T and the computation of increased density due to sodium chloride (NaCl).

$$\rho = \rho_T + \Delta\rho_s \tag{3.4}$$

where ρ : density (kg/m^3)

ρ_T : water density as a function of temperature (kg/m^3)

$\Delta\rho_s$: density increment due to NaCl

The density of pure water (ρ_T) as a function of temperature can be computed to within 0.1% (1 kg/m^3) using (Head, 1983):

$$\begin{aligned}\rho_T = \{ & 0.9998395 + (6.7914 \cdot 10^{-5} \times T) \\ & + (-9.0894 \cdot 10^{-6} \times T^2) + (1.0171 \cdot 10^{-7} \times T^3) \\ & + (-1.2816 \cdot 10^{-9} \times T^4) + (1.1592 \cdot 10^{-11} \times T^5) \\ & + (-5.0125 \cdot 10^{-14} \times T^6) \} / 0.001\end{aligned} \tag{3.5}$$

The measured conductivity value requires a temperature compensation process based on the reference temperature. The temperature compensation equation for NaCl in water is given as:

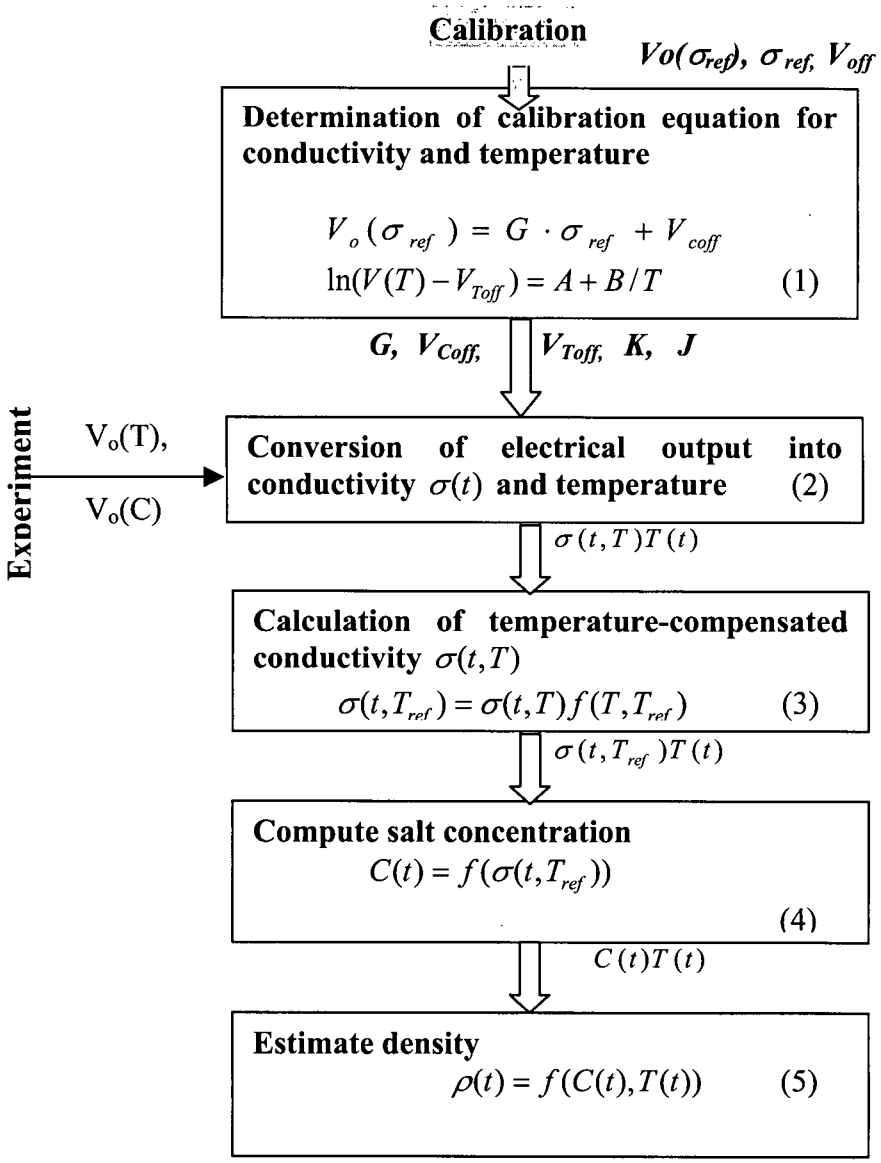

Figure 3.14 Calculation procedure of fluid density (After Head, 1983)

$$C_{25} = C_T/(1+(0.0191\times(T-25)) \tag{3.6}$$

where C_{25} and C_T are conductivity at 25 °C and temperature T, respectively. The salinity (wt %) at 25 °C is obtained by

$$\begin{aligned} \text{Salinity}(\%) \;=\; & 0.01498478 + (-0.01458078\times C_{25}^{1/2}) \\ & + (0.05185288\times C_{25}) + (0.00206994\times C_{25}^{3/2}) \\ & + (-0.00010365\times C_{25}^{2}) + (0.00006269\times C_{25}^{5/2}) \end{aligned} \tag{3.7}$$

This equation is valid for seawater but it can also be used for NaCl solution with standard deviation of 0.02% (Head, 1983). Density increment ($\Delta\rho_s$) due to sodium chloride is estimated as:

$$\begin{aligned} \Delta\rho_s = & (45.5655\times M_o) + (-0.2341\times M_o\times T) + (3.4128\cdot 10^{-3}\times M_o\times T^2) \\ & + (-2.7030\cdot 10^{-5}\times M_o\times T^3) + (1.4037\cdot 10^{-7}\times M_o\times T^4) + (-1.8527\times T^{1.5}) \\ & + (5.3956\cdot 10^{-2}\times M_o^{1.5}\times T) + (-6.2635\cdot 10^{-4}\times M_o^{1.5}\times T^2) + (-1.6368\times M_o^2) \\ & + (-9.5653\cdot 10^{-4}\times M_o^2\times T) + (5.2829\cdot 10^{-5}\times M_o^2\times T^2) + (0.2274\times M_o^{2.5}) \end{aligned} \tag{3.8}$$

M_o is the molar concentration calculated from estimated conductivity at 25 °C. Calculation of molar concentration (M_o) for NaCl in water is given (Head, 1983) as:

$$\text{Molar concentration } (M_o) = \frac{\dfrac{\text{Salinity}(\%)}{(100-\text{Salinity}(\%))}}{0.058443} \tag{3.9}$$

This equation is valid for the temperature range 0 to 50 °C and salinity 0 to saturation (Head, 1983).

Chapter 4

Results and Discussion: Fluid Jets

4.1 Introduction

To conduct wastewater discharge into receiving water in an effective and environmentally-safe manner it is essential to understand the behavior of buoyant fluid jets under various discharge schemes and ambient fluid conditions. Understanding the dynamics of buoyant fluid jets also provides a basis to interpret the behavior of particle-laden jets.

Buoyant fluid jets discharged at 3^{o} downward orientation were examined i) to identify the important factors affecting the flow dynamics under various source conditions, ii) to understand the effect of the ambient fluid condition and, in particular, the presence of the pycnocline and iii) to identify discharge conditions preventing buoyant jet fluids from penetrating into the upper layer in two-layer systems.

4.2 Buoyant jet in a two-layer system

This section presents the experimental results and dimensional analysis of buoyant jets discharged into in two-layer systems. The general behavior of buoyant jets is described and important flow regimes are determined. Backflow occurrence and Coanda bottom attachment are investigated. The gross flow characteristics of buoyant jets such as maximum rise height and spreading layer thickness are analyzed using dimensional analysis and compared with the experimental results.

4.2.1 Behavior of buoyant jets

Three flow regimes were observed for buoyant fluid jets: weak impingement, strong impingement and penetration as illustrated in Figure 4.1. The behavior of buoyant jets was obtained from flow visualization, and the density and dye concentration profiles. Detailed characteristics of these flow regimes and analysis of their behavior are given in the following sections.

4.2.1.1 Weak impingement

As a buoyant jet rises and approaches the pycnocline, a density step across the pycnocline suppresses the vertical momentum of the jet. As a result, the rising buoyant jet bends immediately after impingement and spreads laterally and horizontally in the lower layer (Figure 4.1(a)). The buoyant jet does not cause mixing in the upper layer due to substantial reduction in the vertical mixing and the density fluctuation at the pycnocline is also small. Figure 4.2 shows a set of typical density profiles of a buoyant jet, showing the weak impingement. The density profiles were taken from five downstream locations along the jet trajectory. In this case, the buoyant jet actively rises and impinges on the pycnocline at approximately $x/L = 0.12 - 0.19$. Here, x and L are the downstream distance and the length of the experimental tank respectively. The jet stopped rising at $x/L = 0.25$, at which point a horizontal spreading layer formed.

4.2.1.2 Strong impingement

When the density of a jet flow impinging on the pycnocline is slightly smaller or similar to that of the upper layer, the jet may overshoot across the density step into the upper layer. However, the jet falls back to its neutral buoyancy level immediately and proceeds horizontally (Figure 4.1(b)). The thickness of the spreading layer grows rapidly until the jet

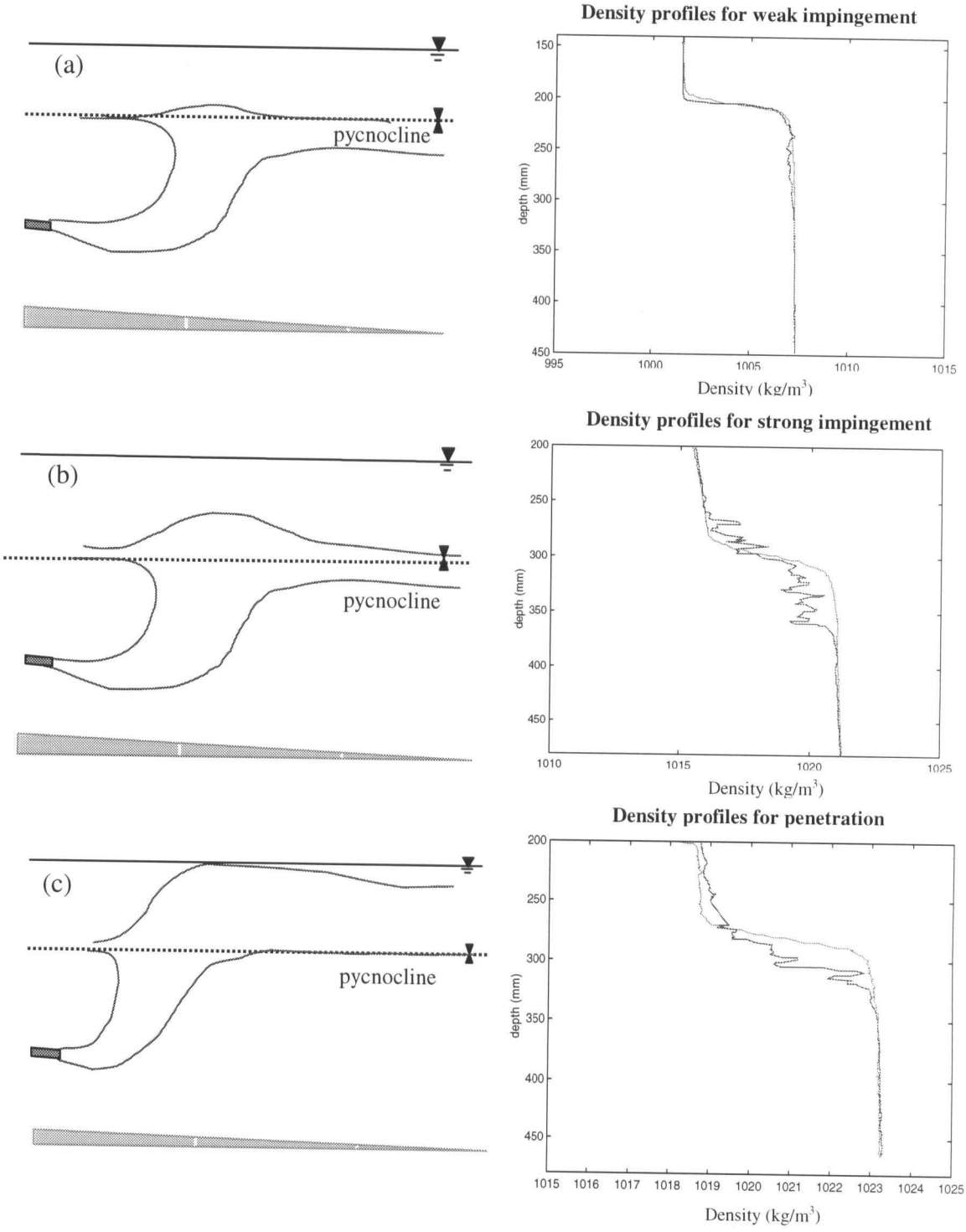

Figure 4.1 Sketches of behavior of buoyant jets and density profiles in two-layer systems: (a) weak impingement (A19) (b) strong impingement (A71) and (c) penetration (A70), (----) : density profile before discharge, (—): after discharge

reaches the maximum rise height and then it reduces as the jet propagates as a gravity current. The density profiles before and after discharge at $x/L = 0.31$ clearly indicates that strong impingement of a jet flow causes permanent mixing in a considerable depth of the upper layer and significantly increases the density of the upper layer. However, the density at surface does not change. This is a distinctive difference between weak and strong impingement. Figure 4.3 (a)(b) are photographs showing examples of weak and strong impingement respectively of buoyant jets on the pycnocline.

4.2.1.3 Penetration

If a highly buoyant jet is injected under a small density step or the density of a jet impinging on the pycnocline is significantly smaller than that of the upper layer, the jet can penetrate into the upper layer as illustrated in Figure 4.1 (c). Once a jet penetrated the pycnocline, it spreads above the pycnocline. The density profiles of a penetrating buoyant jet into the upper layer indicates that the pycnocline became eroded and the upper layer was disturbed significantly by the penetration of the jet flow. The density significantly increased in the entire upper layer, implying that a considerable amount of the lower layer fluid was transferred into the upper layer through entrainment and penetration. Since jet fluid is always lighter than the ambient fluid in the lower layer, the density increase in the upper layer is due only to the entrainment of the lower layer. Figure 4.4 are photographs showing the process of buoyant jet penetration and spreading in the upper layer. As the jet reaches the water surface, lateral spreading increases greatly and then it forms a horizontal spreading layer.

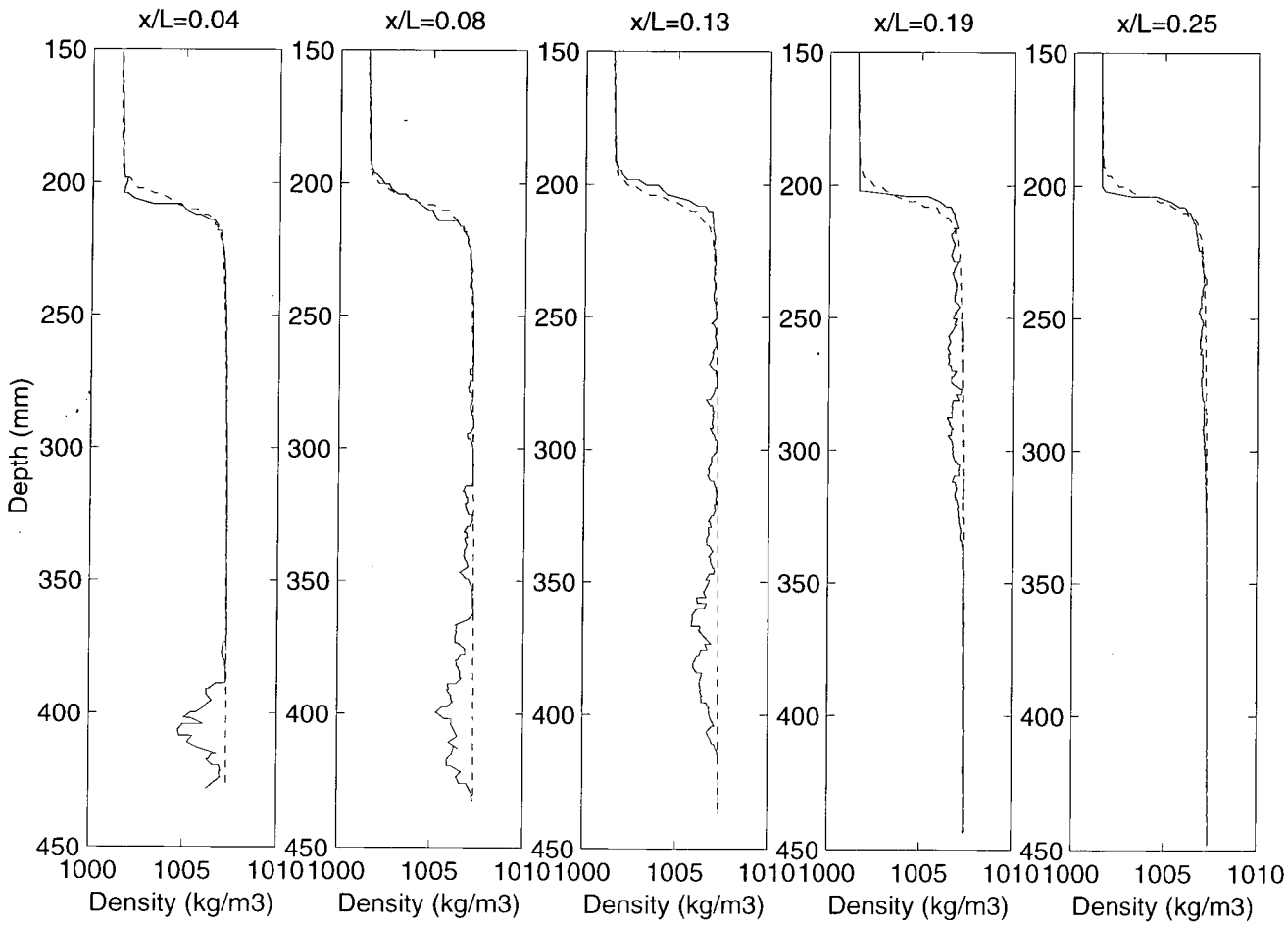

Figure 4.2 Density profiles before (----) and after (—) a buoyant jet discharge along the tank for weak impingement (A19)

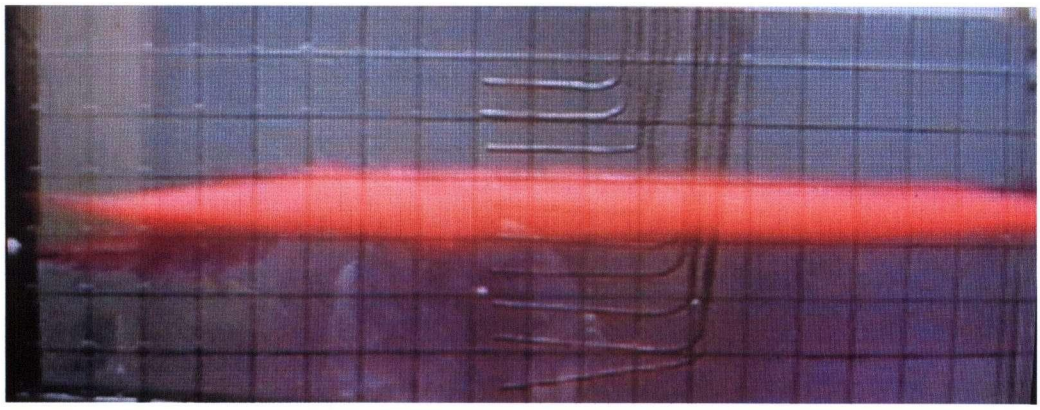

(a) Weak impingement

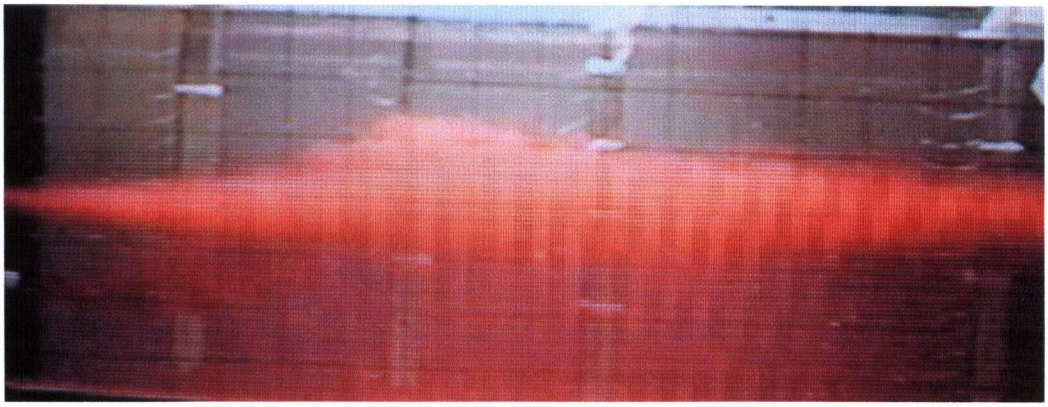

(b) Strong impingement

Figure 4.3 Impingement of buoyant jets in two-layer systems: (a) weak impingement (A37) and (b) strong impingement (A51)

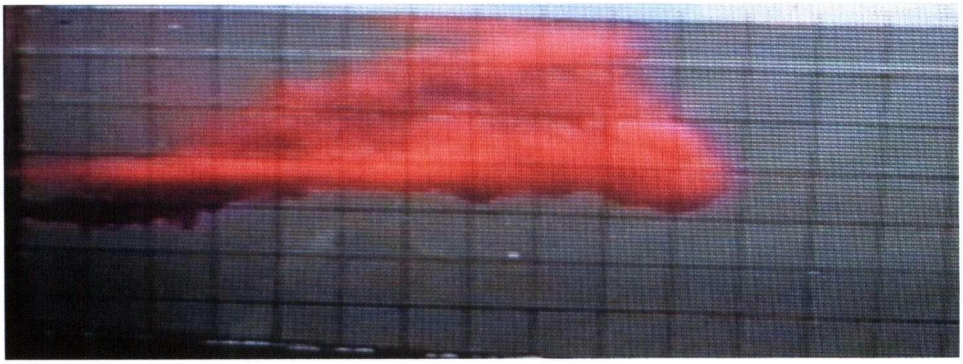

(a) t=36 second

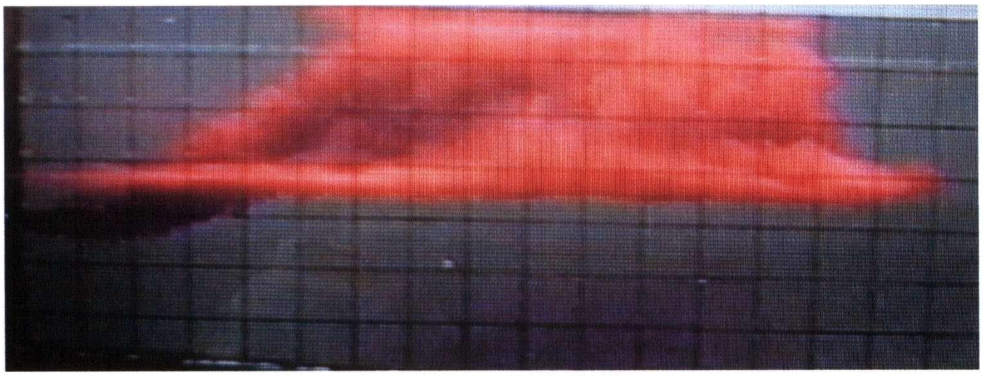

(b) t=65 second

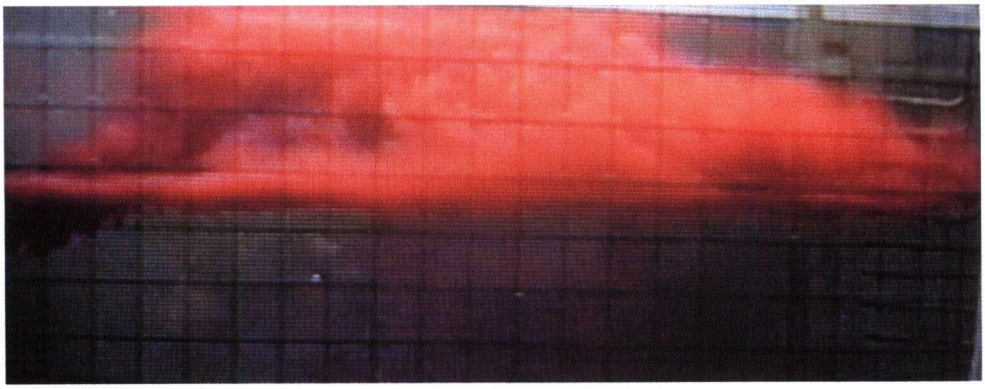

(c) t= 69 second

Figure 4.4 Process of a buoyant jet penetration in two-layer system: (a) penetration (b) lateral-horizontal spreading and (c) horizontal spreading

4.2.2 Determination of flow regimes

4.2.2.1 Penetration/impingement parameter, Ψ

The direction of source momentum of a buoyant jet is fixed at 3° downward in this study. Thus a buoyant jet spreads out predominantly in the source momentum direction and it constantly entrains heavy ambient fluid (ρ_2). This results in density increase in jet flow before it bends and rises to the pycnocline as illustrated in Figure 4.5. If there is sufficient dilution the density of the jet will approach ρ_2 as it rises to the pycnocline. However, the density is always less than the lower layer fluid and the jet rises above the pycnocline.

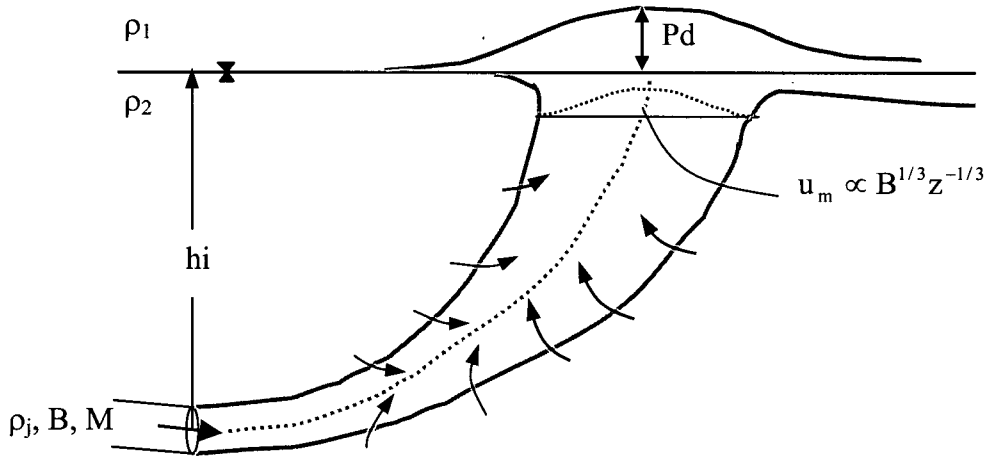

Figure 4.5 A buoyant jet in two-layer system

Since the direct effect of source momentum on the jet at the pycnocline is insignificant, a buoyant jet can be approximated as a plume. The rising distance of a jet above the pycnocline, P_d depends on the relative strength of vertical velocity of the plume when it impinges on the pycnocline and the strength of the density step.

The balance between kinetic energy and potential energy in the impingement region yields:

$$P_d \sim \frac{u_m^2}{\frac{\rho_j - \rho_1}{\rho_2} g} \tag{4.1}$$

If there is sufficient dilution in the jet as it rises towards the pycnocline, then $\rho_j \to \rho_2$. For the purposes of the derivation of the most relevant dimensionless this problem, assume $\rho_j = \rho_2$ at the point of impingement so that:

$$P_d \sim \frac{u_m^2}{g_a'} \tag{4.2}$$

$$\text{where} \quad g_a' = \frac{\rho_2 - \rho_1}{\rho_2} g$$

The time-averaged vertical velocity on the axis of the plume is given as a function of the buoyancy flux and the vertical distance (Fischer et al., 1979):

$$u_m \propto (B/z)^{1/3} \tag{4.3}$$

Therefore the ratio of the rise height above the pycnocline (P_d) to the discharge distance (h_i) can be rewritten using eq(4.3) as

$$\frac{P_d}{h_i} \approx \frac{B^{2/5}}{g_a'^{3/5} h_i} \tag{4.4}$$

Subsequently, the ratio can be defined as a dimensionless parameter (Ψ):

$$\Psi = \frac{B^{2/5}}{g_a'^{3/5} h_i} \tag{4.5}$$

Ψ is a measure of the ratio of the strength of the plume as it impinges on the pycnocline to the resistance offered by the density step. Given the assumptions presented above the impingement height P_d should increase linearly with increasing Ψ.

Baines (1975) presented a similar result for a negatively buoyant plume impinges on a density interface but does not penetrate it. He expressed his results in terms of a Froude number F_r, which has the same general form as Ψ. In fact, if the centerline velocity $u_m = 4.7(B/z)^{1/3}$, see Fischer (1979), then $\Psi = (F_r/4.7)^{6/5}$. Kumagai (1984) also conducted a similar experiments and theoretical investigation on impingement of pure plumes on the density interface. However, these studies are different from the present study in that this study is associated with 3° downward directed turbulent jets which cause significant entrainment of the ambient fluid while the previous studies dealt with pure plumes without source momentum. Also, the previous studies covered only impingement cases whereas the present study concerned with both impingement and penetration.

Figure 4.6 shows the dimensionless impingement height (P_d / h_i) versus Ψ, where P_d is the impingement height above the pycnocline. The flow became trapped under the pycnocline when $\Psi < 0.5$, which covered the weak impingement regime. The impingement height above the pycnocline (P_d) was less than $0.3h_i$ from 14 measurements. Penetration occurred when $\Psi > 0.9$ and the strong impingement regime covered $0.5 < \Psi < 0.9$.

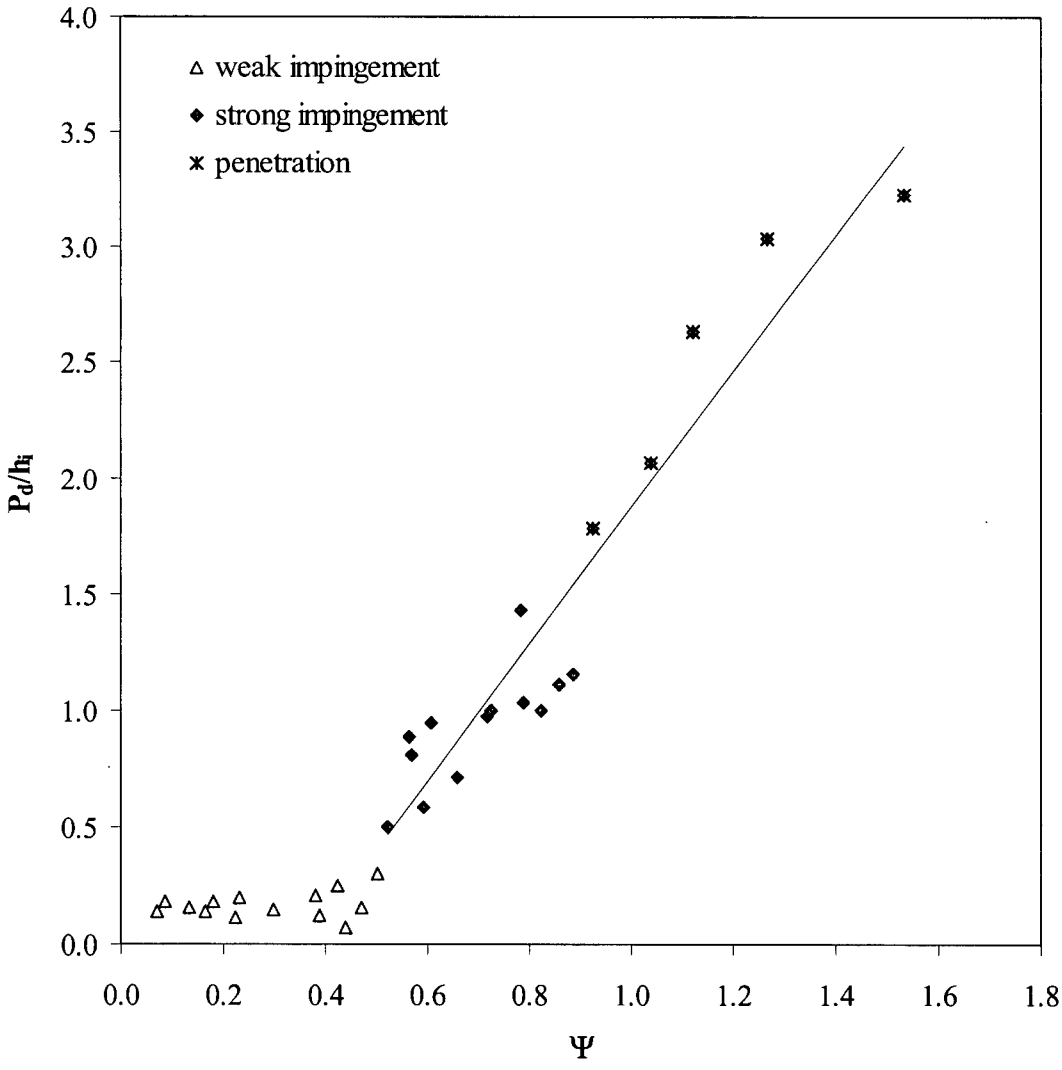

Figure 4.6 Flow regimes of buoyant jets in two-layer systems

4.2.2.2 Density Relation

To understand under what circumstances a buoyant jet impinges or penetrates the pycnocline, the relationship between the density of a jet when it reaches the pycnocline and that of the lower and upper layer is considered. The density ratio γ can be defined as:

$$\gamma = \frac{\rho_1 - \rho_i}{\rho_2 - \rho_i} \tag{4.6}$$

where ρ_i, ρ_1 and ρ_2 are the density of a jet flow at the pycnocline and the density of the upper and lower layers respectively. If $\gamma = 1$, the ambient fluid is homogeneous, while $\gamma > 1$ indicates that the ambient fluid is statically unstable since the upper layer is heavier than the lower layer. For a stable two-layer stratified fluid the lower layer density is always greater than that of the upper layer ($\rho_2 > \rho_1$). As a buoyant jet ascends it entrains heavy ambient fluid, however the density of the lower layer (ρ_2) is always larger than that at the density step ρ_i ($\rho_2 - \rho_i > 0$). Consequently, a jet can penetrate into the upper layer only if $\rho_1 - \rho_i > 0$, that is:

$$0 < \gamma < 1 \tag{4.7}$$

However, if $\rho_1 - \rho_i < 0$, a submerged jet does not penetrate but becomes trapped at the pycnocline. As the jet rises, it slightly impinges on the density step due to the weak vertical momentum resulting from buoyancy. The weak impingement occurs if:

$$\gamma < 0 \tag{4.8}$$

On the other hand, if $\rho_1 \approx \rho_i$, a jet flow impinges on the pycnocline with varying strength depending on the density difference with the lower layer, $\rho_2 - \rho_i$. If $\rho_2 \geq \rho_i$ impingement can occur only weakly since the jet does not obtain sufficient vertical

momentum from the lower layer. However, if $\rho_2 >> \rho_i$, a strong impingement may occur due to the strong vertical driving force generated by the large density difference even for $\rho_1 \leq \rho_i$ although penetration does not occur. Therefore, if strong impingement regime satisfies

$$\gamma \approx 0 \tag{4.9}$$

However, the definition of strong impingement is rather vague and thus this regime can be supplemented quantitatively with experimental data in section 4.2.2.1. Figure 4.7 presents the estimated dimensionless density ratio γ showing that the defined regimes agree with the experimental data. Density at the pycnocline ρ_i was estimated using CORMIX1.

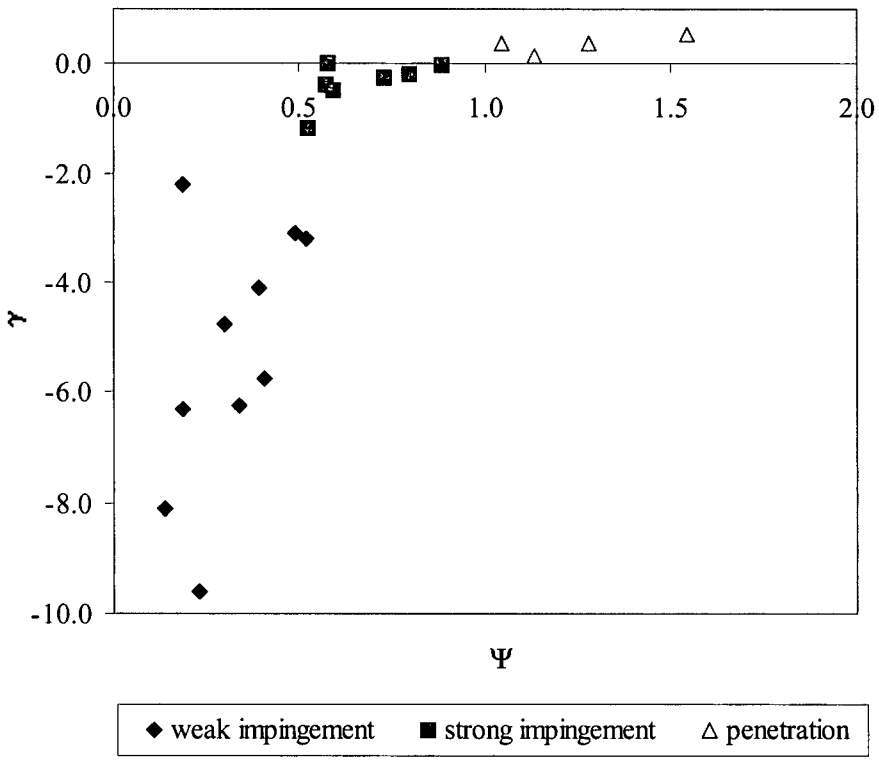

Figure 4.7 Dimensionless density (γ) of buoyant jets in two-layer systems

4.2.2.3 Comparison of flow regimes with prediction of CORMIX1

CORMIX1 v3.2 was run to compare with the flow regimes defined in this study. All submerged buoyant jets tested were predicted to be Class H4-0 except for the Coanda bottom attachment condition. When this type of flow is discharged into the stagnant ambient fluid, the weakly bent buoyant jet impinges on the pycnocline and spreads radially (Jirka et al, 1996).

CORMIX1 does not explicitly distinguish between impingement and penetration as different flow classes but it recognizes the density step as an internal boundary. The model determines whether (a) the flow penetrates to water surface or (b) bends and propagates under the density step by the following relations: (a) $Z_t + h \geq H_s$ and (b) $Z_t + h \leq H_s$, where Z_t and h are the vertical height of rise relative to the discharge elevation and the discharge height above the bottom respectively. H_s is a finite layer depth which can be either total water depth or discharge height to the pynocline depending on the strength of the density step (Jirka and Doneker, 1991).

When the density step is influential, only lower layer depth is important. Thus, $H_s = h_i + h$, where h_i is the distance to the pycnocline from discharge level. As the top of the spreading layer approaches the boundary, $Z_t \leq h_i$, the flow is trapped under the pycnocline and if $Z_t \geq h_i$, the jet rises to the water surface.

Experiments showed that when $Z_t - h_i < 1.5$ weak impingement occurred along the pycnocline and if $Z_t - h_i > 5.5$ the flow rose to the surface regardless of the presence of the pycnocline. The model agreed with the defined flow regimes in the present study except for a strong impingement case (A51). In this exceptional case $Z_t - h_i = 5.9$ and thus the model predicted the jet to penetrate to the upper layer. This discrepancy may have occurred because the model underestimates the influence of the small density step. Once the model

determines the effect of the density step to be negligible, it regards the ambient fluid as homogeneous with average density of the upper and the lower layer, thus allowing a buoyant jet to rise to the top of the upper layer.

4.2.3 Backflow

The prevention of discharge flows back to the intakes is one of the principal design factors in many industrial applications. A backflow, an upstream intrusion, is formed when a rising buoyant jet encounters a horizontal pressure gradient. It is necessary to distinguish between a backflow and a return flow for a small scale laboratory experiments, where the limited basin length may affect flow pattern. A return flow forms when a discharged jet pushes the fluid ahead toward the end-wall in the tank resulting in reversing the direction at the end wall (Darden et al., 1972).

For all experimental conditions, backflows occurred when buoyant jets approached the density step. However, there was a great deal of variation in the thickness and location of the backflow. Some of the backflows emerged along the pycnocline immediately near the jet nozzle while some formed far downstream and exerted little impact on the discharge area. Hereafter, the former is termed as *backflow* and the latter defined as *no-backflow.* Figure 4.8 shows photographs of both backflow and no-backflow.

To identify the condition of backflow generation, the horizontal momentum, m_h and vertical momentum, m_v of a buoyant jet are considered. The horizontal momentum of a jet is constant at any cross-section, i.e. $m_h = M\cos\theta$, where M is the source momentum flux. For a small discharge angle $m_h = M$ since $\cos\theta \approx 1$.

The momentum of a vertically oriented jet can be approximated by the vertical momentum of a plume:

$$m_v = b_2\, B^{2/3} z^{4/3} \tag{4.10}$$

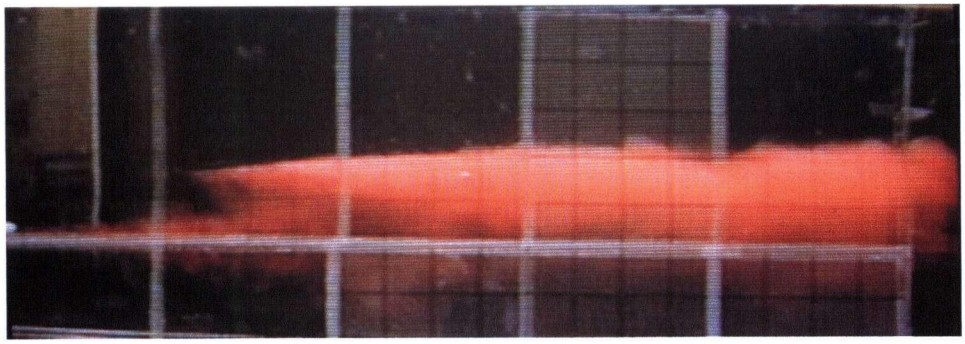

(a) No-backflow

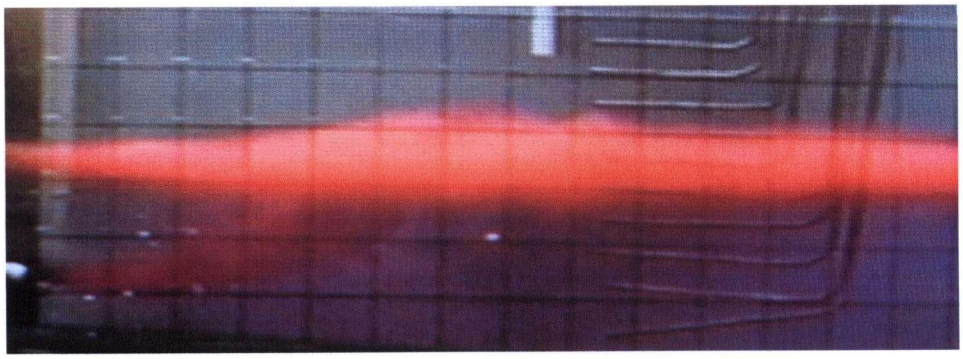

(b) Backflow

Figure 4.8 Backflows in two-layer systems: (a) no-backflow (A24, $\Psi = 0.34, F_d = 30.1$**) and (b) backflow (A40,** $\Psi = 0.52, F_d = 8.9$**)**

where b_2 is an experimental coefficient to be 0.35 for a round plume (Fischer et al., 1979). The vertical momentum flux at the pycnocline is $m_v = b_2 B^{2/3} h_i^{4/3}$, where h_i is the distance to the pycnocline from a jet nozzle. A sketch of a buoyant jet forming a backflow is shown in Figure 4.9.

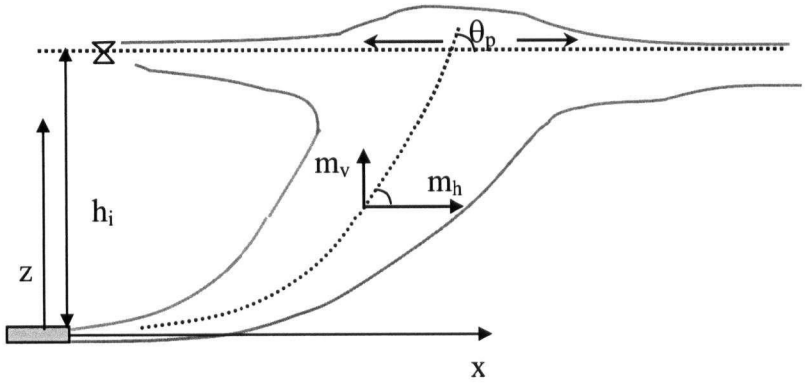

Figure 4.9 Development of a backflow at the pycnocline

A buoyant jet approaches the pycnocline at the angle θ_P, which is determined by the relative magnitude of two momentum i.e. $\tan\theta_p = \frac{m_v}{m_h}$. If the horizontal momentum is larger than the vertical momentum, the angle becomes small and thus the jet spreads horizontally without forming a backflow. However, if the relative strength of vertical momentum to the horizontal momentum is large, then a backflow forms as a jet reaches the pycnocline. The relative momentum is given as:

$$\frac{m_v}{m_h} = \frac{0.35\, B^{2/3} h_i^{4/3}}{M} \tag{4.11}$$

Eq. (4.11) can be rewritten using a characteristic length scale $\ell_M = M^{3/4} / B^{1/2}$:

$$\frac{m_v}{m_h} = 0.35\left(\frac{h_i}{\ell_M}\right)^{4/3} \tag{4.12}$$

Consequently, the jet angle at the pycnocline becomes functions of the distance to the pycnocline, h_i and the characteristic length scale ℓ_M :

$$\theta_p = \tan^{-1}\left[0.35\left(\frac{h_i}{\ell_M}\right)^{4/3}\right] \tag{4.13}$$

The results are likely to be relevant to small angles of discharge flow since but overall nature of jets are the same as horizontal jets although small angle difference can cause jets to rise to the pycnocline at different locations.

Backflow occurred when the estimated $\theta_p > 7^\circ$ but no backflow occurred when $\theta_p < 7^\circ$. This result was confirmed by experiments as shown in Figure 4.10. Occurrence of backflows was plotted against ℓ_M / h_i and impingement/penetration parameter Ψ. It is shown that as the relative strength of the source momentum to the vertical momentum (ℓ_M / h_i) increases, the possibility of backflow formation at the pycnocline decreases. On the other hand, for the penetration regime, $\Psi > 0.9$, some jet flow accumulated along the pycnocline with varying degrees while the jet penetrated into the upper layer and a thick backflow formed at the water surface.

4.2.4 Coanda bottom attachment

When a jet is discharged parallel to the bottom bed, the jet clings more abruptly to the boundary due to the increased entrainment demand. Rising of a buoyant jet is delayed which causes a jet to entrain the more heavy ambient fluid. Thus, the jet trajectory and dilution can be significantly affected. Figure 4.11 shows the Coanda bottom attachment of a

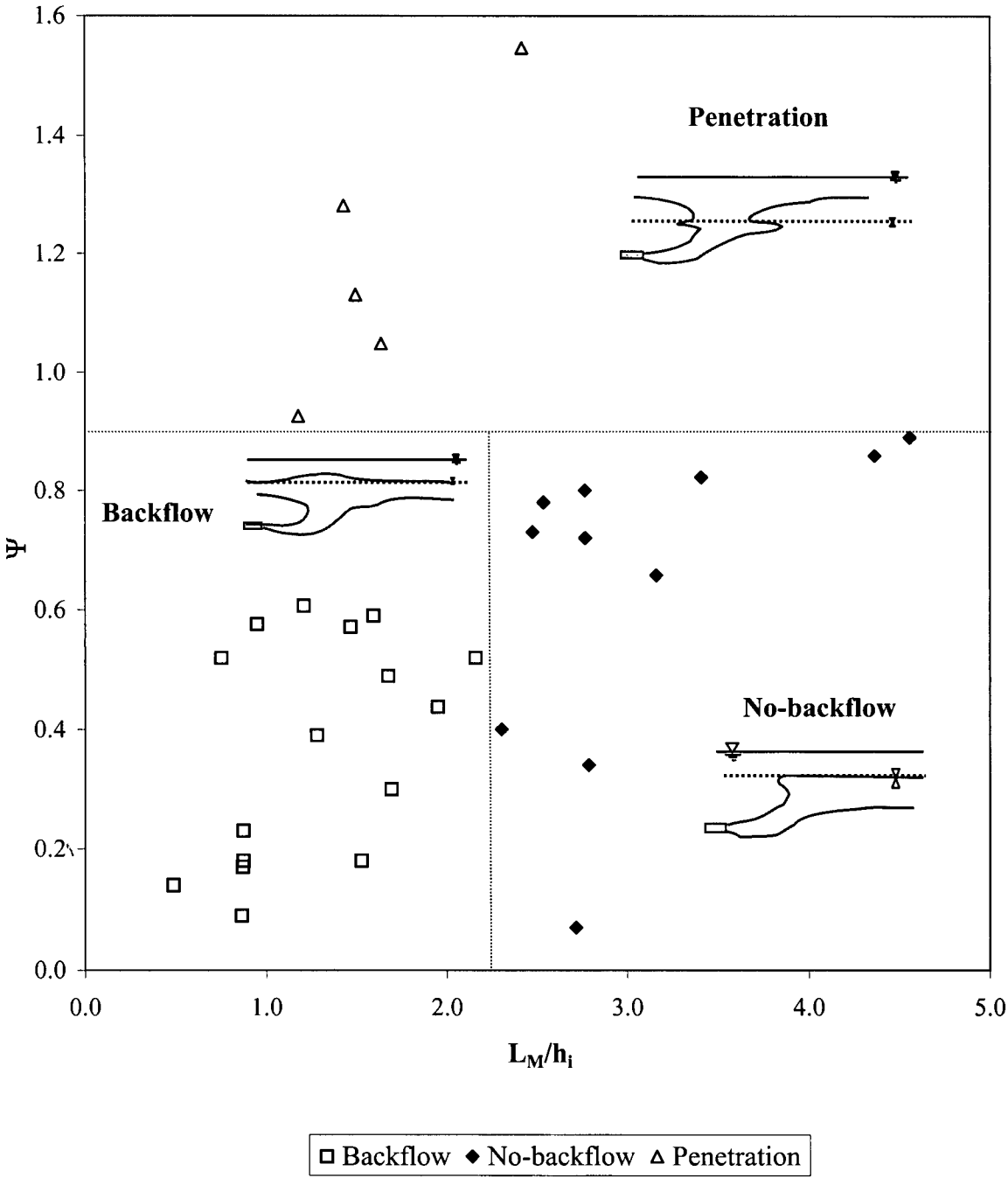

Figure 4.10 Backflows of fluid jets in two-layer system

buoyant jet in a homogeneous ambient fluid. After an extended bottom attachment, a buoyant jet lifts off from the bed and rises to its neutral buoyancy level.

The Coanda bottom attachment of buoyant jets discharged at 3° downward was tested for different ambient fluid conditions: homogeneous, linearly stratified fluid and two-layer system. However, the majority of the experiments were conducted for homogeneous ambient fluid for the purpose of comparison with past studies. The experimental conditions employed for the Coanda attachment were $0.065 < h/\ell_M < 2.1$ and $8.7 < F_d < 55.5$.

The results showed that the bottom attachment occurred when the submergence parameter satisfied $h/\ell_M < 0.22$, regardless of the ambient conditions shown in Figure 4.12. This is because the source discharge condition and geometry are influential on the jet development in the vicinity of the jet exit whereas the ambient fluid condition plays an important role far downstream.

4.2.4.1 Comparison with previous studies

As illustrated in Figure 3.2, the discharge direction of the buoyant jet was parallel to the bottom bed but at a 3° downward direction relative to the ambient fluid. The Coanda bottom attachment occurred when $h/\ell_M < 0.22$, which is considerably larger than the value of 0.1 observed in two previous experiments for horizontal jets by Sobey et al. (1988) and Johnston et al. (1994), shown in Figure 4.13.

This difference is probably due to the different range of densimetric Froude numbers used. The range of F_d tested here was 8.7 – 55.5 where most of cases were $F_d > 15.0$ whereas Sobey et al. (1988) and Johnston et al. (1994a) performed experiments for $F_d < 16.0$. The definition of bottom attachment may also have caused the difference in results. The previous two studies defined attachment based on the measured density deficit after discharge whereas the present study used the flow visualization. Consequently, the former obtained relatively conservative results.

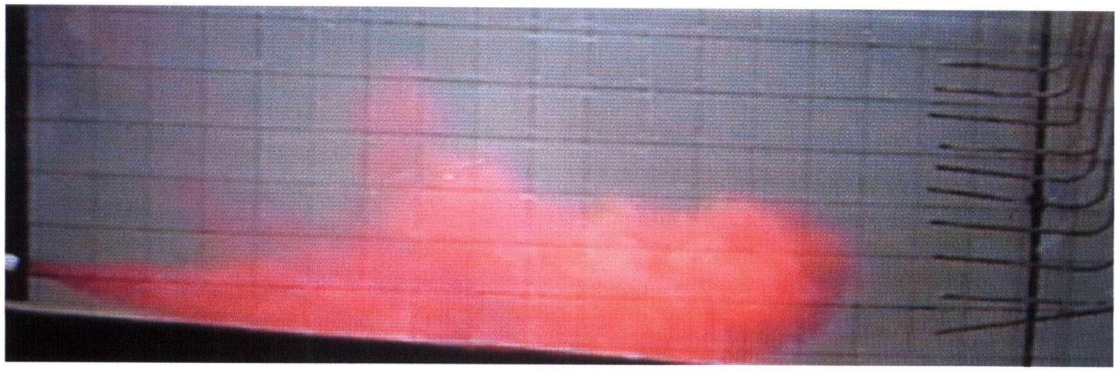

(a) Coanda bottom attachment

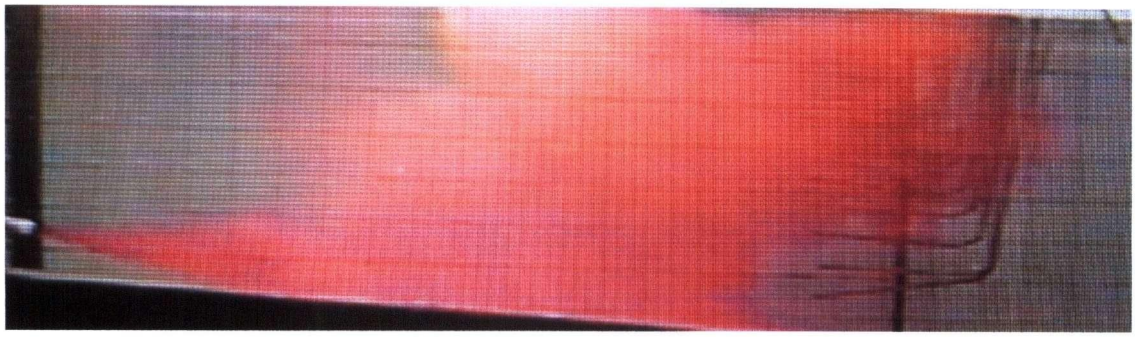

(b) Coanda bottom attachment and lift-off

Figure 4.11 Coanda bottom attachment (A45, $F_d = 33.4$, $h/\ell_M = 0.21$**)**

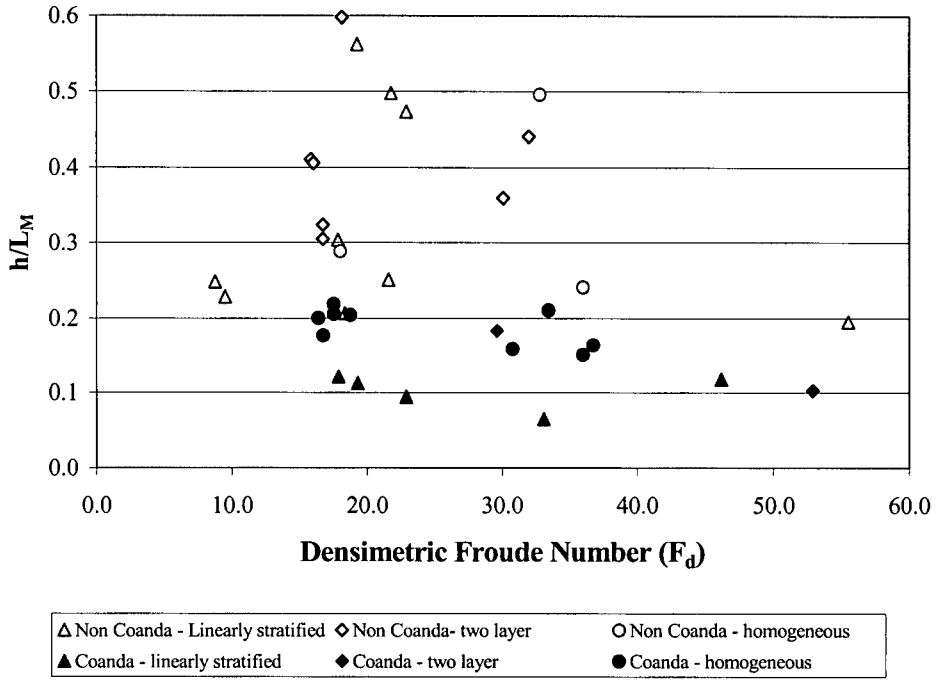

Figure 4.12 Coanda attachment in various ambient fluid conditions

4.2.4.2 Comparison with CORMIX prediction

CORMIX1 was also run in order to provide another comparison. In fact, CORMIX1 does not consider jets discharged into ambient fluid with a sloped bottom. However, jets were discharged horizontally to the bed and the discharge angle is small in this study, it is possible to neglect the discharge angle to the ambient fluid. A simple criteria for bottom attachment by the CORMIX1 is given as (Jirka and Doneker, 1991):

$$\tan\theta < (0.2 - h/\ell_M) \qquad (4.14)$$

where θ is a discharge angle. According to above equation, the Coanda effect occurs if $h/\ell_M < 0.25$ for 3° downward discharge, which agrees with the results observed here.

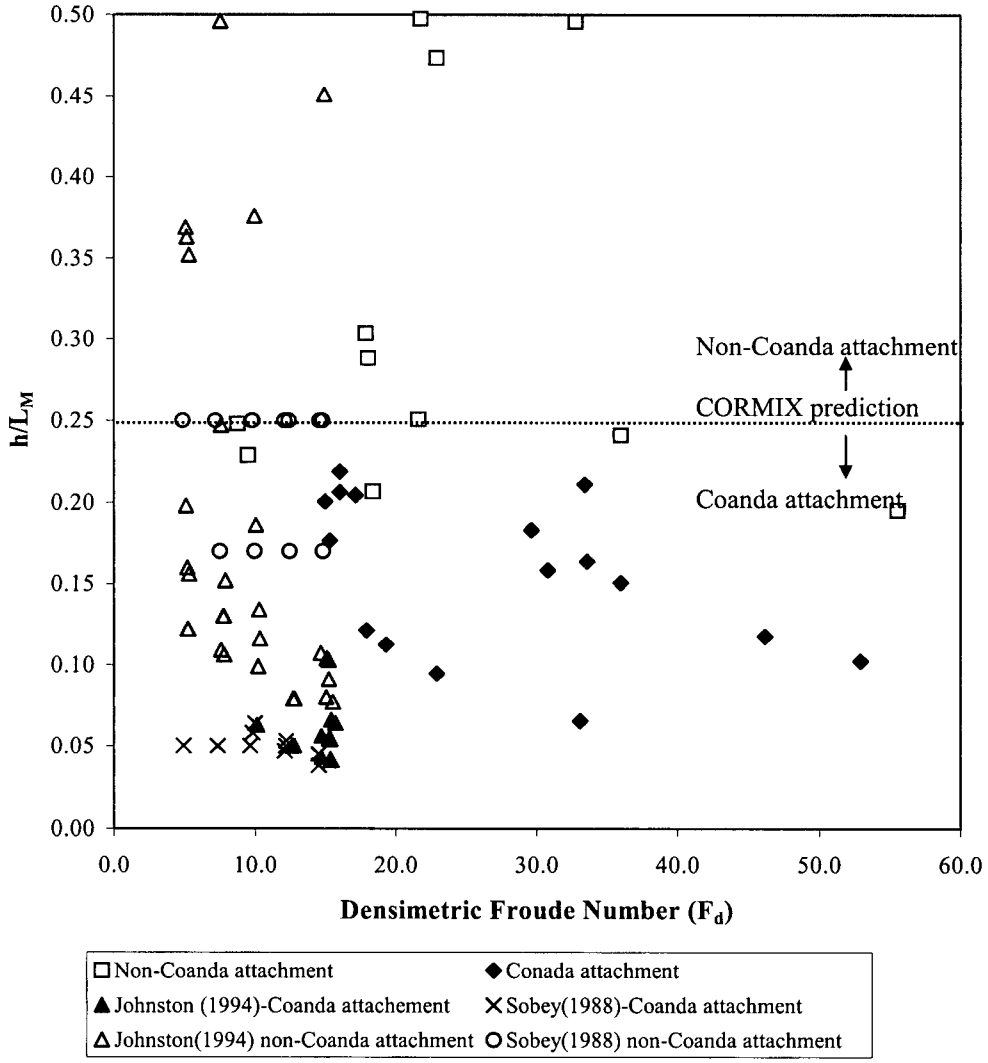

Figure 4.13 Comparison of the Coanda attachment with previous studies (Sobey et al., 1988; Johnston et al., 1994b)

4.2.5 Analysis of gross flow characteristics

Important independent parameters that were considered for buoyant jets in a two-layer system include 1) the jet properties, such as density (ρ_j) and velocity (u), 2) the discharge configuration such as the nozzle diameter (d), the distance from the jet nozzle to the pycnocline (h_i), the discharge angle (θ) and the injection height above the bed (h), and 3) the ambient fluid condition characterized by the density step between two layers ($\Delta\rho_a = \rho_2 - \rho_1$) and the total water depth above the jet discharge nozzle (H). The definition sketch of parameters is shown in Figure 4.14. The dependent parameters (Φ) include the maximum rise height (Z_m) and its location (X_m), the impingement height above the density step (P_d), the top and bottom of the spreading layer (Z_t, Z_b) and the spreading layer thickness (T_f).

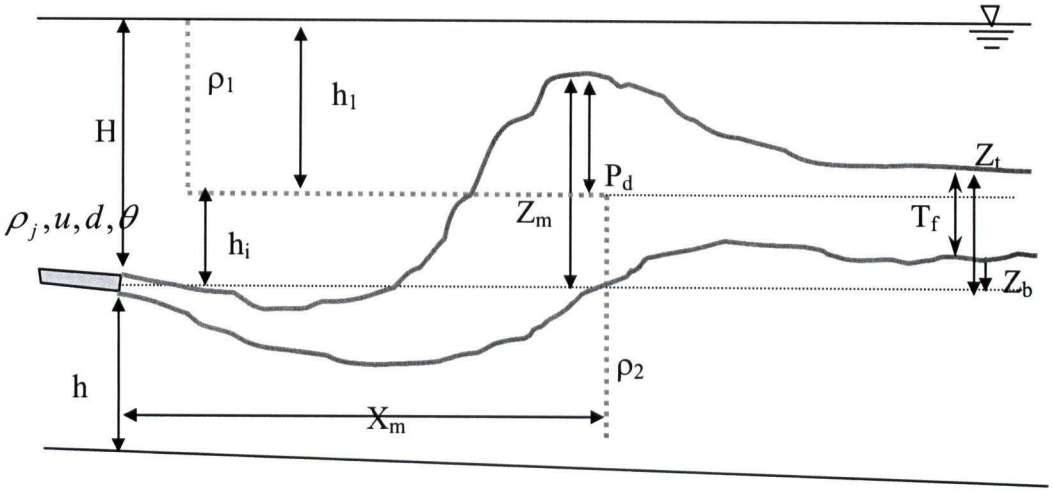

Figure 4.14 Definition sketch of parameters in a two-layer system

The source condition of a buoyant jet can be characterized by the initial fluxes of kinematic momentum M, kinematic source buoyancy B, and source volume flux Q. Since the discharge angle, θ is fixed at -3°, the dependent variables (Φ) are:

$$\Phi = f(M, B, Q, g'_a, h_i, H) \tag{4.15}$$

where M, B and Q are defined in section 2.3. The parameter g'_a is the modified gravitational acceleration based on the density difference between two layers and is given as $g'_a = g(\rho_2 - \rho_1)/\rho_2$. The effect of the initial volume flux becomes negligible when a characteristic length ℓ_Q is small (Wright and Wallace, 1979). In this study $\ell_Q = 0.87$ in all experiments and thus Q can be ignored. If the discharge angle is constant, the dimensionless groups can be formed by means of dimensional analysis:

$$\Phi = f\left(\frac{B^{2/5}}{g'^{3/5}_a h_i}, \frac{h_i}{H}, \frac{M^{3/4}}{h_i B^{1/2}}\right) \tag{4.16}$$

where $\Psi = \dfrac{B^{2/5}}{g'^{3/5}_a h_i}$: impingement/penetration parameter,

$\dfrac{h_i}{H}$: relative distance of the jet exit to the pycnocline to the total water depth above the jet exit,

$\dfrac{M^{3/4}}{h_i B^{1/2}}$: relative influence of the distance to the pycnocline and initial momentum and buoyancy.

4.2.5.1 Maximum rise height and the top of the spreading layer

For the impingement and penetration of the jet on the pycnocline, the vertical momentum of the flow is most important. Vertical momentum M_v due to -3^o oriented buoyant jets is negligible at the pycnocline since the vertical momentum, M_v due to source momentum $M_v = M\,sin(-3^o))$ is significantly smaller than the source momentum. Consequently, the effect of $\dfrac{M^{3/4}}{h_i B^{1/2}}$ is insignificant on the jet behavior at the pycnocline.

If two homogeneous ambient fluids are separated by a strong density step, a jet impinges slightly on the density step and then it spreads only below the pycnocline. Therefore, the total water depth H is insignificant and only h_1 affects jet behavior. Eq. (4.16) can be simplified as:

$$\frac{Z_m}{h_i}, \quad \frac{Z_t}{h_i} = c_1, \; c_2 \tag{4.17}$$

The constants c_1 and c_2 are obtained from the experiments. However, if a density step is small and the vertical momentum generated due to the positive buoyancy is large, then the jet flow can strongly impinge on the pycnocline. In such case, $\frac{B^{2/5}}{g_a'^{3/5} h_i}$ is an important parameter to be considered. Consequently, Eq. (4.16) becomes:

$$\frac{Z_m}{h_i}, \quad \frac{Z_t}{h_i} = f\left(\frac{B^{2/5}}{g_a'^{3/5} h_i}\right) \tag{4.18}$$

Experimental results

Maximum rise height

Figure 4.15 presents the dimensionless maximum rise height (Z_m/h_i) of fluid jets showing two distinctive regimes in a two-layer system. Under the weak impingement regime ($\Psi < 0.5$), the maximum rise heights of buoyant jets are constant. Therefore, Eq. (4.17) has an asymptotic solution (c_1) with standard deviation ± 0.2 for the weak impingement regime:

$$\frac{Z_m}{h_i} = 1.17 \; (\pm \; 0.2) \tag{4.19}$$

The constant 1.17 was obtained by averaging across the 14 measurements. On the other hand, for $\Psi > 0.5$, the maximum height of rise increases proportionally with Ψ with standard deviation $\pm$ 0.05:

$$\frac{Z_m}{h_i} = (1.53 \times \Psi) + 0.186 \qquad (4.20)$$

In the strong impingement and penetration regimes, the relative strength of the pycnocline to buoyancy is weak and thus the maximum rise height is primarily influenced by the buoyancy of the jet flow for a constant discharge depth.

Location of maximum height of rise

Although initial momentum is unimportant to the vertical component such as the maximum rise height, it has significant effect on the location of the maximum height of rise (X_m). Figure 4.16 shows the locations of maximum rise height in two-layer systems. X_m is functions of the densimetric Froude number (F_d) and discharge angle (θ). As F_d increases, the path length of the jet is extended and thus buoyancy begins to prevail further downstream. Also the negative discharge angle causes the jet flow to stay longer in the lower layer and rises further downstream later than horizontal jets.

However, since X_m is primarily controlled by initial momentum the influence of small negative discharge is less important.

Top of the spreading layer

The trajectory of the top of the spreading layer (Z_t) versus discharge depth below the pycnocline and the densimetric Froude number in two-layer systems is shown in Figure 4.17. As a buoyant jet approaches the pycnocline, the top of the spreading layer becomes

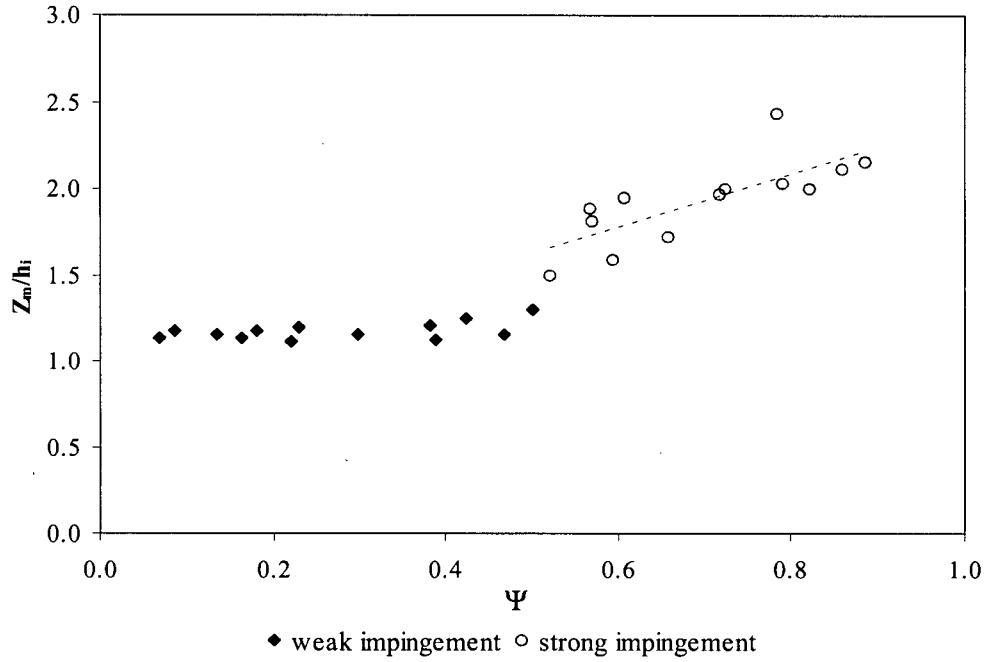

Figure 4.15 Dimensionless maximum rise height (Z_m/h_i) in two-layer systems

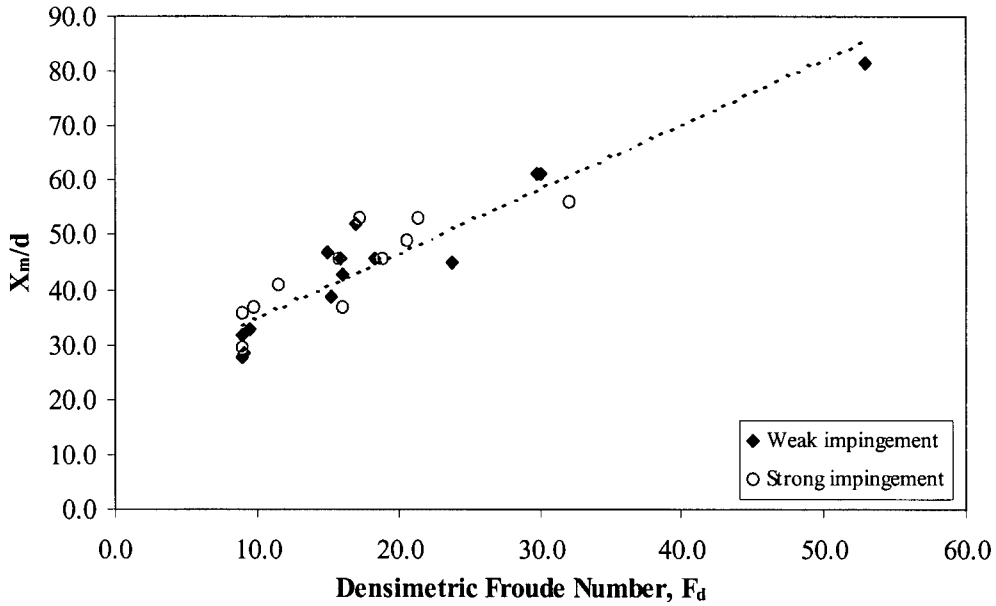

Figure 4.16 Location of maximum rise height (X_m/d) in two-layer systems

flat under the density step. For the same h_i/d Z_t/h_i varies with F_d until the jet reaches the pycnocline but after impingement it becomes independent of F_d. Jets with small F_d rises at nearer distance compared with those with large F_d.

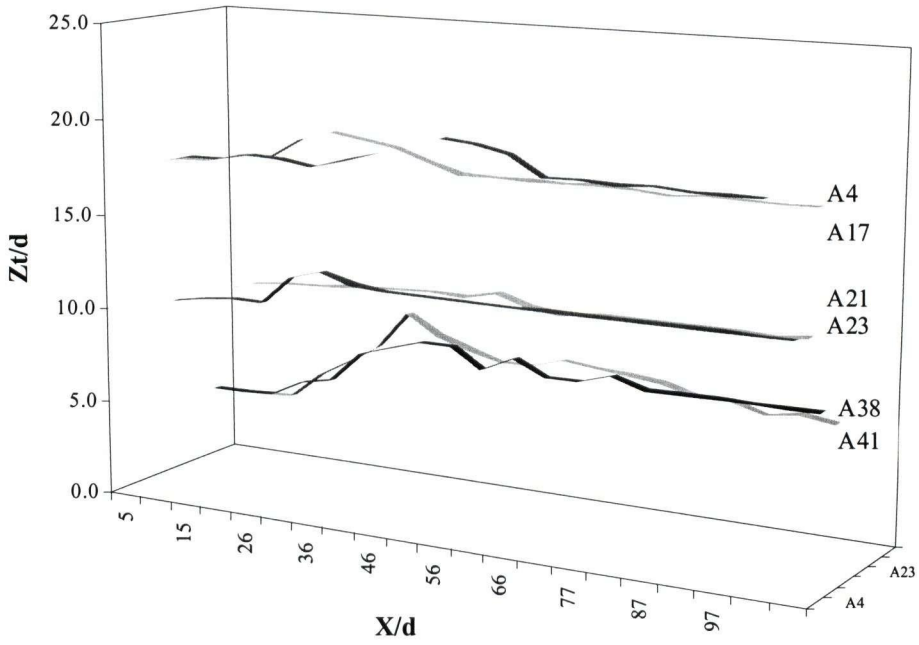

Figure 4.17 Trajectory of the top of the spreading layer in two – layer system
A4 (h_i/d= 18.4 F_d= 16.7), A17 (h_i/d= 18.4 F_d= 8.9), A21 (h_i/d= 10.2 F_d= 9.3)
A23 (h_i/d= 10.2 F_d= 18.1), A38 (h_i/d= 5.1 F_d= 18.7), A41 (h_i/d= 5.1 F_d= 16.0)

Figure 4.18 shows that the dimensionless top of the spreading layer also has the following asymptotic solution (c_2) for the weak impingement regime:

$$\frac{Z_t}{h_i} = 1.07\ (\pm 0.04) \qquad (4.21)$$

The constant c_2 was obtained by averaging across 14 measurements. However, for the strong impingement and penetration regime the top of the spreading layer shows a slight increase with the dimensionless parameter Ψ. The formula obtained by regression analysis is:

$$\frac{Z_t}{h_i} = 2.47 \times \Psi - 0.19 \quad (R^2 = 0.8) \tag{4.22}$$

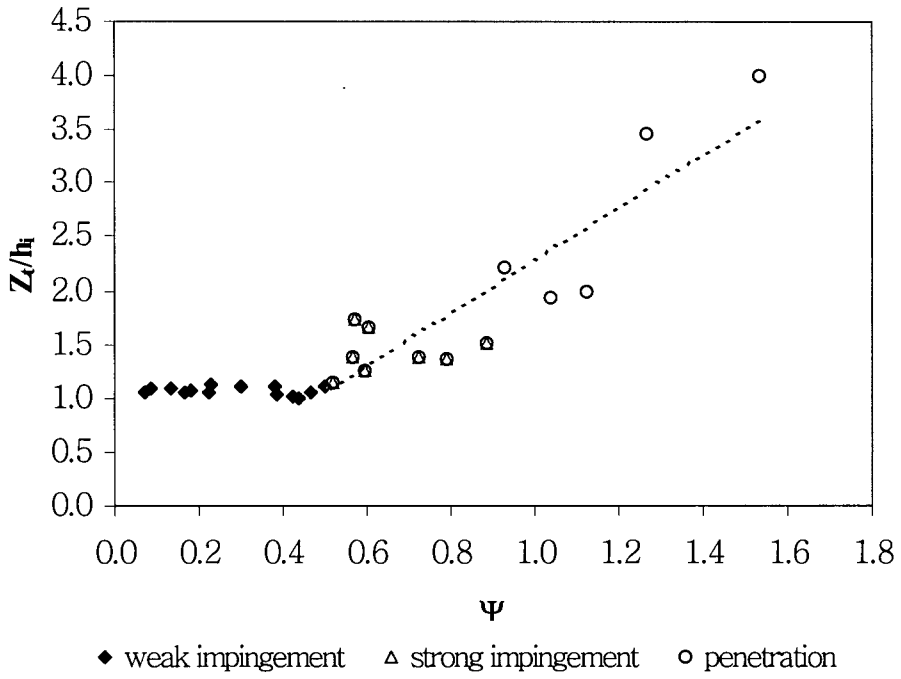

Figure 4.18 Dimensionless top of the spreading layer (Z_t/h_i) of buoyant fluid jets

The top of the spreading layer is primarily influenced by the maximum rise height. For $\Psi < 0.5$, jet flows are confined under the pycnocline and both Z_m/h_i and Z_t/h_i converge to the constants c_1 and c_2 . However, for $\Psi > 0.5$ the higher a jet initially impinges, the higher the final top of the spreading layer becomes. This point is important in that the strength of impingement and penetration determines the elevation of the final spreading layer.

4.2.5.2 Spreading layer thickness

As the jet proceeds in the homogeneous dense lower layer, the density difference between the jet and ambient fluid constantly decreases with distance due to entrainment. If the

density of a jet flow becomes sufficiently large as it approaches the pycnocline, the rising buoyant flow can be suppressed by even a small density step across the pycnocline. Thus, $B^{2/5}/g_a'^{3/5}h_i$ becomes negligible. Consequently, for the spreading layer thickness only the dimensionless source momentum term is significant. Therefore, Eq. (4.16) reduces to:

$$\frac{T_f}{h_i},\ \frac{Z_b}{h_i} = f\left(\frac{M^{3/4}}{h_i B^{1/2}}\right) \tag{4.23}$$

The experimental results agree with the dimensionless analysis as shown in Figure 4.19.

$$\frac{T_f}{h_i} = 0.50\frac{M^{3/4}}{h_i B^{1/2}} + 0.2 \quad (\pm 0.05) \tag{4.24}$$

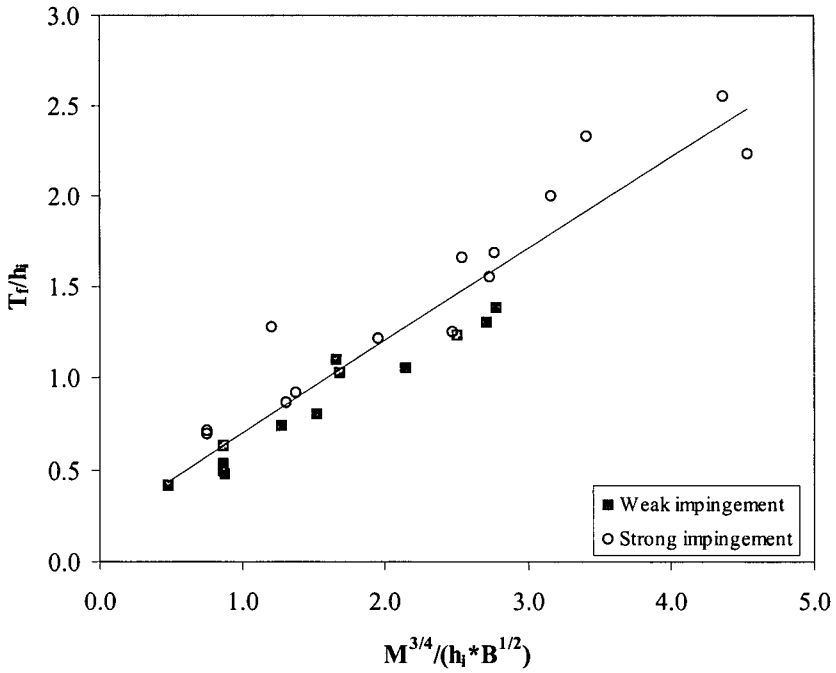

Figure 4.19 Dimensionless spreading layer thickness (T_f/h_i) of buoyant fluid jets in two-layer systems

4.3 Summary of fluid jets

This chapter investigated the dynamics of buoyant jets in two-layer systems. The findings also provide the basis of understanding the dynamics of particle-laden jets with buoyant interstitial fluid. The investigation results of fluid jets are summarized as follows:

Three parameters were found to have a critical influence on jet behavior at the near-field: the magnitude of density step, buoyancy of the jets and the discharge distance to the pycnocline. These were combined into a dimensionless parameter Ψ $(=\frac{B^{2/5}}{g_a'^{3/5}h_i})$, which determines the flow regimes: weak impingement, strong impingement and penetration.

Weak impingement regime: when $\Psi < 0.5$, a buoyant jet initially rose and reached the pycnocline, where the jet impinged weakly without any significant mixing of the upper layer. Then it bent and advanced under the pycnocline. This condition was also found to satisfy the condition, $\gamma << 0$ where $\gamma = \rho_1 - \rho_i / \rho_2 - \rho_i$, in which ρ_1, ρ_2 and ρ_i are density of the upper and the lower layer fluid, and density at the pycnocline.

Strong impingement regime: for $0.5 < \Psi < 0.9$, buoyant jets overshot the density step and immediately fell back to its neutral buoyancy. Jet flows disturbed considerable depth of the upper layer, causing density increases by transporting entrained lower layer fluid. However density change does not occur at the surface.

Penetration regime: for $\Psi > 0.9$, a buoyant jet penetrated into the upper layer immediately after the source momentum decays. The penetrated jet flow initially occupied the entire upper layer and proceeded above the pycnocline. While the jet rose it entrained the lower layer fluid, resulting in a significant density increase in the upper layer. This regime also satisfies $0 < \gamma < 1$.

Backflows occurred along the pycnocline depending on the relative magnitude of vertical and source momentum flux, which determines jet angles at the pycnocline. Backflow occurred when $\theta_p > 7^o$ but no backflow occurred when $\theta_p < 7^o$. This result was obtained from the theoretical analysis and confirmed by experiments. For the penetration regime, $\Psi > 0.9$, some jet flow accumulated along the pycnocline and backflows also formed at the surface of the upper layer.

The Coanda bottom attachment occurred when $h/\ell_M < 0.22$, independently of the ambient fluid conditions for constant water depth $H/h_o = 34.7$. This value is similar to the CORMIX v3.2 prediction ($h/\ell_M < 0.25$) but is considerably larger than those from Sobey et al (1988) and Johnston et al. (1994b) for horizontal jets in shallow water ($h/\ell_M < 0.1$).

The gross flow characteristics suggested that for the weak impingement regime the dimensionless maximum rise height (Z_m/h_i) and the top of the spreading layer (Z_t/h_i) converged to constants $c_1 = 1.17$ and $c_3 = 1.07$ respectively. For the strong impingement regime, Z_m/h_i and Z_t/h_i linearly increase as $B^{2/5}/g'_a h_i$ increases. On the other hand, the final spreading layer (T_f/h_i) was found to be a function only of the dimensionless parameters $M^{3/4}/B^{1/2}h_i$ regardless of the presence of density step, and increasing with this dimensionless parameter.

Chapter 5

Results and Discussion: Particle-laden jet

5.1 Introduction

The dynamics of particle-laden jets is more complicated than that of fluid jets because particles settle out of the jet constantly, thereby modifying the bulk density. Thus, it is important to understand both the characteristics of fluid jets and the effect of particles on the interstitial fluid.

The primary purpose of the studies of particle-laden jets is to understand the effect of suspended particles on turbulent buoyant flows and to identify whether particles can prevent the penetration of highly buoyant interstitial fluid. A series of experiments were performed with buoyant interstitial fluid containing spherical glass beads. The conditions of ambient fluid and jet fluid were kept the same as that of fluid jets in order to identify the effect of particles on flows.

5.2 Particle-laden jets in two-layer systems

The qualitative features of particle-laden jets in two-layer systems are described and the flow regimes are determined in this section. The particle distribution and dye concentration profiles of the interstitial fluid are analyzed. The gross flow characteristics are analyzed by means of dimensional analysis and compared with experimental results. The flow classification and dilution of interstitial fluid are compared with CORMIX v3.2 predictions and the suitability of this model for particle-laden jets is discussed.

5.2.1 Behavior of particle-laden jets

When buoyant fluid jets carrying particles are discharged into stagnant ambient fluid, initially the source momentum maintains particles in suspension. However, with increasing distance from the source the influence of the source momentum weakens and the dynamics of particle-laden jets is determined by the buoyancy of the jet and the ambient conditions. In the present experimental conditions, when $\ell_M > 30\ cm$, all particle-laden jets began to display plume-like behavior.

Experimental observation showed that when the particle concentration in flow was small, a particle-laden jet behaved like a fluid jet. The jet penetrated into the upper layer (Figure 5.1(a)) or impinged on the pycnocline (Figure 5.1(b)). As the jet spread along the density step, the interstitial fluid was constantly mixed with the ambient fluid while individual particles settled out of the jet without significant impact on the jet behavior.

The flow exhibited a distinctive behavior as the particle concentration increased. The bottom of the jet constantly expanded downward due to the initial discharge angle and active particle settling. Initially, the mixture of fluid and particle clouds descends as a group of individual particles and gradual separation between particles and parent fluid occurs as Noh and Fernando (1993) observed. However, the entrainment decreased with distance and thus the internal circulation became insufficient to keep the particles in suspension. Moreover, the constant influx of particle-laden flow supplied more particles into the spreading layer in which the previously discharged particles were still in suspension. Consequently, the particles accumulated due to settling at a certain position within the flow, resulting in a wide, U-shaped configuration at the bottom of the flow as shown in Figure 5.1 (c).

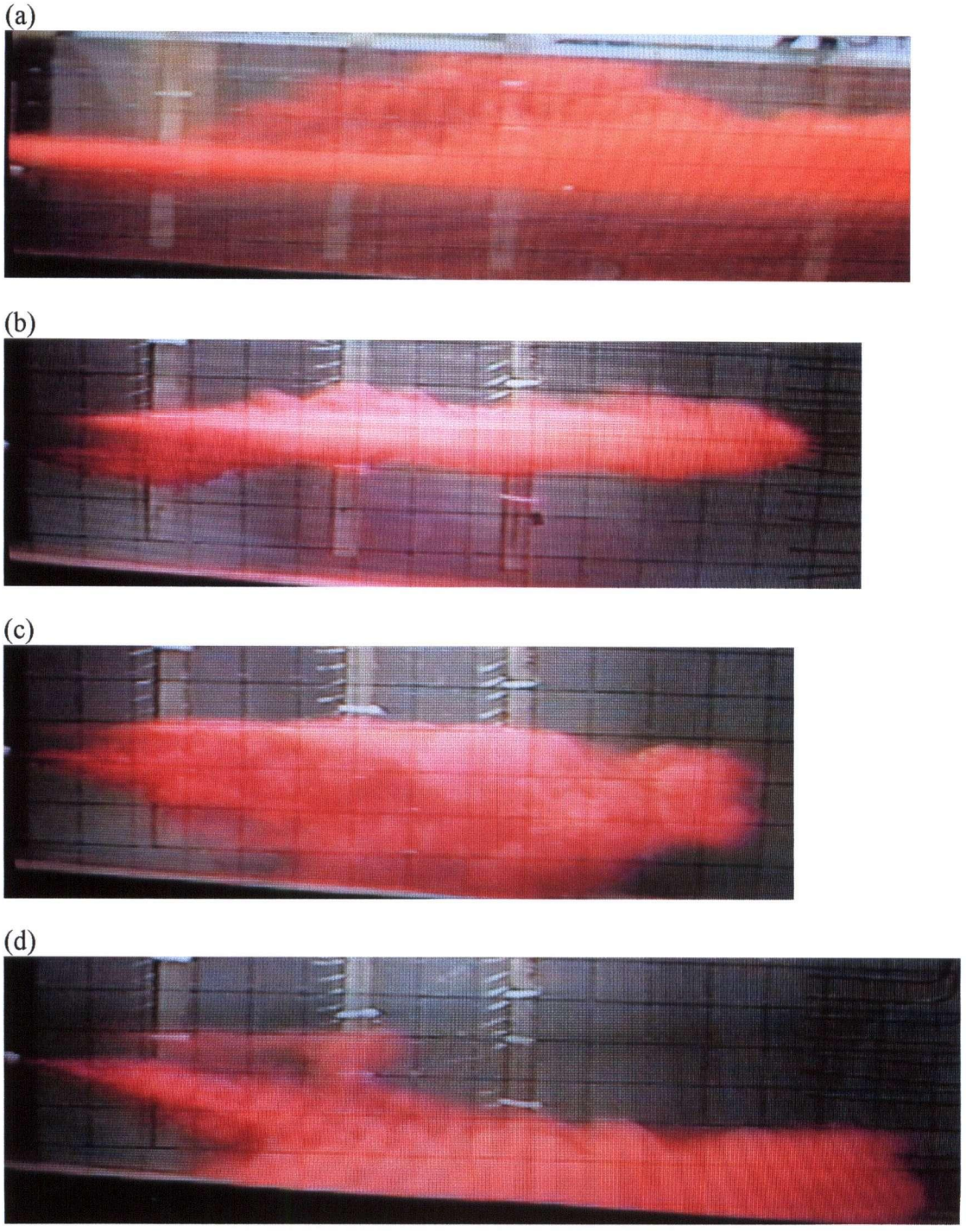

Figure 5.1 Behavior of particle-laden jets in two-layer systems: (a) penetration (P20) (b) impingement (P24), (c) weak plunging (P22) and (d) strong plunging (P23)

When the bulk density of a jet was much larger than the ambient fluid density, the jet plunged down to the bed and propagated like a turbidity current (Figure 5.1 (d)). This initial plunging process was similar to the behavior of negatively buoyant fluid jets except for the separation of buoyant interstitial fluid from the jet during plunging. Abrupt settling of particles occurred at the plunging point, where the jet looked and behaved like the turbidity current with reversing buoyancy as described by Simpson (1987), Spark et al. (1993) and Hüzerler (1996). The buoyant interstitial fluid continuously rose and a backflow was generated on the bottom.

Note that a patch of dyed fluid along the pycnocline in Figure 5.1(d) is an experimental artifact caused by the inevitable release of interstitial fluid separated from the mixture during initial discharge. Although it is not shown in the figure, the jet flow occupied almost the entire lower layer far downstream. When sufficient particles settled, the flow lifted off the bed and formed a horizontal gravity current under the pycnocline.

5.2.2 Determination of flow regimes

Experimental observation indicated that both the initial difference between the bulk density of a jet and the ambient fluid density and the density difference between the interstitial fluid and the ambient fluid are critical in determining the initial jet behavior. The relationship between the two density differences can be expressed as a non-dimensional density R which is the inverse of a parameter suggested by Turner and Huppert (1992):

$$R = \frac{\rho_a - \rho_b}{\rho_a - \rho_f} \tag{5.1}$$

where ρ_a : ambient fluid density at the discharge level

ρ_f : interstitial fluid density

ρ_b : bulk density of particle-laden jet

For fluid jets, $R = 1$, since $\rho_b = \rho_f$ and for particle-laden jets $R < 1$. The present study considers the case where the interstitial fluid is always buoyant relative to the ambient fluid (i.e. $\rho_a > \rho_f$), therefore, if $0 < R < 1$, then the ambient density is always greater than the bulk density ($\rho_a > \rho_b$). Under this condition the influence of particles on the flow is insignificant and a particle-laden jet behaves like a buoyant fluid jet regardless of the particles. Therefore, the flow penetrates or impinges on the pycnocline depending on the dimensionless parameter Ψ defined in fluid jet analysis in section 4.2.2. The former is defined as penetration regime and the latter as impingement regime. Note that the present experimental condition for particle-laden jets covered only the strong impingement ($0.5 < \Psi < 0.9$) but not the weak impingement regime.

For $R < 0$ the jet is initially negatively buoyant, in which case the density difference between ρ_a and ρ_b plays a significant role in the behavior of the jet. Under this circumstance if R is less than a critical value R_c, rapid change occurs in jet trajectory. If $R_c < R < 0$ then the jet flow is initially negatively buoyant but the bulk density is insufficient to completely sink to the bottom. Thus, the jet begins to rise after sufficient particle settling - this transitional flow regime is classified as weak plunging regime. However, if $R \leq R_c < 0$, then the particle-laden jet is significantly heavier than the ambient fluid and thus it immediately plunges to the bottom and proceeds on the bottom slope - this is defined as strong plunging regime. For weak and strong plunging regimes the ambient fluid condition has little effect on the jet behavior before significant particle settling occurs and the flow rises.

Consequently, the behavior of particle-laden jets in two-layer systems can be classified into four flow regimes based on Ψ as in fluid jets and R. Table 5.1 summarizes the classification of particle-laden jets.

The critical value R_c was estimated to be –2.0 from the experiments and the flow regimes are shown in Figure 5.2.

Table 5.1 Classification of particle-laden jets

Regime	**Density Relations** $\rho_a > \rho_f$ always true	***R and*** Ψ $\left(\frac{\rho_a - \rho_b}{\rho_a - \rho_f}\right), \left(\frac{B^{2/5}}{g_a'^{3/5} h_1}\right)$	**Behavior of particle-laden jets in two-layer systems**
Penetration	$\rho_a > \rho_b$	$0 < R < 1$, $\Psi > 0.9$ Initially buoyant	Penetration (Figure 5.1(a))
Impingement	$\rho_a > \rho_b$	$0 < R < 1$, $\Psi < 0.9$ Initially buoyant	Impingement on the pycnocline (Figure 5.1 (b))
Weak Plunging	$\rho_a < \rho_b$	$R_c < R < 0$ Initially negatively buoyant	Initial plunging and abrupt group settling, detrainment of interstitial fluid (Figure 5.1 (c))
Strong Plunging	$\rho_a << \rho_b$	$R < R_c < 0$ Initially negatively buoyant	Plunge down to the bottom and active detrainment of interstitial fluid (Figure 5.1 (d))

5.2.3 Particle distribution and interstitial fluid dilution

5.2.3.1 Particle distribution in ambient fluid

Particles carried by the fluid motion start settle out of the turbulent flow when the particle settling velocity w_s approaches the flow velocity (u) (Popper et al., 1974). That is, if $u/w_s >> 1$, particles move with flow whereas when $u/w_s << 1$, individual particle settling occurs. The settling velocity of the glass beads used in the present study was 1.14 mm/s based on the mean diameter 38.72 μm. The velocity ratio ranged $366.3 < u/w_s < 732.7$ at the source, which satisfied $u/w_s >> 1$ to the end of the tank. In this case, individual particles were expected to follow the flow motion and the turbulence of flow due to entrainment also maintains particles in suspension. However, jets with high particle

concentration exhibited grouping settling behavior near the nozzle. This caused a rapid flow velocity decrease resulting in abrupt settling behavior.

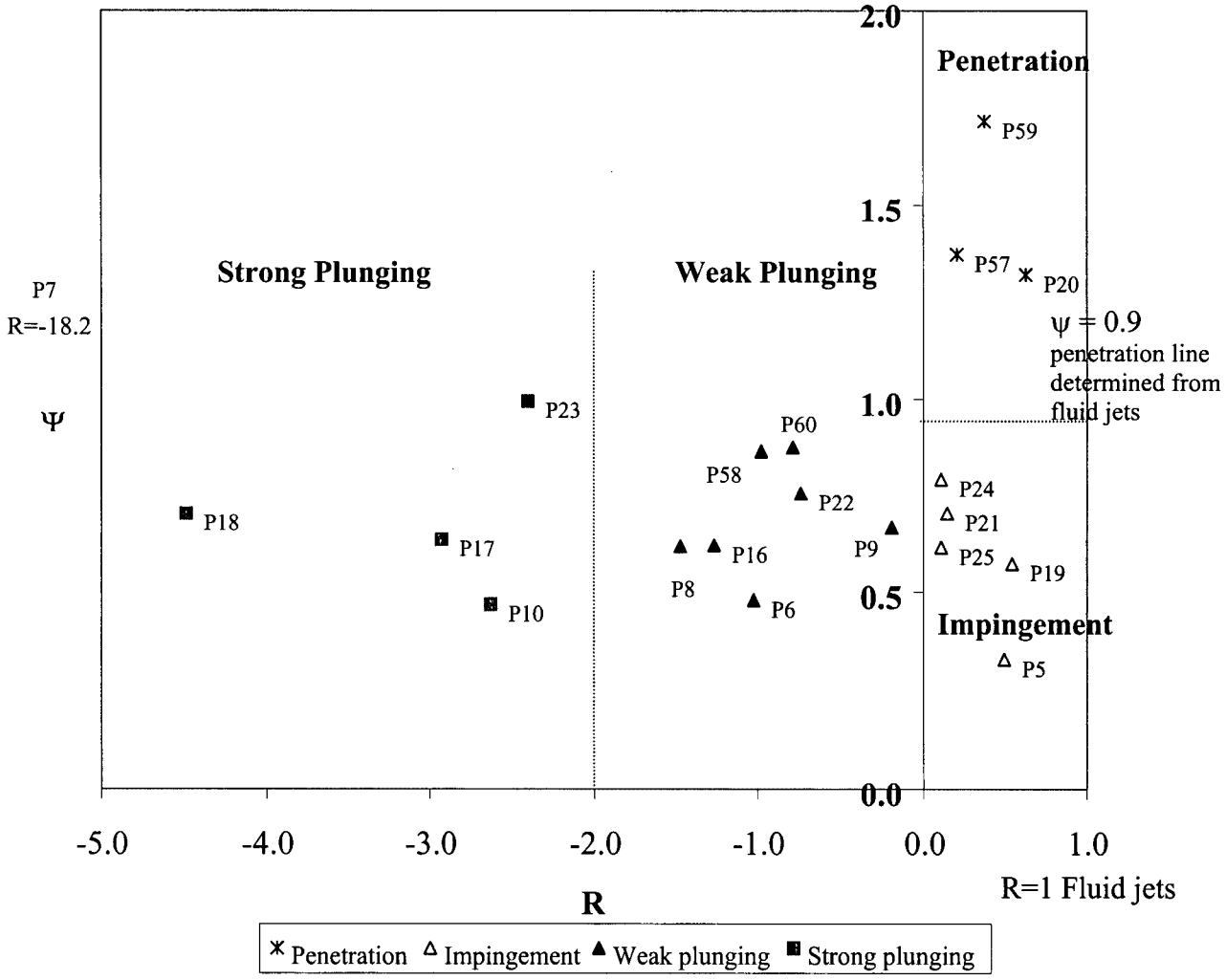

Figure 5.2 Flow regimes for particle-laden jets in two-layer systems

Figure 5.3 (a) (b) shows the particle distribution and interstitial fluid dye concentration profile for penetration and the weak plunging cases respectively. It is shown that the particle distribution follows the motion of interstitial fluid. When a jet penetrate into the upper layer it transports a significant amount of particles into the upper layer, where some particles travel in suspension for a considerable horizontal distance (Figure 5.3 (a)).

However, for the weak plunging regime, overall particles move with fluid but considerable particle settling also occurs under the centerline of flow (Figure 5.3 (b)). It is probably due to the grouping behavior of particles in high particle concentration and individual settling of large particles.

5.2.3.2 Dye concentration profile

The dye concentration profiles were fitted with a Gaussian distribution described by

$$c = c_m \exp(-\frac{z^2}{b^2}) \qquad (5.2)$$

where z : vertical distance from the jet centerline

c_m : centerline concentration

b : characteristic width of concentration at a radial position where the concentration $c/c_m = \exp(-1) = 0.37$

Figure 5.4 (a)-(d) show an example of the dye concentration profiles of particle-laden jets. Near the jet exit ($x/L = 0.13$), the concentration profiles of all particle-laden jets were identical, however as the source momentum weakened the jets rose or plunged down depending on R. In addition to the constant settling of the particles, the release of buoyant interstitial fluid also caused the jet flow to fluctuate as it proceeded along the tank. This centerline displacement was expressed by modifying a Gaussian distribution:

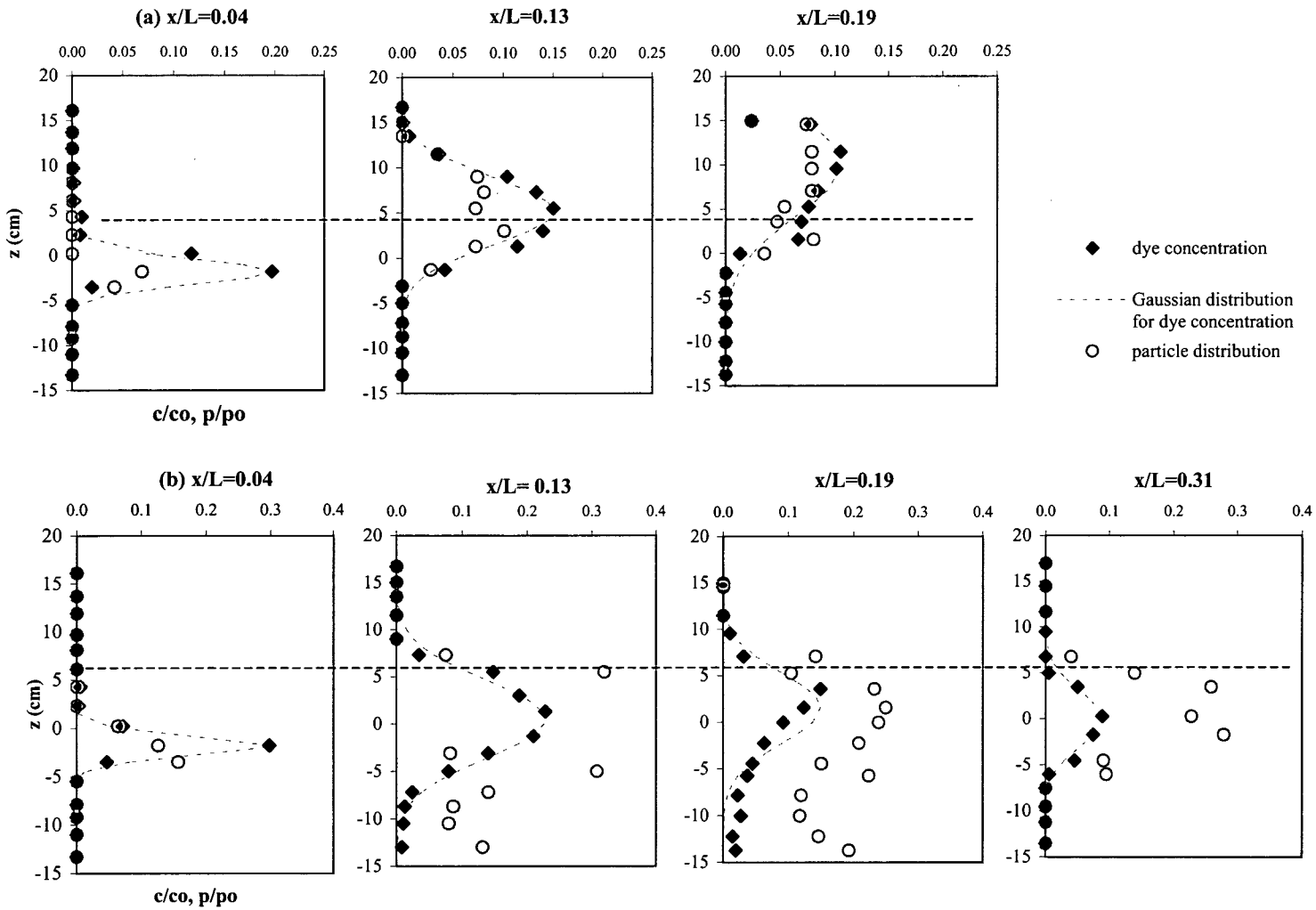

Figure 5.3 Relative dye concentration and particle distribution for (a) Penetration (P57)
(b) Weak Plunging (P58) (----): pycnocline

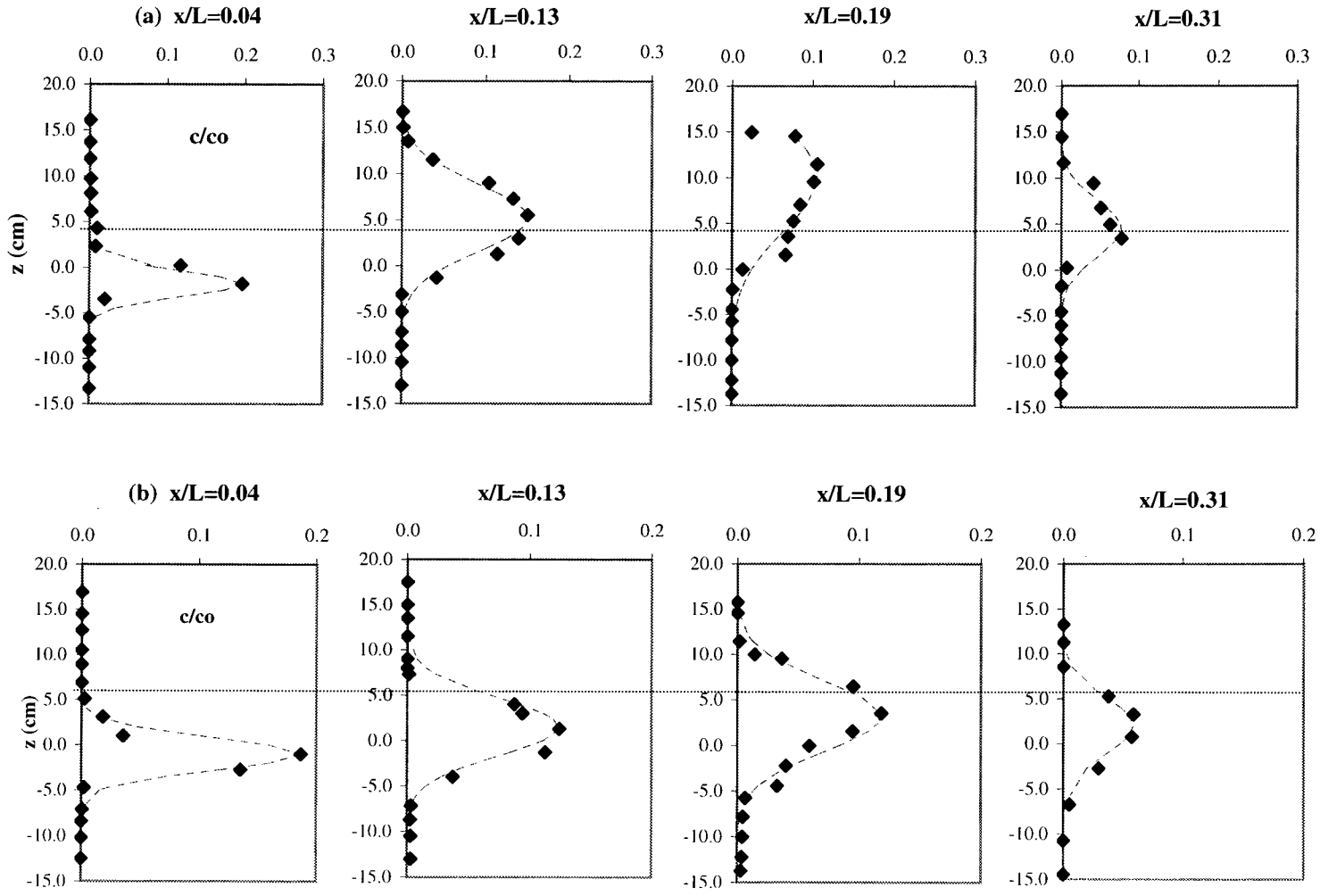

Figure 5.4 Dye concentration and Gaussian distribution for (a) Penetration (P57) and (b) Impingment regime (P24) ----: pycnocline

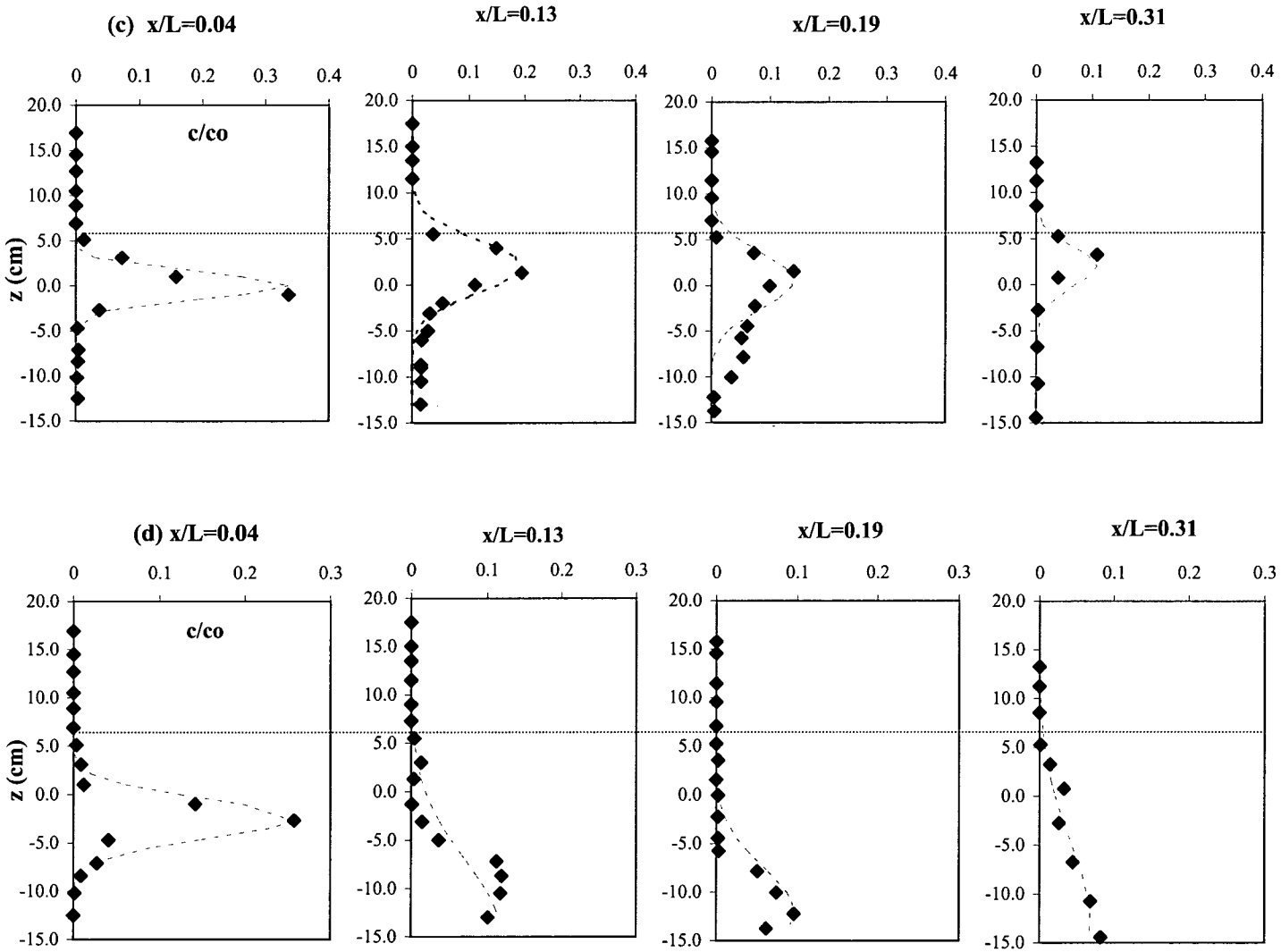

Figure 5.4 (continued) Dye concentration profile and Gaussian distribution for (c) Weak Plunging (P22) and (d) Strong Plunging Regime (P23), ---: pycnocline

$$C = C_m \exp\left(-\frac{(z+s)^2}{b^2}\right) \tag{5.3}$$

where s is a constant which describes the centerline displacement from the jet nozzle.

The centerline displacement (s) of the flow regime versus dimensionless downstream distance (x/L) was plotted for all flow regimes in Figure 5.5. The profiles clearly indicate that as the particle concentration increased the centerline position fell and as the densimetric Froude number (F_d) increased the maximum centerline occurred further downstream. This is consistent with the location of the maximum rise height (X_m) for fluid jets as discussed in section 4.2.5.

Jets of penetration and impingement regimes rose to the maximum rise height and fell. Two particle-laden jets of strong plunging regime have negative centerline positions and depending on R, different particle settling behavior and detrainment of interstitial fluid caused difference in the centerline displacement. At $x/L = 0.13 - 0.19$, the centerline shifted due to plunging. At $x/L = 0.31$, the centerline of P17 rose slightly due to rising buoyant interstitial fluid after sufficient particle settling occurred. However, P23, with larger particle concentration, propagated as a turbidity current without significant rising of interstitial fluid within the experimental tank length.

5.2.3.3 Effect of R on the characteristic width (b)

The relationship between the jet centerline position and the b along the jet trajectory is shown in Figure 5.6. The source momentum-dominant location $x/L = 0.04$ was excluded in the plot. For penetration and impingement regimes, b is independent of the centerline displacement, however, b increases proportionally for weak and strong plunging regimes

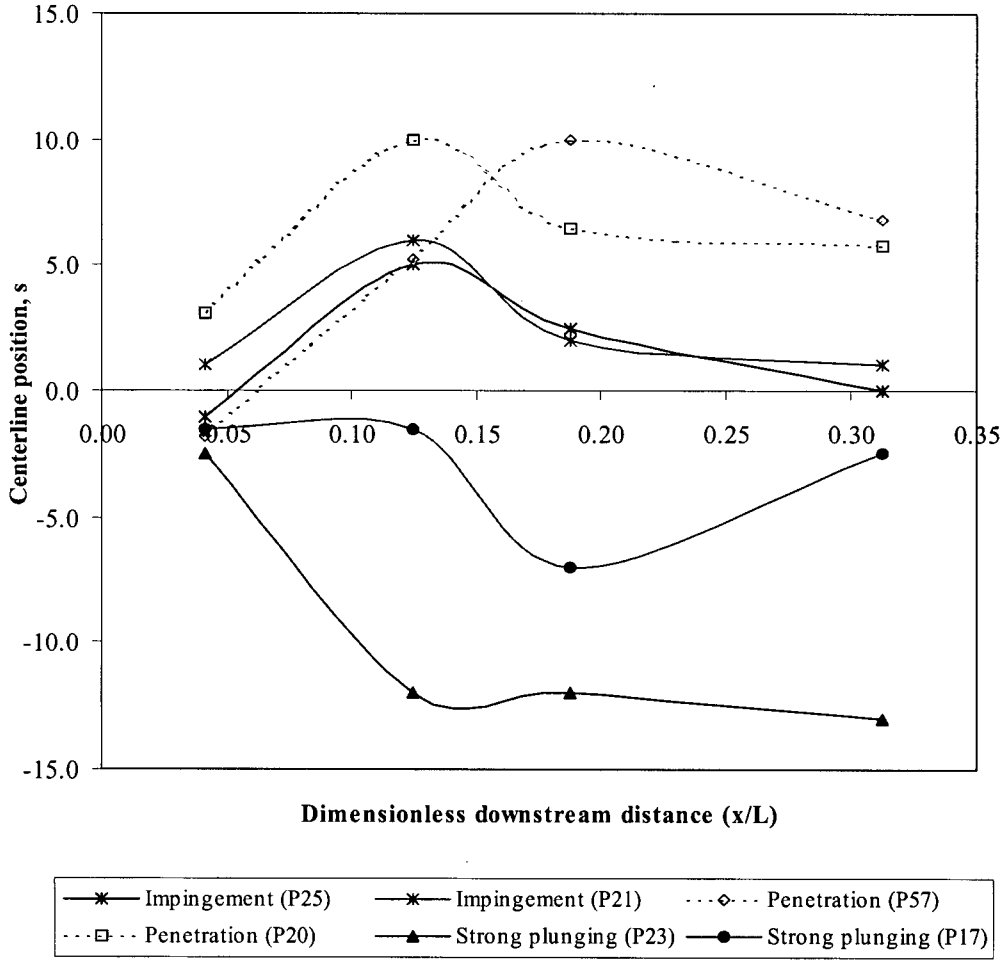

Figure 5.5 Jet centerline displacement (s) along the jet trajectory (x/L)

as the centerline shifts downward. This is because some portion of buoyant interstitial fluid plunged while particles plunged and some in the upper part of the flow rose as particle-free fluid.

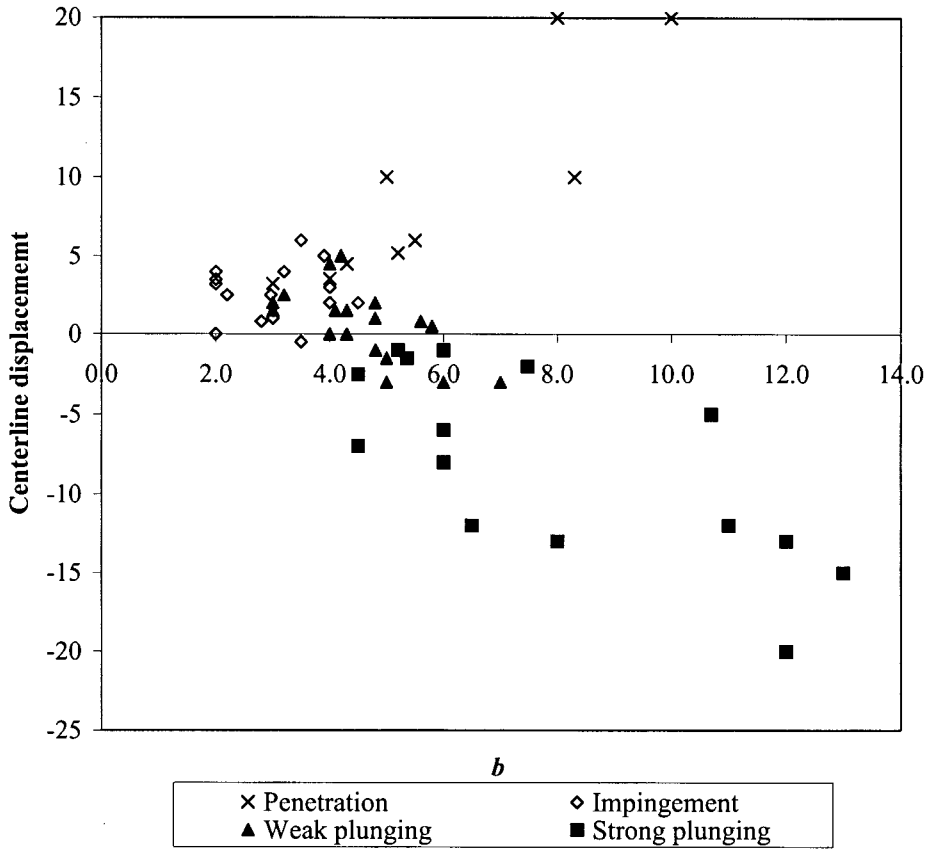

Figure 5.6 Centerline displacement and concentration characteristic width (b) of particle-laden jets

5.2.4 Analysis of gross flow characteristics

This section analyzes the gross flow characteristics of particle-laden jets and also seeks asymptotic solutions to the equations. The experiments for particle-laden jets in two-layer systems were performed for $0.33 < \Psi < 1.72$, $-18.15 < R < 0.63$, $\theta = -3^\circ$ and $h/d = 15.3$. According to the flow regimes defined for fluid jets in section 4.2.3, the experiments covered mostly the strong impingement and penetration regime.

In addition to the independent variables relevant to fluid jets (Q, M, B, g'_a, h_i, H)

described in section 4.2, two important additional parameters need to be considered for particle-laden jets: the distance from the bed (h), and the ratio of density differences R. The dependent variables (Φ_p) include the maximum height of rise (Z_m), the top of the spreading layer (Z_t) and the spreading layer thickness (T_f). A definition sketch of a particle-laden jet in a two-layer system is shown in Figure 5.7.

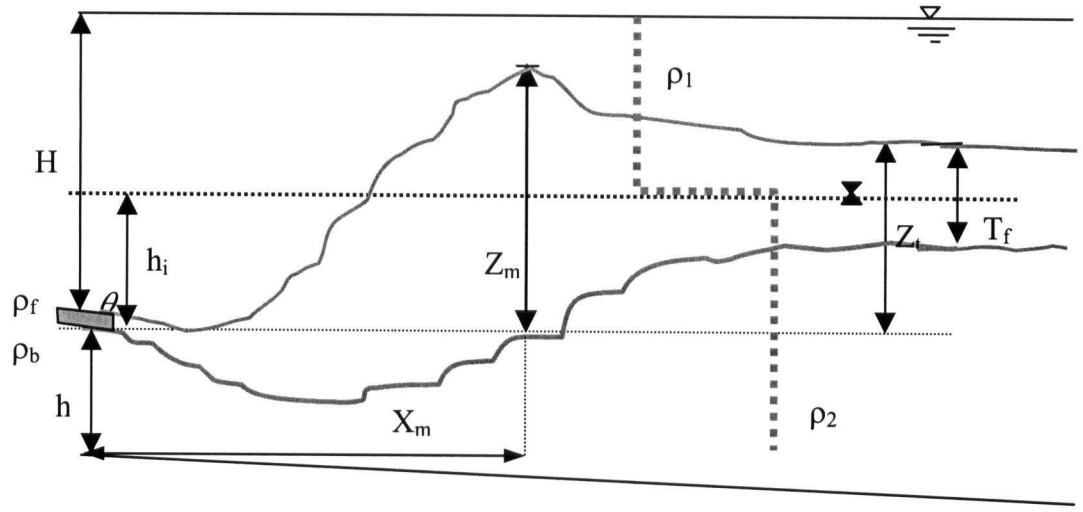

Figure 5.7 Definition of parameters of a particle-laden jet in a stagnant two-layer system

Consequently, dimensionless groups for particle-laden jets are:

$$\Phi_p = f\left(\frac{B^{2/5}}{g_a'^{3/5}h_i},\ \frac{h_i}{H},\ \frac{M^{3/4}}{h_i B^{1/2}},\ R,\ \frac{h}{d}\right) \tag{5.4}$$

where $\frac{B^{2/5}}{g_a'^{3/5}h_i}$, $\frac{h_i}{H}$, $\frac{M^{3/4}}{h_i B^{1/2}}$ and R are defined in section 4.2 and 5.1. The dimensionless depth parameter $\frac{h}{d}$ is defined as the ratio of the discharge height above the bed to the nozzle diameter.

5.2.4.1 Maximum rise height and the top of the spreading layer

Due to the initial downward discharge angle and particle sedimentation, the direct effect of the source momentum on the jet behavior at the pycnocline is insignificant, resulting in $M^{3/4}/h_i B^{1/2} \to 0$.

For the jets of penetration, impingement and weak plunging regime, $\frac{B^{2/5}}{g_a'^{3/5} h_i}$ and $\frac{h_i}{H}$ are important while the effects of particles (R) and $\frac{h}{d}$ on the jet dynamics are negligible. Consequently, Eq. (5.4) reduces to:

$$\frac{Z_m}{h_i}, \frac{Z_t}{h_i} = f\left(\frac{B^{2/5}}{g_a'^{3/5} h_i}, \frac{h_i}{H}\right) \tag{5.5}$$

On the other hand, for strong plunging regime a particle-laden jet immediately plunges down to the bottom and thus the role of the pycnocline on the jet behavior is unimportant in the near field. Only the relative distance becomes influential to the plunging particle-laden jets. Therefore,

$$\frac{Z_m}{h_1}, \frac{Z_t}{h_1} = f\left(\frac{h}{d}\right) \tag{5.6}$$

Since $\frac{h}{d}$ is constant in this study, Eq. (5.6) becomes:

$$\frac{Z_m}{h_i}, \frac{Z_t}{h_i} = c_3, c_4 \tag{5.7}$$

The constants c_3 and c_4 are determined experimentally.

Experimental results

Maximum rise height

The dimensionless maximum height of rise (Z_m / h_i) of particle-laden jets in a two-layer system is shown in Figure 5.8. The Z_m / h_i for impingement regime increases with the impingement-penetration parameter Ψ, and tended to be slightly higher than for weak plunging regime. Neglecting the minor difference among the two regimes, regression analysis of the combined experimental results are:

$$\frac{Z_m}{h_i} = 3.43 \times \Psi - 0.31 \ (\pm 0.4) \tag{5.8}$$

On the other hand, a jet of strong plunging regime plunged down to the bed and the plunging depth became constant as $\frac{h}{d} = 15.3$ in this study. Therefore, the constant (c_3) in Eq.(5.7) becomes:

$$\frac{Z_m}{h_i} = c_3 = -3.0 \ (\pm 0.01) \tag{5.9}$$

However, if the discharge height above the bed (h) increases, the plunging depth is no longer constant but increases with $\frac{h}{d}$.

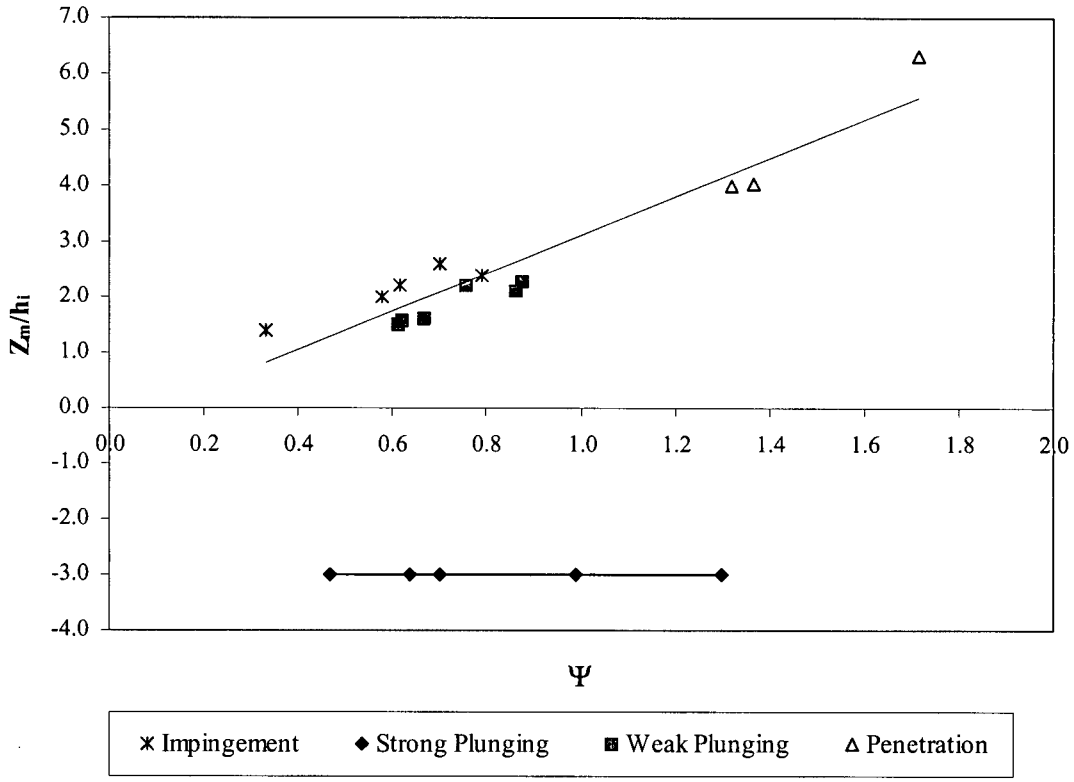

Figure 5.8 Dimensionless maximum rise height (Z_m/h_i) of particle-laden jets in two-layer systems

Top of the spreading layer

The dimensionless top of the final spreading layer was plotted in Figure 5.9. In penetration and impingement regimes, it increased linearly with $\frac{B^{2/5}}{g_a'^{3/5}h_i}$ as was observed for the maximum rise height, regression analysis gives:

$$\frac{Z_t}{h_i} = 0.95\frac{B^{2/5}}{g_a'^{3/5}h_i} + 0.66\ (\pm\ 0.17) \qquad (5.10)$$

However, for weak plunging regime the top of the final spreading layer shows an irregular pattern due to the interaction between particle settling and detrainment of the interstitial fluid and it also tends to lower than that of impingement regime.

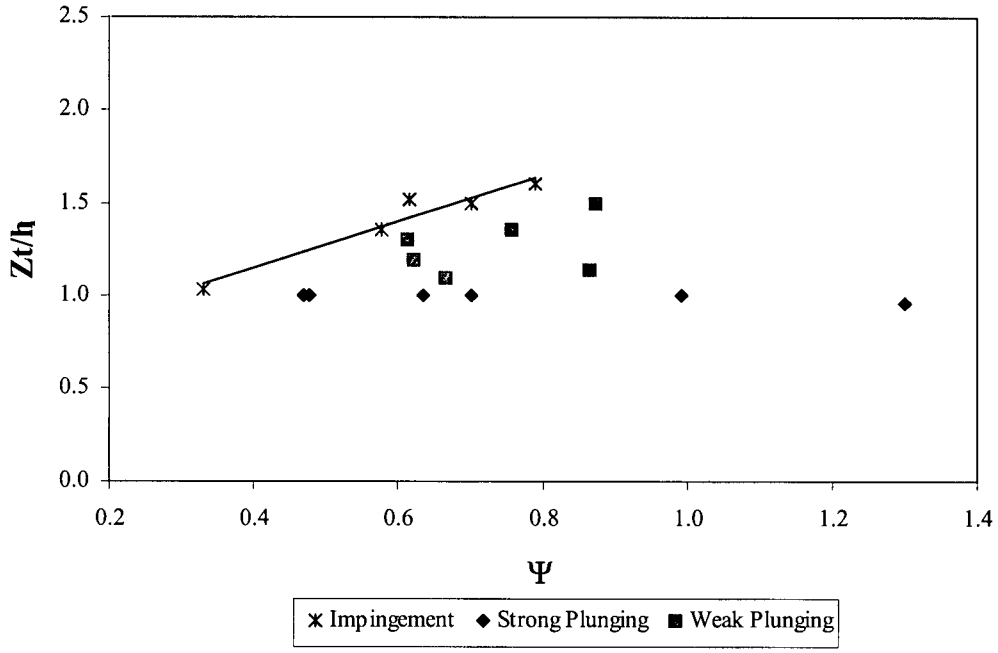

Figure 5.9 Dimensionless top of the spreading layer (Z_t/h_i) of particle-laden jets in two-layer systems

On the other hand, jets of strong plunging regime initially plunge down to the bed and thus the top of the flow becomes negative relative to the jet exit. However, immediately after considerable settling occurs the jet flow begins to rise due to positive buoyancy of the interstitial fluid. Thus, the top of the final spreading layer converges along the density jump. Consequently, Eq.(5.7) has an asymptotic solution (c_4).

$$c_4 = \frac{Z_t}{h_i} = 0.9 \ (\pm 0.01) \qquad (5.11)$$

5.2.4.2 Spreading layer thickness

Particle-laden jets in penetration and impingement regimes behave like buoyant fluid jets and thus the spreading layer increases with $M^{3/4}/B^{1/2}h_i$ as discussed in Chapter 4. As particle concentration increases, the flow thickness increases significantly in the near field. However, once a considerable amount of particles settle out the final spreading layer thickness depends only on $M^{3/4}/B^{1/2}h_i$.

For strong plunging regime, jets plunge down and thus initially $B^{2/5}/g_a'^{3/5}h_i$ and h_i/H have little impact on the thickness of the spreading layer. However, the source momentum and dimensionless distance to the bed (h/d) are influential. Consequently, if h/d is constant, the dimensionless final layer thickness is a function only of $M^{3/4}/B^{1/2}h_i$ regardless of the flow regime:

$$\frac{T_f}{h_i} = f\left(\frac{M^{3/4}}{h_i B^{1/2}}\right) \tag{5.12}$$

Experimental results

Initially the spreading layer thickness varies along the trajectory due to particle sedimentation. However, as substantial sedimentation occurs the flow spreads out as a layer with a relatively constant thickness. Figure 5.10 shows the dimensionless spreading layer thickness after substantial settling has occurred.

For jets of impingement and weak plunging regimes, the spreading layer thickness increases with initial momentum and slightly with R. At a low source momentum R is influential, but it becomes insignificant as momentum increases. Neglecting the minor difference due to R and combining the two regimes, the relationship describing the spreading layer thickness is estimated to be:

$$\frac{T_f}{h_i} = 0.26\frac{M^{3/4}}{B^{1/2}h_i} + 0.96\ (\pm 0.4) \qquad (5.13)$$

For strong plunging regime it was impossible to obtain the final spreading layer thickness because the experimental tank was not long enough for the bottom turbidity current to lose sufficient particles and rise. However, the results imply that jets plunged down and the spreading layer became independent of the source momentum and was determined mostly by the detrainment of buoyant interstitial fluid from the bed.

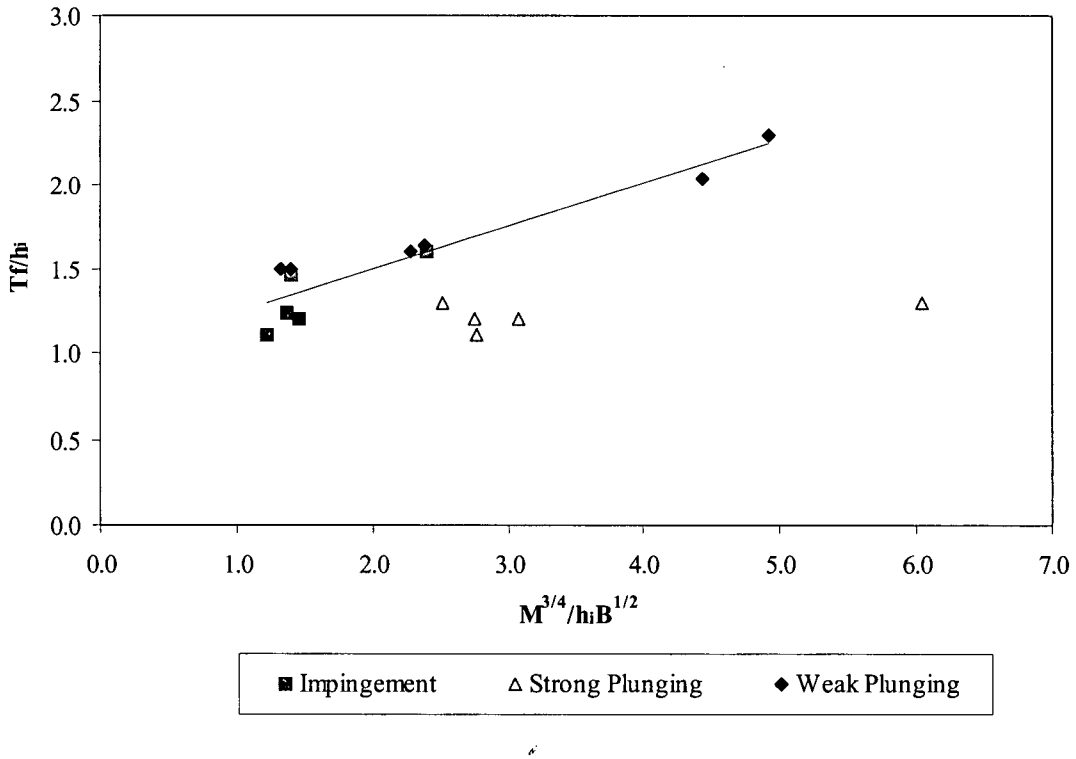

Figure 5.10 Dimensionless spreading layer thickness of particle-laden jets

5.2.5 Comparison with CORMIX prediction

CORMIX1 v3.2 was run to compare with the present experimental results and thus examine the suitability of the model for analyzing particle-laden jets. CORMIX1 was initially applied to fluid jets without particles and to 19 particle-laden jets in two-layer systems. The comparison was made in terms of classification of flow regimes and maximum (centerline) concentration of the jet flow.

5.2.5.1 Flow classification

CORMIX1 classified all particle-laden jets as Class NH1 or Class H4. Class NH1 describes submerged negatively buoyant jets discharged horizontally or near horizontally while Class H4 describes positively buoyant jets rises and impinges on the upper boundary of the ambient water

- If a jet is momentum-dominant near the nozzle, the initial discharge is usually attached to the bottom. After some distance, the jet flow is vertically mixed over the full layer depth and a re-circulating eddy regime may occur downstream (Jirka, et al 1996).

Penetration, impingement and weak plunging regimes in the present study are equivalent to CORMIX1 Class H4 and the strong plunging regime is equivalent to the CORMIX1 Class NH1. When the interstitial fluid density (ρ_f) was applied to the model, all flow regimes were determined as Class H4 as expected. However, the predicted flow class based on the initial bulk density ρ_b varied depending on R. Table 5.2 compares the flow regimes that CORMIX1 predicts using bulk density with the experimental results.

The CORMIX1 prediction agreed with the flow regime determined in this study for penetration impingement and strong plunging regime, defining them as Class NH1. In contrast, the model classified weak plunging regime as Class NH1, in which a jet is subject

to plunging down to the bottom. However, the experiments showed that these jets did not plunge to the bottom but only locally expanded downward and then spread as a gravity current as described in section 5.2.2.

Table 5.2 Comparison of CORMIX1 prediction and experimental results for flow classification

EXP #	Density ratio (R)	Flow classification	
		CORMIX prediction	Experiment results (Regime)
P20	0.63	H4	Penetration
P57	0.21	H4	Penetration
P59	0.38	H4	Penetration
P5	0.5	H4	Impingement
P19	0.54	H4	Impingement
P21	0.15	H4	Impingement
P24	0.12	H4	Impingement
P25	0.11	H4	Impingement
P9	-0.19	NH1	Weak Plunging
P16	-1.26	NH1	Weak Plunging
P8	-1.35	NH1	Weak Plunging
P22	-0.73	NH1	Weak Plunging
P58	-0.97	NH1	Weak Plunging
P60	-0.79	NH1	Weak Plunging
P18	-0.05	NH1	Strong Plunging
P23	-2.38	NH1	Strong Plunging
P7	-16.6	NH1	Strong Plunging
P10	-2.63	NH1	Strong Plunging
P17	-2.94	NH1	Strong Plunging

This discrepancy occurred because the model interprets the particle-laden jets as single-phase fluid (i.e. negatively buoyant fluid jets), not considering the density change due to particle sedimentation. Therefore, if the initial bulk density is smaller or larger than the ambient fluid density, the model simply classifies the flow as positive buoyant fluid (H4) or negatively buoyant flow (NH1) respectively.

This limitation can cause a significant prediction error if the model is applied to particle-laden jets, in particular, to heavy particle-laden jets with highly buoyant interstitial fluid.

5.2.5.2 Centerline concentration

CORMIX1 overestimated the dye concentration for all flow regimes, the difference increasing with R. In particular, the model overestimated the concentration significantly for strong plunging regime. As a particle-laden jet proceeded and particle settling continued, the error between the model prediction and the measurements decreased ($x/L = 0.19$). At $x/L = 0.31$ most particles settled out and the jet behaved like a fluid jet, the CORMIX1 prediction becoming closer to the measured concentration. However, for penetration regime and impingement, the model underestimated the dye concentration as in the case of fluid jets.

Figure 5.11 shows the relative error between the concentration predicted by CORMIX1 v3.2 and the measured values for particle-laden jets as the dimensionless density ratio R varied. The bulk density (ρ_b) was applied to the model and subsequently the model estimated and used the bulk buoyancy flux B_b. The relative error was calculated using:

$$E_R = \frac{(C_M - C_C)}{C_M} \tag{5.14}$$

where E_R: relative error

C_M: measured dye concentration

C_C: predicted dye concentration by CORMIX1

As described above, fluid jets and particle-laden jets of penetration and impingement regimes showed positive error and as R decreased, the error became negative.

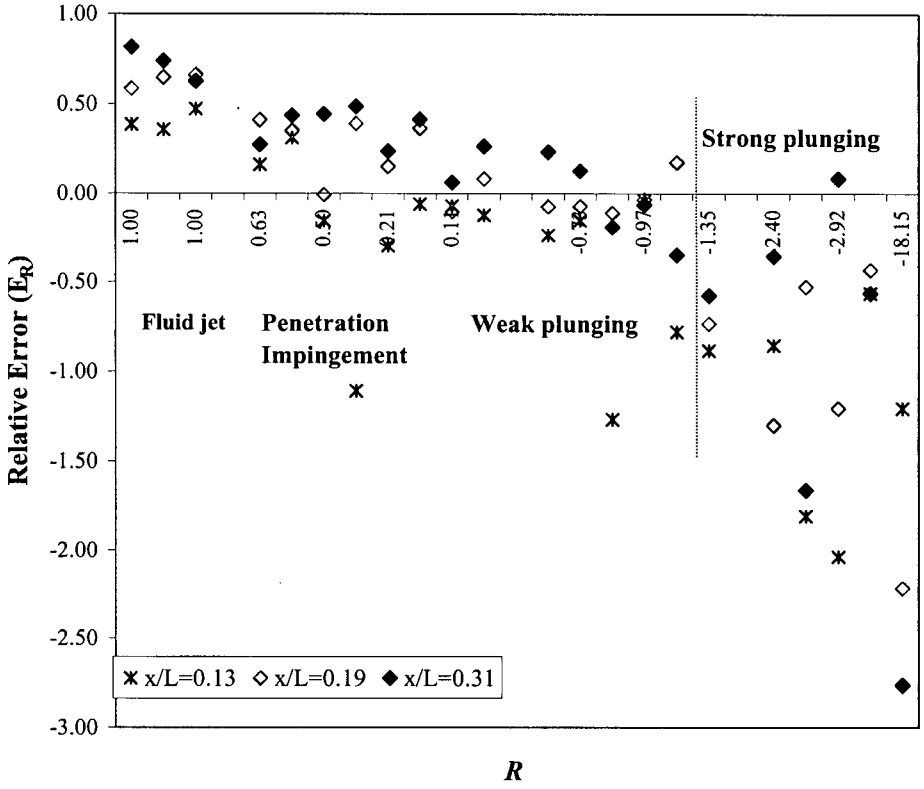

Figure 5.11 Relative error between the experimental results and CORMIX1 prediction

5.3 Summary of particle-laden jets

The behavior of particle-laden jets studied is summarized as follows. The difference between fluid jets and particle-laden jets are discussed in Chapter 6.

- At the source momentum-dominant zone, the jets behaved like fluid jets regardless of the particles. As jets proceeded, those with low particle concentration exhibited buoyant fluid-jet like behaviors, penetrating into the upper layer or strongly impinging on the

pycnocline and propagating horizontally. As particle concentration increased, jets initially plunged and proceeded like an intermediate jet or plunged down to the bottom and advanced like a turbidity current containing buoyant interstitial fluid.

- Four flow regimes of particle-laden jets were identified based on the density difference ratio R and Ψ.

  - Penetration Regime: the bulk density of a particle-laden jet (ρ_b) is smaller than the ambient fluid density (ρ_a) and the density interstitial fluid is significantly smaller than lower layer density. Thus the jet penetrates into the upper layer. This regime satisfies $0 < R < 1$ and $\Psi > 0.9$.

  - Impingement Regime: ρ_a is greater than ρ_b but the jet buoyancy is sufficiently low relative to the density step that penetration does not occur. Thus the jet strongly impinges on the pycnocline. Active particle settling occurs at the near field. This regime occurs when $0 < R < 1$ and $\Psi < 0.9$.

  - Weak Plunging Regime: this regime is transitional, exhibiting both buoyant fluid jet-like behavior and negatively buoyant jet behavior. The jets are initially heavier than the ambient fluid but not heavy enough to plunge down to the bottom. Abrupt group settling of particles and active detrainment of interstitial fluid occurs. The ambient condition is insignificant at the near field. This regime occurs when $-2.0 < R < 0$.

  - Strong Plunging Regime: Despite the positive buoyancy of interstitial fluid, jets plunge down to the bed and proceed along the bed slope due to having high bulk density. The ambient fluid condition is unimportant until sufficient interstitial fluid is released. This regime occurs when $R < -2.0$.

- Concentration profiles and particle distribution of the particle-laden jets showed that particles move with flow and a significant amount of particles were transported to the upper layer and traveled for a considerable distance during strong impingement and penetration.

- Dimensional analysis and the experimental results indicated that for penetration, impingement and weak plunging regimes, the dimensionless maximum rise height (Z_m/h_i) and the top of the spreading layer (Z_t/h_i) increases with $B^{2/5}/g_a'^{3/5}h_i$ while for Strong Plunging Regime the parameters converge to constants $c_3 = -3.0\,(\pm 0.01)$ and $c_4 = 0.9\,(\pm 0.01)$. The dimensionless final spreading layer thickness (T_f/h_i) depended only on $M^{3/4}/B^{1/2}h_i$ regardless of the flow regime. It was also found that penetration of particle-laden jets into the upper layer was prevented by the presence of particles regardless of the buoyancy of interstitial fluid.

- The CORMIX1 v3.2 predictions of flow classification agreed with the experimental results when the particle concentration was either very low (penetration and impingement regimes) or very high (strong plunging regime). However, for intermediate jets (weak plunging regime) the model predicted them to be plunging to the bed (strong plunging regime). In general, the model underestimated the dye concentration of fluid jets while overestimating for particle-laden jets.

Chapter 6

Comparison between Fluid Jet and Particle-laden Jet

This chapter discusses the difference in the flow characteristics of fluid jets and particle-laden jets. Comparisons are first made in the absence of the influence of ambient fluid. The effect of ambient fluid conditions on the two types of jet is then considered by comparing the results presented in Chapters 4 and 5.

6.1 Homogeneous ambient fluid

Observation of fluid jet and particle-laden jet behavior in homogeneous ambient fluid provides insight into the effect of particles on jet trajectory and the role of the ambient condition. Figure 6.1 (a)(b) shows the behavior of fluid jets and particle-laden jets in homogeneous ambient fluid. The density of the fluid jet is identical to that of the interstitial fluid of particle-laden jets and less than ambient fluid. Therefore, the density difference between the two jets is due only to the presence of particles.

At the near jet exit ($x/L = 0.04$) where the source momentum was still dominant, both the jets showed similar behavior. As the jets propagated, however, the fluid jet started to rise due to its positive buoyancy and propagated as a surface jet whereas the particle-laden jet initially sank due to high bulk density. Most interstitial fluid was incorporated into the

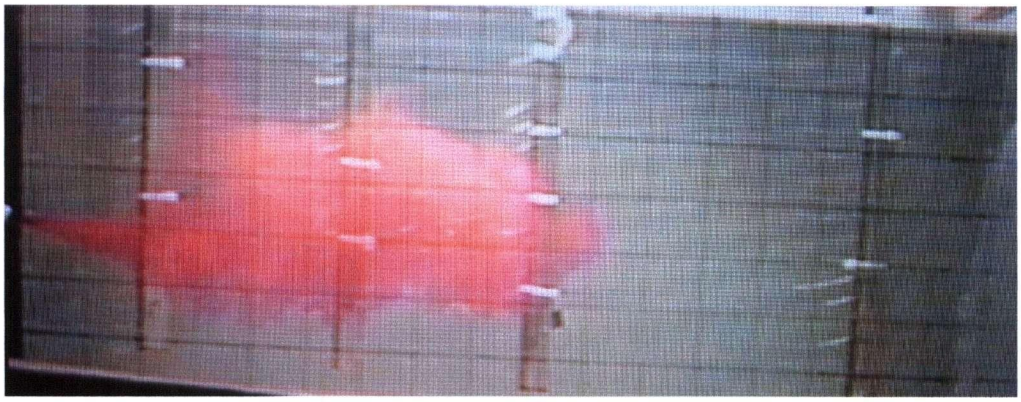

(i) t = 10 second

(ii) t = 32 second

Figure 6.1 (a) Behavior of a buoyant fluid jet in homogeneous ambient fluid (A47)

(i)

(ii)

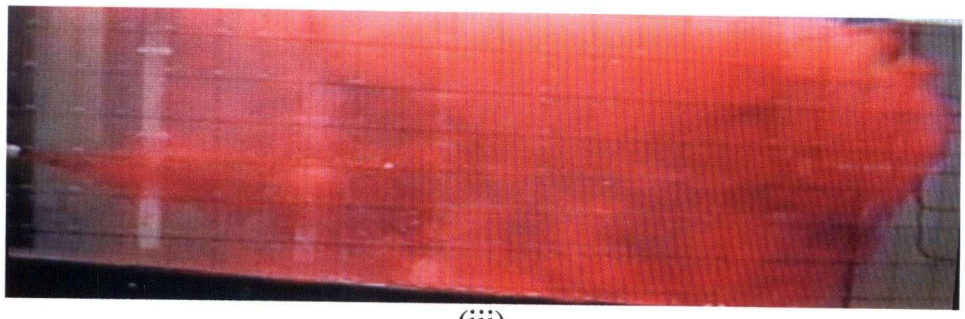

(iii)

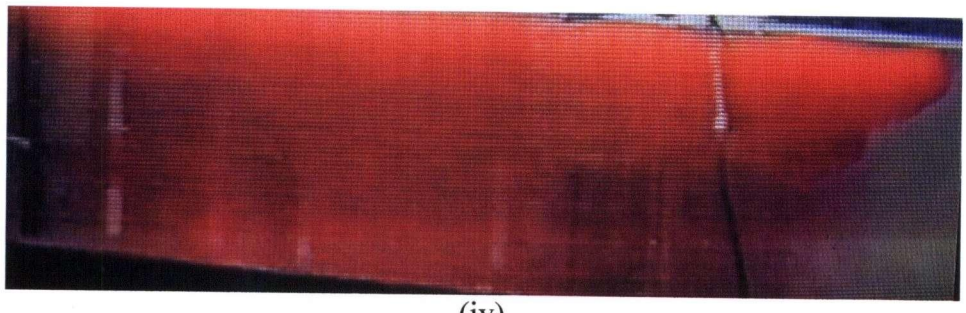

(iv)

Figure 6.1 (b) Behavior of a particle-laden jet with buoyant interstitial fluid in homogeneous ambient fluid: (i) momentum-dominant jet behavior, (ii) plunging, (iii) detrainment of interstitial fluid and bulk particle settling and (iv) forming a horizontal spreading layer after active particle settling (P61)

particle settling while the particle-free buoyant fluid at the upper boundary of the jet flow rose to its neutral buoyancy level. Consequently, the particle-laden jets occupied almost the entire water column in the near field. The fine particles constantly settled along the entire length of the tank but this had little impact on the jet trajectory. Far downstream, the final spreading layer formed near the surface like fluid jets. Figure 6.2 shows the dye concentration profile for each case. The profiles agree with the description of the jets above. Two flows behave similarly until $x/L = 0.13$ but at $x/L = 0.19$ the fluid jet rises rapidly to the surface.

6.2 Two-layer system

6.2.1 Maximum rise height and penetration

The primary concern is the height of rise and the possibility of penetration of a buoyant jet in a two-layer system. Figure 6.3 shows the dimensionless maximum rise height for fluid and particle-laden jets in two layer systems. In general, only minor differences occurred in maximum rise height and penetration for Penetration and Impingement Regimes. Also, Weak Plunging regime appeared to rise slightly less than the corresponding fluid jets.

However, jets of Strong Plunging Regime plunged down to the bed and propagated along the bed slope regardless of Ψ. This behavior is the main difference between the two jets. Even for the penetration regime where the interstitial fluid is highly buoyant, jets plunged to the bottom. For example, although P7 ($\Psi = 1.3$) and P23 ($\Psi = 0.99$) could penetrate into the upper layer but jets plunged down to the bed due to particles. This implies that the presence of particles in flow above a certain concentration in flow can prevent buoyant interstitial fluid from penetrating into the upper layer. Otherwise, the jet would penetrate and spread out in the upper layer.

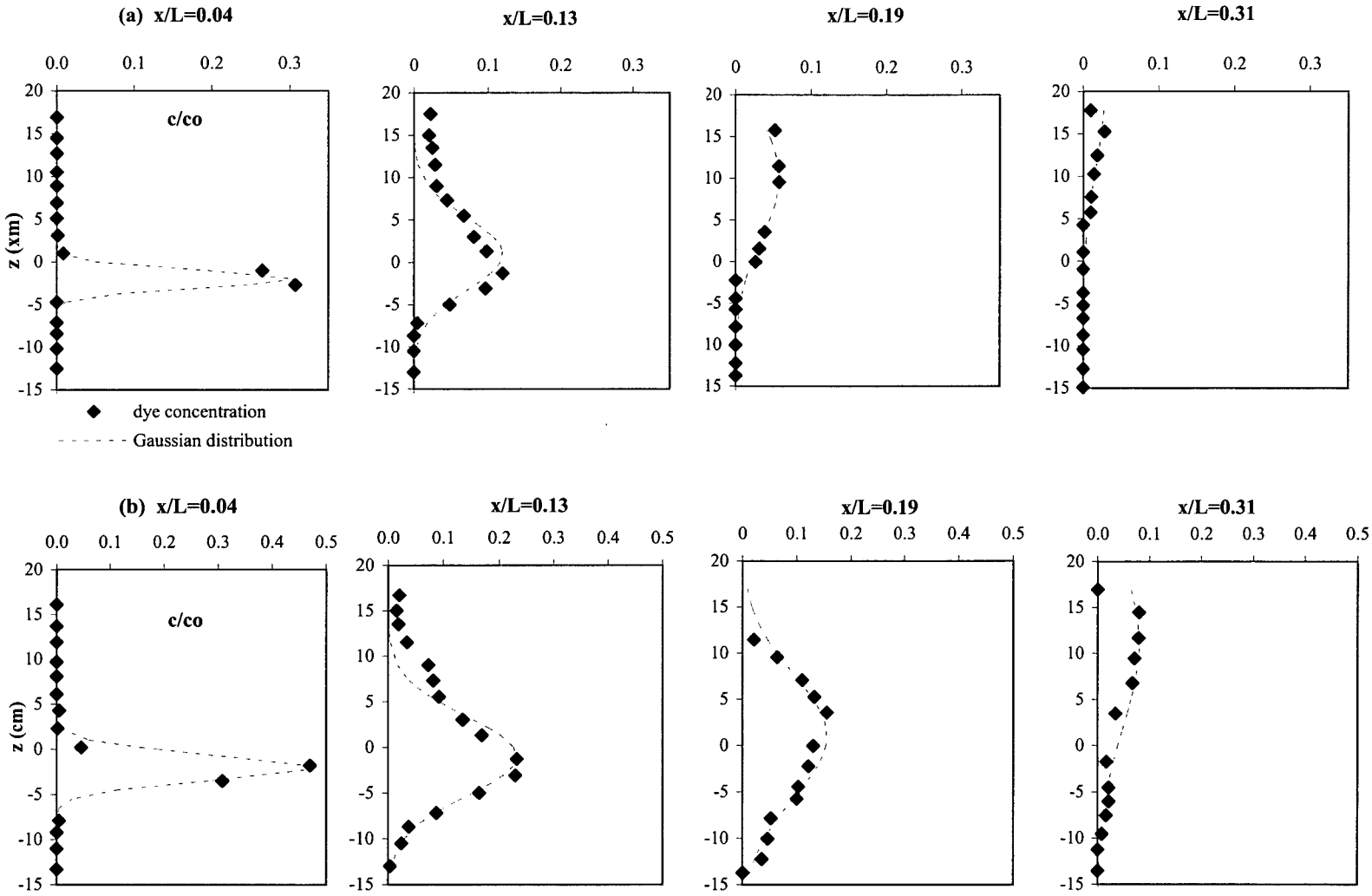

Figure 6.2 Dye concentration profiles and Gaussian distributions of (a) a fluid jet (A48) and (b) a particle-laden jet (P55) in homogeneous ambient fluid

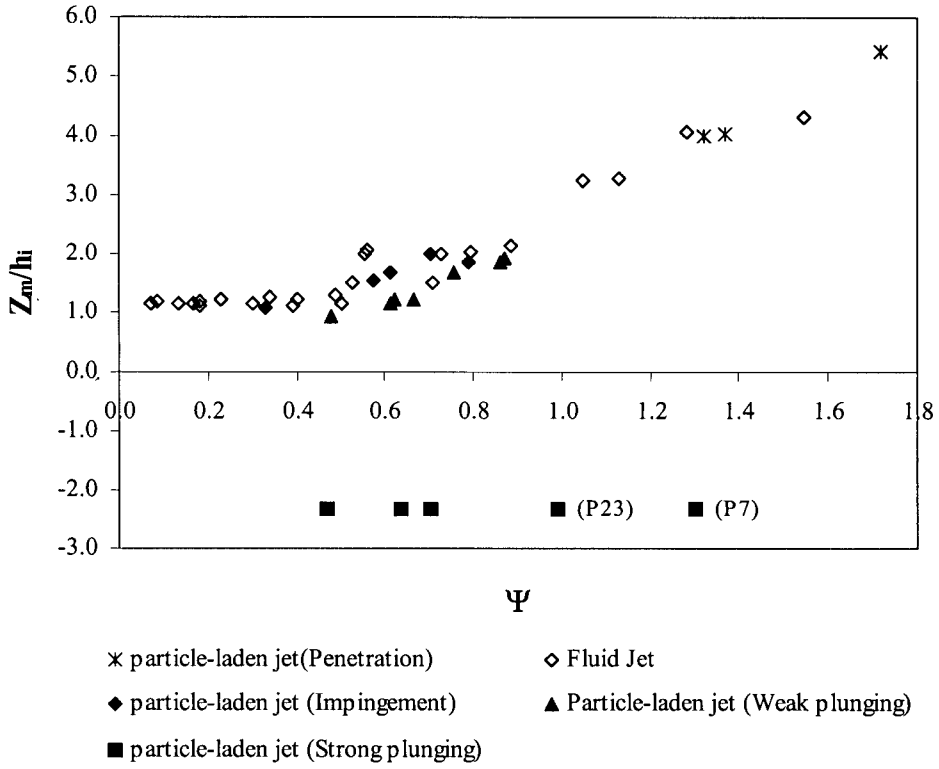

Figure 6.3 Comparison of the maximum rise height (Z_m/h_i) between fluid jets and particle-laden jets in two-layer systems

6.2.2 Top of the spreading layer

In the strong impingement regime, Z_t/h_1 for the fluid jets increased linearly with Ψ as shown in Figure 6.4. The particle-laden jets of Impingement and Weak Plunging Regimes did not rise as high as the fluid jets. In addition, the jets of Strong Plunging Regime released buoyant interstitial fluid during instantaneous plunging and the interstitial fluid constantly entrained heavy ambient fluid. Eventually, the top of the final spreading layer was trapped under the pycnocline, which is another unique characteristic of particle-laden jets relative to the fluid jets.

The results also indicate that the difference in the top of the spreading layer between fluid jets and particle-laden jets is larger than that of the maximum rise height. It is because the maximum rise height occurs before significant settling occurs, and thus the buoyancy of the interstitial fluid of particle-laden jets is still as large as in fluid jets. However, the final spreading layer forms further downstream after the settling and thus the interstitial fluid entrains more heavy fluid in the lower layer. Consequently, as the particle concentration increases, the top of the spreading layer tends to lower.

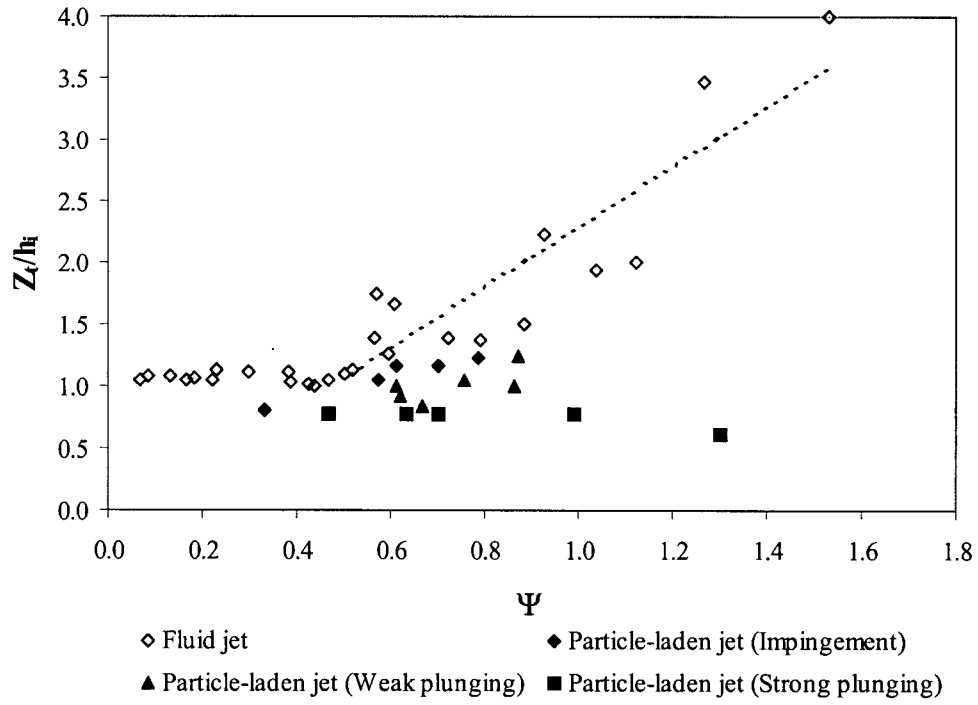

Figure 6.4 Comparison of the top of the spreading layer (Z_t/h_i) between fluid jets and particle-laden jets in two-layer systems

6.2.3 Spreading layer thickness

The particle-laden jets formed an abrupt thick spreading layer in the vicinity of the

nozzle compared to fluid jets. However, surprisingly, the particles exerted little impact on the final spreading layer thickness. Figure 6.5 compares the final spreading layer thickness between fluid jets and particle-laden jets showing that both jets increased with dimensionless parameter $M^{3/4}/h_1 B^{1/2}$. At low $M^{3/4}/h_1 B^{1/2}$, Weak Plunging Regime appeared to have only a slightly thicker spreading layer compared with fluid jets and jets of Weak Plunging Regime, implying the effect of particle presence on the final spreading layer was insignificant.

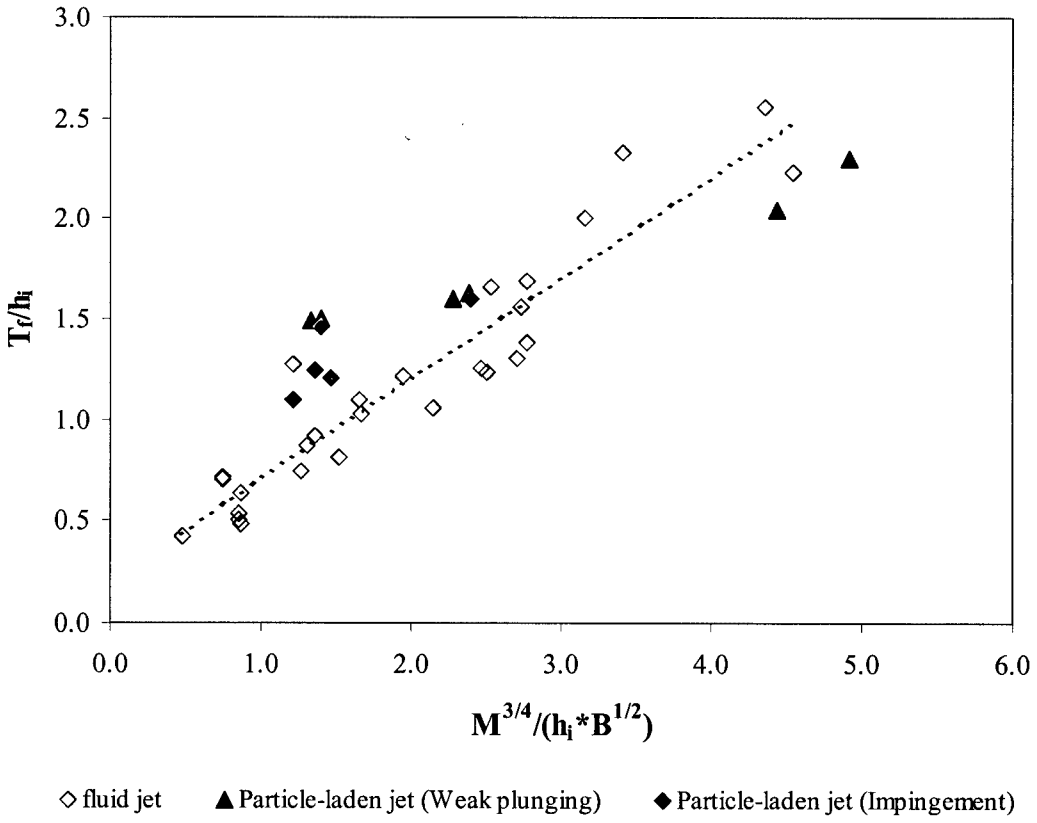

Figure 6.5 Comparison of the spreading layer thickness (T_f/h_i) of fluid jets and particle-laden jets in two-layer systems

Chapter 7

Conclusions and Recommendations

7.1 Conclusions

The dynamics of buoyant fluid jets and particle-laden jets discharged into two-layered stagnant ambient fluid were studied through a series of experiments and analysis. The following conclusions were drawn from this investigation.

7.1.1 Buoyant fluid jets in two-layer system

Three parameters were identified to have crucial influence on the buoyant jet behavior in two-layer systems: buoyancy of the jet fluid B, the magnitude of the density step expressed as a modified gravitational acceleration (g_a') and the distance of discharge exit to the pycnocline h_i. A useful dimensionless parameter $\Psi = \frac{B^{2/5}}{g_a'^{3/5} h_i}$ was found by combining these three parameters.

The following flow regimes were identified based on Ψ.

- $\Psi < 0.5$: buoyant jets rose and impinged on the pycnocline weakly, causing no density change in the upper layer. Immediately after impingement, the jet advanced horizontally under the pycnocline, entraining the lower layer fluid.

- $0.5 < \Psi < 0.9$: buoyant jets impinged strongly on the pycnocline but did not penetrate into the upper layer. The upper layer was significantly disturbed and the jet

entrained lower layer fluid which was transported into and mixed with the upper layer.

- $\Psi > 0.9$: buoyant jets penetrated into the upper layer. On penetration, rapid vertical growth occurred and a spreading layer proceeded in the upper layer. A density increase occurred at the surface of the upper layer due to the entrained fluid from the lower layer. Once a jet penetrates it spreads above the pycnocline, which is an important issue for the water quality in the upper layer.

A small discharge angle (-3°) was found to result in insignificant difference in jet behavior relative to horizontal jets (0°).

Occurrence of backflows was estimated theoretically and confirmed by experiments. Backflow was found to occur along the pycnocline depending on the relative magnitude of vertical buoyancy flux and the source momentum flux. The relative strength of the two momentum fluxes was found to determine jet angles at the pycnocline. When the estimated jet angles at the pycnocline were greater than 7° backflows occurred but when $\theta_p < 7^o$ no backflow occurred. For the penetration regime, $\Psi > 0.9$, some jet flow accumulated along the pycnocline and backflows also formed at the surface of the upper layer.

The ambient fluid condition near the jet appeared to have no influence on Coanda bottom attachment. The bottom attachment occurred at $h/\ell_M < 0.22$ for all the given experimental conditions. The Coanda effect is a beneficial phenomenon for buoyant wastewater discharged under the pycnocline. This is because discharge flow stays longer in the lower layer, entraining more heavy ambient fluid, resulting in a reduced possibility of penetration.

The dimensionless maximum rise height and the top of the spreading layer were found to be constant in the weak impingement regime, whereas they increased with Ψ in the strong impingement regime. The spreading layer thickness was independent of the presence

and the strength of the density step and increased with a dimensionless parameter $M^{3/4}/h_1 B^{1/2}$. The location of the maximum rise height (X_m) increased with the densimetric Froude number.

7.1.2 Particle-laden jets in two-layer system

The initial concentration of particles was found to have a significant influence on the behavior of particle-laden jets. Jets with low particle concentration behaved like buoyant fluid jets whereas those with high particle concentration behaved like negatively buoyant jets regardless of interstitial fluid buoyancy. Particles tended to be carried by the interstitial fluid and transported downward.

For the source momentum dominant zone, the effect of particles on the jet behavior was insignificant. However, as source momentum decayed the flow pattern was controlled by the particle concentration, interstitial fluid density and ambient fluid density. A density difference ratio R was found to be the most important factor determining the initial dynamics of particle-laden jets. The critical value R_c was found to be –2.0, under which the particle-laden jets plunged to the bed despite the interstitial fluid being highly buoyant.

The behavior of particle-laden jets were categorized into four flow regimes depending on the critical dimensionless density R and Ψ . The regimes were as follows:

- Penetration Regime was defined as flow behavior characterized by jet penetration. For the conditions $0 < R < 1$, particle-laden jets behaved like fluid jets regardless of the presence of particles. If $\Psi > 0.9$, jets penetrate into the upper layer.

- Impingement Regime was defined as flow behavior characterized by strong impingement without penetration. The conditions $0 < R < 1$ and $\Psi < 0.9$ were satisfied and active separation of individual particles from the interstitial fluid

occurred. However, the general behavior was similar to that of buoyant fluid jets.

- Weak Plunging Regime was defined as flow behavior where the presence of particles began to exert a significant impact on the flow patterns. This transitional regime occurred for $-2.0 < R < 0$ and involved abrupt group settling and active detrainment of interstitial fluid. The influence of the ambient fluid condition was insignificant in the vicinity of the discharge exit.

- Strong Plunging Regime was defined as flow behavior with particle-laden jets that rapidly plunged down to the bed and advanced as a turbidity current and for which $-2.0 < R$. The ambient fluid condition had no influence on the flow pattern until the buoyant interstitial fluid rose from the bottom current.

The dimensionless maximum rise height and the top of the spreading layer increased with Ψ for particle-laden jets of Penetration, Impingement and Weak Plunging Regimes. However, the jets plunged to the bottom for the Strong Plunging Regime while the top of the spreading layer was highly dependent on detrainment of interstitial fluid and converged along the pycnocline. Moreover, the high particle concentration effectively prevented buoyant interstitial fluid from penetrating into the upper layer. On the other hand, the thickness of spreading layer was found only to be a function of the dimensionless parameter $M^{3/4}/B^{1/2}h_1$, after abrupt particle settling occurred.

A substantial proportion of the particles and of the lower layer fluid were found to transport into the upper layer and travel for a considerable horizontal distance during strong impingement and penetration.

The CORMIX1 v3.2 prediction on flow classification was incorrect for the intermediate jets (Weak Plunging Regime), predicting them as plunging jets (Strong Plunging Regime). The model underestimated the dye concentration of fluid jets but

overestimated for particle-laden jets. When most particles settled, adversely, the model underestimated the dye concentration of particle-laden jets. Therefore, using CORMIX1 to predict two-phase flow characteristics is questionable.

7.2 Contributions

- This research increases our knowledge of the behavior of buoyant discharge flow in two-layer stagnant ambient fluid. It was found that buoyant jets can either penetrate into the upper layer during discharge or only impinge on the density step but spread horizontally, depending on the source and the ambient fluid conditions. The penetration of a jet flow can cause serious problems for real-world disposal of wastewater. A useful dimensionless parameter was identified by combining most influential parameters. This parameter can be applied in practice to predict the trajectory of discharge in two–layer structured receiving water. It allows discharge conditions to be identified that prevent the penetration of highly buoyant discharge into the upper layer and minimize the disturbance of the slurry layer in a tailings pond. In addition, the analysis of the gross flow characteristics based on the dimensional analysis and experimental results provide a basis for predicting the gross spreading behavior of buoyant jets such as the maximum rise height, top of the spreading layer and final spreading layer thickness.

- The present study also provides insights into the significance of the presence of particles in the discharge, in particular for particle-laden jets with high particle concentration. Flow regimes of particle-laden jets depending on discharge conditions were identified which allow us to predict whether the particle-laden jets behave like fluid jets or negatively buoyant fluid in the near field. The practical significance of this is that the penetration of buoyant discharge flow may be prevented simply by adding sufficient fine particles to the jet. Although eventually the interstitial fluid rises, the constant entrainment of heavy fluid in the lower layer increases the density of the jet fluid. Thus disturbance of the upper layer due to discharge activity becomes insignificant, which is a benefit for

tailings disposal below the pycnocline.

- The experimental results indicated that the CORMIX1 v3.2 model is unsuitable for predicting two-phase negative buoyant jets. Thus, the unique flow behavior due to the particles in two-phase flow is not captured by the model, which may result in significant error in predictions at near-field.

7.3 Recommendations for further research

For a better understanding of the physical processes in buoyant fluid jets and particle-laden jets, the following recommendations for future research are made:

- Large scale experimental facility: it is necessary to perform the experiments in a sufficiently long and wide experimental tank to achieve the fully developed steady-state and to obtain sufficient measurement time and to avoid side and end wall effects. It is also necessary to use various discharge nozzles and thus examine the effect of the initial volume flux on the jet dynamics. A sufficiently powerful pump should be used to prevent separation of particles from the interstitial fluid in the pipe during discharge, especially for the jets with high particle concentration.

- Realistic ambient conditions: in order to simulate realistic ambient conditions, the ambient turbulence or crossflow should be considered. Also, a two-layer system with linearly stratified lower layer should be simulated.

- Discharge angles and bottom slopes: the effect of various discharge angles including horizontal direction and bottom slope on particle-laden jets and fluid jets should be investigated.

- Discharge above the pycnocline: To investigate the possibility of tailings disposal into the upper layer, it is useful to conduct experiments on the discharge of particle-laden jets above the pycnocline.

- Velocity profile: vertical velocity distribution along the jet trajectory should be measured to identify the effect of particles on the flow field and especially the relation between particle concentration and velocity distribution.

- Particle-size distribution and types: various sizes and types of particles (i.e. actual soils or tailings) should be tested to obtain practically useful results.

- Theoretical studies on particle-laden jets should be conducted including not only individual particle settling but also bulk (grouped) settling behavior.

- Implications for prototype such as the effect of viscosity due to increased Reynolds number in the lower layer should be tested.

- Investigation whether the two dimensionless parameters, R and Ψ can be combined is recommended.

- Further study on turbulent particle-laden jets in linearly stratified ambient fluid is also recommended.

References

Abraham, G., Horizontal jets in stagnant fluids of other density, Journal of the Hydraulic Division, ASCE, Vol. 90, No. HY4, Proceeding paper 4411, pp. 139-154, 1965a

Abraham, G., Entrainment principles and its restrictions to solve problems of jets, Journal of the Hydraulic Research, Vol. 3, No. 2, pp. 2-23, 1965b

Baines, W. D., Entrainment by a plume or jet at a density interface, Journal of fluid Mechanics, Vol. 68, Part 2, pp. 309-320, 1975

Baines, W. D., and Hopfinger, E. J., Thermals with large density difference, Atmospheric Environmental Science, Vol. 18, No. 6, pp. 1051-1067, 1984

Balasubramanian V. and Jain S. C., Horizontal buoyant jets in quiescent shallow water, Journal of the Environmental Engineering Division, Vol. 104, No. EE4, pp. 717-730, 1978

Bonnecaze, R. T., Huppert, H. E., and Lister, J. R., Particle-driven gravity currents, Journal of Fluid Mechanics, Vol. 250, pp. 339-369, 1993

Britter, R. E. and Simpson. J. E., A note on the structure of the head of an intrusive gravity current, Journal of Fluid Mechanics, Vol. 112, pp. 459-466, 1981

Brooks N. H., Synthesis of stratified flow phenomena for design of outfalls, Proceedings of the Second International Symposium on Stratified Flows, Norway, pp. 809-831, 1980

Carey, S. N., and Sigurdsson, H., Experimental Studies of particle-laden plumes, Journal of Geophysical Research, Vol. 93, No. B12, pp. 15,314, 1988

Darden R. B., Imberger, J., Fischer, H. B., Jet discharge into a stratified reservoir, Journal of Hydraulics Division, ASCE, Vol. 101, No. HY9, pp. 1211- 1220, 1975

Dietrich, W. E., Settling velocity of natural particles, Water Resources Research, Vol. 18, No. 6, pp. 1615-1626, 1982

Doneker, R. L. and Jirka, G. H., Expert systems for mixing zone analysis and design of pollutant discharge, Journal of Water Resources Planning and Management, Vol.117, No. 6, pp. 679 - 697, 1991

Fan, L. N. and Brooks. N. H., horizontal jets in stagnant fluid of other density, Journal of the Hydraulic Division, pp. 423-429, 1966

Fan, L-N and Brooks, N., Numerical solutions of turbulent buoyant jet problems, W.M. Keck Laboratory of Hydraulics and Water resources Division of Engineering and Applied Science, California Institute of Technology, Pasadena, California, Report No. KH-R-18, 1969

Fischer, H. B., List, J. E., Koh, R. C. Y, Imberger, J., Brooks, N. H., Mixing in Inland and Coastal Waters, London, Academic Press, 1979

Fischer, H. B. and Smith, R. D., Observations of transport to surface waters from a plunging inflow to Lake Mead, Limnology and Oceanography, Vol. 28, No 2, pp. 258-272, 1983

Goldschmidt, V. W., Householder, M. K., Ahamadi, G and Chuang, S. C., Turbulent diffusion of small particles suspended in turbulent jets, Progress in Heat and Mass transfer, Vol. 6, pp.487-508, 1972

Green T. The importance of double diffusion to the settling of suspended material, Sedimentology, Vol. 34, pp.319-331, 1987

Gu, R. and Stefan H. G., Analysis of turbulent buoyant jet in density stratified water, Journal of Environmental Engineering, Vol. 114, No. 4, pp. 878-897, 1988a

Gu, R. and Stefan H. G., Mixing of temperature-stratified lakes and reservoirs by buoyant jets, Journal of Environmental Engineering, Vol. 114, No.4, pp.898-913, 1988b

Hallworth M. A., Huppert H. E., Abrupt transitions in high-concentration, particle-driven gravity currents, Physics of Fluids, Vol. 10 (5), pp. 1083-1087, 1998

Hallworth M. A., Huppert H. E., Phillips J. C., Sparks R. S. J., Entrainment into two-dimensional and axisymmetric turbulent gravity currents, Journal of Fluid Mechanics Vol. 308 pp. 289-311, 1996

Hallworth, M. A., Hogg, A. J. and Huppert H. E., Effects of external flow on compositional and particle gravity currents, Journal of Fluid Mechanics, Vol. 359, pp.109-142, 1998

Head M. J., The use of miniature four-electrode conductivity probes for high resolution measurement of turbulent density or temperature variations in salt stratified water flows, Ph.D. dissertation, University of California, San Diego, 1983

Hinze, J. O., Turbulent fluid and particle interaction, Progress in Heat and Mass Transfer, Vol. 6, pp. 433-452, 1972

Hirst, E., Buoyant jet with three dimensional trajectories, Journal of the Hydraulics Division, Vol. 98, No HY11, pp. 1999-2014, November, 1972

Hofer, K. and Hutter, K., Turbulent jet diffusion in stratified quiescent ambient, part II; experiments, Journal of non-Equilibrium Thermodynamics, Vol. 6, pp. 49-64, 1981

Hogg A. J., Huppert H. E., Hallworth M. A., Reversing buoyancy of particle-driven gravity currents, Physics of Fluids, Vol. 11(10), pp. 2891-2900, 1999

Holly, F. M., and Grace, J. L., model study of dense jet in flowing fluid, Journal of the Hydraulic Division, ASCE, Vol. 98, NO. HY11, pp. 1922-1932, 1972

Holyer, J. Y. and Huppert, H. E., Gravity currents entering a two-layer fluid, Journal of Fluid Mechanics, Vol. 100, part 4, pp. 739-767, 1980

Huppert, H. E., Kerr, R. C., Lister, J. R. and Turner, J. S., Convection and particle entrainment driven by differential sedimentation, Journal of Fluid Mechanics, Vol. 226, pp. 349-369, 1991

Huppert H. E., Turner J. S., Hallworth, M. A., Sedimentation and mixing of a turbulent fluid suspension – A laboratory study, Earth and Planetary Science Letters, Vol. 114 (2-3), pp. 259-267, 1993

Huppert H. E., Turner J. S., Hallworth, M. A. Sedimentation and entrainment in dense layers of suspended particles stirred by an oscillating grid, Journal of Fluid Mechanics, Vol. 289, pp. 263-293, 1995

Hürzeler, B. E., Turbidity currents with reversing buoyancy, A thesis of the Degree of Doctor of Philosophy, Department of Environmental Engineering, University of Western Australia, 1994

Hürzeler, B. E., Imberger, J. and Ivey G. N., Dynamics of turbidity current with reversing buoyancy, Journal of Hydraulic Engineering, Vol. 122, No. 5, pp. 230-236, 1996

Ilic, V., Vincent, J. J., Zhang, R. and Phan-thien, N., sedimentation velocity of some complex-shaped particles in newtonian and non-newtonian liquids, 11th Australian Fluid Mechanics conference, University of Tasmania, Hobart, Australia, December, 1992

Jirka G. H., and Doneker, R. L., Hydrodynamic classification of submerged single-port discharges, Journal of Hydraulic Engineering, Vol. 117, No. 9, pp.1095-1128, 1991

Jirka, G. H. Doneker, R. L. and Hinton, S. W., User's Manual for CORMIX: A hydrodynamic mixing zone model and decision support system for pollutant discharge into surface waters, Prepared for the U.S. Environmental Protection Agency by Defree Hydraulics Laboratory, School of Civil and Environmental Engineering, Cornell University, Ithaca, New York, 1996

Johnson, T. R., Ellis, C. R., Stefan, H. G., "Negatively buoyant flow in diverging channel. IV: entrainment and dilution, Journal of Hydraulic Engineering, Vol. 115, No.4, pp. 437-456, 1989

Johnston, A. J. and Volker, R. E, Round buoyant jet entering shallow water, Journal of Hydraulic Research, Vol.31, No.1, pp. 121-138, 1993

Johnston, A. J., Nguyen, N. and Volker, R. E., Round buoyant jet entering shallow water in motion, Journal of Hydraulic Engineering, Vol. 119, No.12, pp. 1364-1382, 1994a

Johnston, A. J., Philips, C. R., and Volker, R. E., Modeling horizontal buoyant jets in shallow water, Journal of Hydraulic Engineering, Vol. 120, No.1, pp. 41-57, 1994b

Kada, H. and Hanratty, Th. J., AICHE J., Vol. 6, pp. 624, 1960

Koh, R. C. Y. and Brooks, N. H., Fluid mechanics of waste-water disposal in the ocean, Annual Review of Fluid Mechanics, pp. 187-207, 1975

Koh, R. C. Y., and Chang, Y. C., Numerical model for barged ocean disposal of wastes, Prepared for the U.S Environmental Protection Agency, Washington, DC, 1973

Kumagai, M., Turbulent buoyant convection from a source in a confined two-layered region, Journal of Fluid Mechanics, Vol. 147, pp. 105-131, 1984

Lawrence, G. A., Ward, P. R. B., MacKinnon, M. D., wind-wave induced suspension of mine tailings in disposal ponds - A case study", Canadian Journal of Civil Engineering, Vol. 18, pp. 1047 – 1053, 1991

Lee, J. H. W. and Jirka, G. H., Vertical jet in shallow water, Journal of the Hydraulic Division, Vol. 107, No. Hy12, pp. 1651-1675, 1981

Lee, J. H. W. and Cheung, V. W. L., Inclined plane buoyant jet in stratified fluid, Journal of Hydraulic Engineering, Vol.112, No. 7, pp. 580-589, 1986

List, E. J. and Imberger, J., Turbulent entrainment in buoyant jets and plumes, Journal of the Hydraulics Division, Vol. 99, pp. 1461-1474, 1973

MacKinnon, M. D., Development of the tailings pond at Syncrude's Oil sands plant: 1978-1987, AOSTRA Journal of Research, Vol. 5, pp. 109-133, 1989

Manins, P. C., Intrusion into a stratified fluid, Journal of Fluid Mechanics, Vol. 74, part 3, pp. 547-560, 1976

McCorquodale, J. A., Zhou, S. P., Moawad, A., Yuen, E-M., Rajaratnam, N., Near field modeling in the connecting channels of the Great Lakes, The Industrial Research Institute of the University of Windsor for Ontario Ministry of the Environment Great Lakes Branch, 1992

Maxworthy, T., Experimental and theoretical studies of horizontal jets in a stratified fluid, International Symposium on Stratified Flows, pp. 611-618, 1973

Noh, Y. and Fernando, H. J. S., the transition in the sedimentation pattern of a particle cloud, Physics of Fluids, Vol. 5, No 12, pp. 3049-3055, 1993

Owen, P. R., Journal of Fluid Mechanics, Vol. 39, pp. 407, 1969

Petroleum Communication Foundation, Canada's oil sands and heavy oil, April, 2000

Popper, J., Abuaf, N. and Hetsroni, G., Velocity measurements in a two-phase turbulent jet, International Journal of Multiphase Flow, Vol. 1, pp. 715-726, 1974

Proni, J. R. and Hansen, D. V., Dispersion of particulates in the ocean studies acoustically: The importance of gradient surfaces in the ocean, Ocean Dumping of Industrial Wastes, Plenum Press, New York, pp. 161-173, 1981

Rahimipour H. and D. Wilkinson, Dynamic behavior of particle clouds. Proceedings of the 11th Australian Fluid Mechanics. Conf. University of Tasmania, Hobart, Australia, December, pp. 743-746, 1992

Rajaratnam, N., Turbulent jets, Elsevier Scientific Publishing Company, Amsterdam, 1976

Roberts, P. J. W., Two stratified jets in linearly stratified fluid se jets in flowing current, Journal of Hydraulic Engineering, Vol. 113, No. 3, pp. 323-341, 2001

Roberts, P. J. W., Behavior of low buoyancy jets in linearly stratified fluid, Journal of Hydraulic Research, Vol. 25, No. 4, pp. 503-519, 1987

Roberts, P. J. W. and Matthews, R. R., Mixing in pumped storage reservoirs, Applying research to Hydraulic Practice, pp. 199 –205, 1982

Roberts, P. J. W., Matthews, P. R., Dynamics of jets in two-layered stratified fluids, Journal of Hydraulic Engineering, Vol. 110, No. 9, pp. 1201-1217, 1984
Rooij de F., Linden, P. F. and Dalziel, S. B., Saline and particle–driven interfacial intrusions, Journal of Fluid Mechanics, Vol. 389, pp. 303-334, 1999

Ruggaber, G. J., Dynamics of particle clouds related to open-water sediment disposal, A thesis submitted to the Department of Civil Engineering in partial fulfillment of the requirements for the degree of doctor of philosophy at the Massachusetts Institute of Technology, 2000

Ruggaber, G. J. and Adams E. E., Influential of initial conditions on particle clouds entrainment, The fifth of international symposium on stratified flow, Vol. 1, University of British Columbia, Vancouver, Canada, July, 2000

Schneider, H. H., Laboratory experiments to simulate the jet-induced erosion of pycnoclines in lakes, Second international Symposium on Stratified Flows, pp. 697-706, 1980

Schmidt, N, P., Generation, propagation and dissipation of second mode internal solitary waves, Ph.D. Thesis, University of Canterbury, New Zealand, 1997

Sharp, J. J. and Vyas, B. D., The buoyant wall jet, Proceedings of international Civil Engineers, part 2, Vol. 63, pp. 593-611, 1977

Simpson, J. E., Gravity currents in the laboratory, atmosphere and ocean, Annual Review of Fluid Mechanics, Vol. 14, pp. 213-234, 1982

Sobey R. J. and Johnston, A. J., and Keane, R. D., Horizontal round buoyant jet in shallow water, Journal of Hydraulic Engineering, Vol. 114, No. 8, pp. 910-929, 1988

Sparks, R. S. J., Bonnecaze, R.T., Huppert, H. E., Lister, J.R, Hallworth, M. A., Mader, H., and Phillips J, Sediment–laden gravity currents with reversing buoyancy, Earth and Planetary Science Letters, 114, pp. 243-257, 1993

Turner, J. S., Buoyancy effects in Fluid, Cambridge University Press, 1973

Turner, J. S., Turbulent entrainment: The development of the entrainment assumption, and its application to geophysical flows, Journal of Fluid Mechanics, Vol. 173, pp.431-471, 1986

Turner J. S. and Huppert, H. E., Sedimentation and mixing at the top of a suspended particles, Proceedings of the 11th Australian Fluid Mechanics. Conf. University of Tasmania, Hobart, Australia, December, pp. 747-750, 1992

Wallace, R. B. and Wright, S. J., Spreading layer of two-dimensional buoyant jet, Journal of Hydraulic Engineering, Vol. 110, No 6, pp. 813-828, 1984

Ward, P. R. B. Personal communication, 2001

Ward, P. R. B., Lawrence, G. A., MacKinnon, M. D., Wind driven resuspension of sediment in a large tailings pond, Proceedings of International Symposium on Ecology and Engineering, VI-37 – 12, 1994

Weast, R. C., CRC Handbook of Chemistry and Physics, CRC Press Inc., 66th edition: 1985-1986, 1985

Wong, D. R. and Wright S. J., Submerged turbulent jets in stagnant linearly stratified fluids, Journal of the Research, Vol. 26, No.2, pp. 199-223, 1988

Wong, D. R., Buoyant jet entrainment of stratified fluids, Ph.D. Dissertation, The University of Michigan, Ann Arbor, 1984

Wood, I. R., Bell, R. G., and Wilkinson, D. L., Ocean disposal of wastewater, World Scientific Publishing Co. Pte. Ltd, 1993

Wright, S. J. and Wallace, R. B., Two-dimensional jets in stratified fluid, Annual Review of Fluid Mechanics, Vol. 105, pp. 1393-1405, 1979

Appendix A

Buoyant jets in linearly stratified ambient fluid

This section presents the results of experiments on buoyant jets discharged at 3° downward in stagnant linearly stratified fluids. The gross flow characteristics of buoyant jets are examined in terms of the maximum rise height, the top of the spreading layer and the spreading layer thickness. The results are presented in terms of dimensionless length scales and compared with previous studies. A total of 14 experiments were performed and the source and ambient condition were $8.7 < F_d < 55.5$ and $0.58 < N < 0.78\ s^{-1}$.

A.1 Behavior of buoyant jets

Figure A.1 presents photographs of buoyant jets under two different source conditions discharged at 3 degree downward. The flow images show that in a linearly stratified ambient fluid, initially a buoyant jet grows linearly with distance near the jet exit, as is the case in a homogeneous ambient fluid. However, the ambient stratification constantly suppresses the vertical turbulent motion and the buoyant jet entrains denser fluid and the density difference between the jet and the ambient fluid decreases. Thus, when neutral buoyancy is achieved the jet reaches the maximum height of rise. Consequently, the jet collapses abruptly and proceeds as a horizontal gravity current. This behavior was also observed by Wong and Wright (1988) and Roberts (1987).

A typical density profile of a buoyant jet along the jet trajectory in linearly stratified ambient are presented in Figure A.2. As a turbulent jet rises to its maximum rise height, the density profile becomes significantly distorted vertically and horizontally. The upper and the lower boundary of the density fluctuation indicate the depth of entrainment. However, note that the density profiles in this study are not time-averaged profiles but instantaneous.

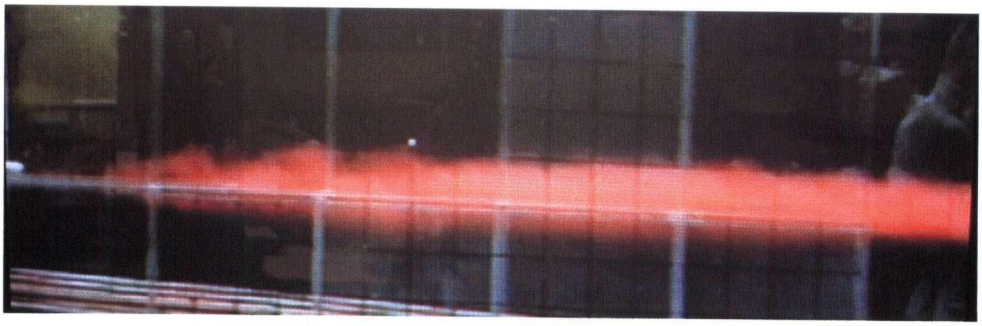

(a) (A13, $F_d = 22.9$, $N = 0.76$)

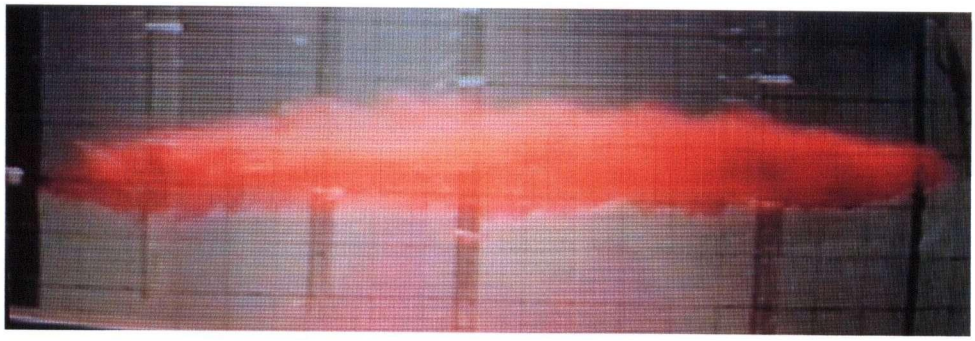

(b) (A53, $F_d = 17.7$, $N = 0.75$)

Figure A.1 Buoyant jets in linearly stratified ambient fluid

(a) A13 ($F_d = 22.9$, $N = 0.76$), (b)A53 ($F_d = 17.7$, $N = 0.75$)

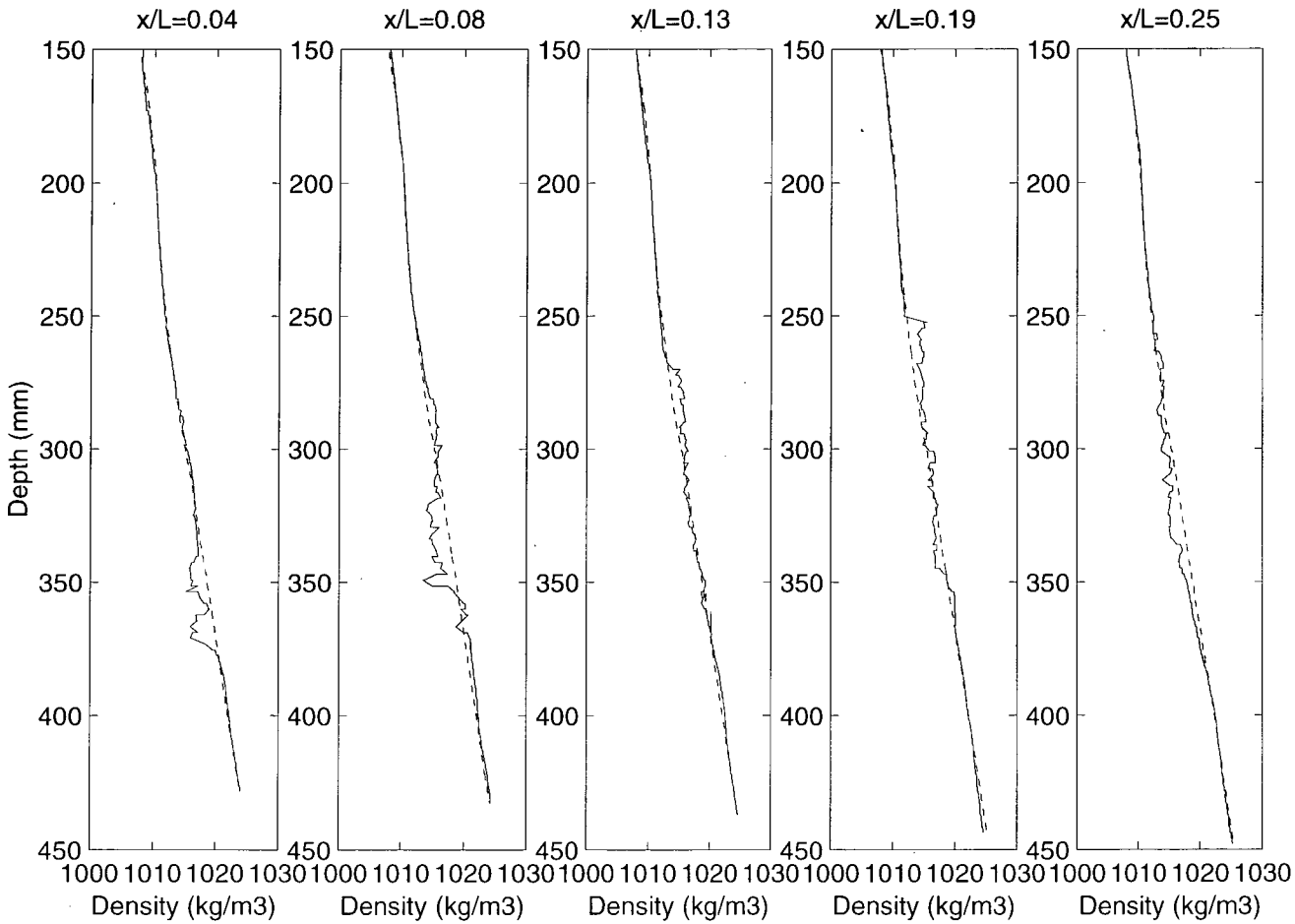

Figure A.2 Density profiles before (----) and after (—) a buoyant jet discharge along the jet trajectory in linearly stratified ambient fluid (A12) .....

A.2 Analysis of gross flow characteristics

The definition of parameters for a buoyant jet in a linearly stratified ambient fluid is shown in Figure A.3. A buoyant jet is discharged at height h above the bed. As the jet reaches its maximum rise height Z_m at the location X_m, it bends and intrudes as a spreading layer with thickness T_f. Z_t and Z_b are defined as the top and the bottom of the spreading layer respectively. The source volume, momentum and buoyancy flux (Q, M, B) are defined in section 2.2.2. The ambient density gradient is expressed by a buoyancy frequency N, defined in section 2.2.4.

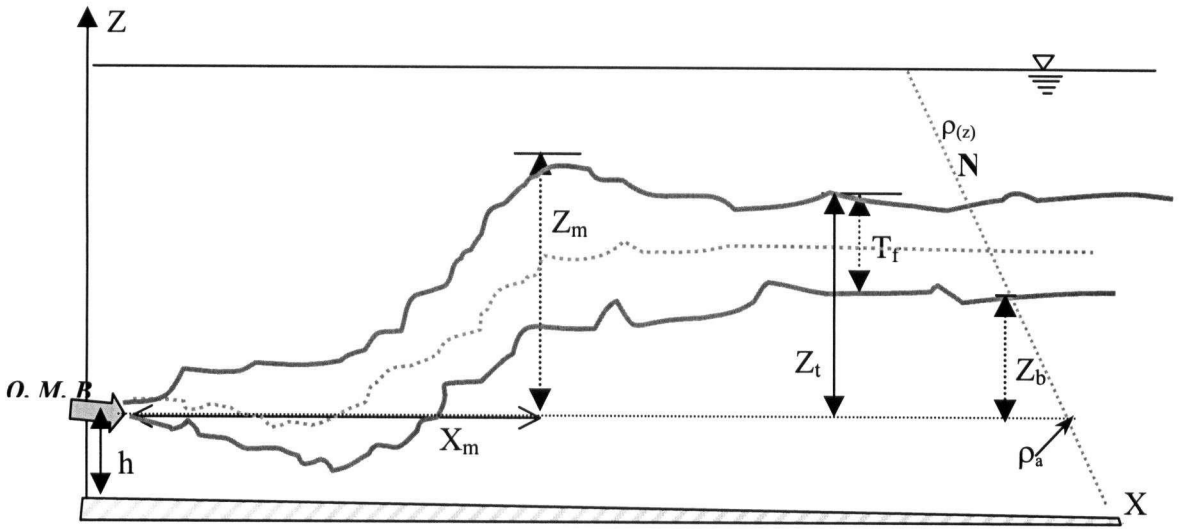

Figure A.3 A definition sketch of a buoyant jet in a linearly stratified fluid

The dimensionless characteristic length ℓ_M / ℓ'_b measures the relative importance of the source momentum, buoyancy and the ambient density stratification.

$$\frac{\ell_M}{\ell'_b} = \left(\frac{M \cdot N}{B} \right)^{3/4} \tag{A.1}$$

where M, B, N are defined in section 2.2. If $\ell_M / \ell'_b > 1$, the buoyant jet behaves like a momentum jet. If $\ell_M / \ell'_b < 1$, a buoyant jet behaves like a plume until the ambient stratification plays a significant role in the jet trajectory (Wallace & Wright, 1984; Wong, 1984; Jirka and Doneker, 1991). The experimental conditions examined here are $0.59 < \ell_M / \ell'_b < 7.27$, which covers a small range of buoyancy-dominant jets but mostly momentum-dominant jets.

A.2.1 Maximum height of rise and its location

The dimensionless maximum height of rise (Z_m / ℓ'_b) of a buoyant jet in linearly stratified stagnant ambient fluids is plotted against ℓ_M / ℓ'_b in Figure A.4. Z_m / ℓ'_b is relatively constant with an average of 0.98 for $\ell_M / \ell'_b > 1$, whereas it tends to decrease for the buoyancy–dominant region, $\ell_M / \ell'_b < 1$. This observation is similar to experimental results of horizontal buoyant jets observed by Wong (1984). However, the numerical results of Gu and Stefan (1988a) give higher values than those of the present study and Wong (1984). Therefore, it is rather difficult to identify the effect of the 3° downward discharge angle on the maximum rise height at this stage.

Figure A.5 shows the dimensionless location of the maximum height of rise (X_m / ℓ_N) of a buoyant jet. To facilitate comparison with previous research, X_m / ℓ_N is plotted against ℓ_M / ℓ_N instead of ℓ_M / ℓ'_b. The results indicate that the location X_m / ℓ_N in a linearly stratified fluid is independent of ℓ_M / ℓ_N and is constant at 4.8. Roberts (1987) estimated the location of jet collapse of non-buoyant jets to be 2.1 - 3.6, with an average value of 2.8, and subsequent experiments (Roberts, 2001) give an average value of 3.5. This large difference is probably due to the initial downward-inclined momentum, which allows jets to take a longer path until reaches the maximum rise height. Thus, for a buoyant jet with large source momentum discharged downward, the location of the maximum rise height is

further downstream compared to that under horizontal discharge.

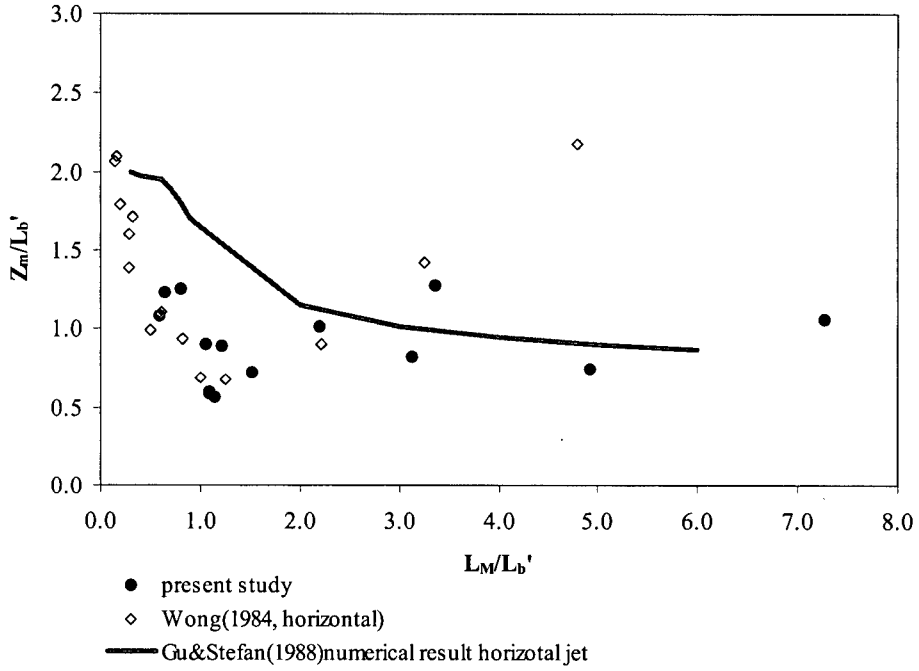

Figure A.4 Dimensionless maximum rise height Z_m / ℓ'_b in linearly stratified ambient fluid

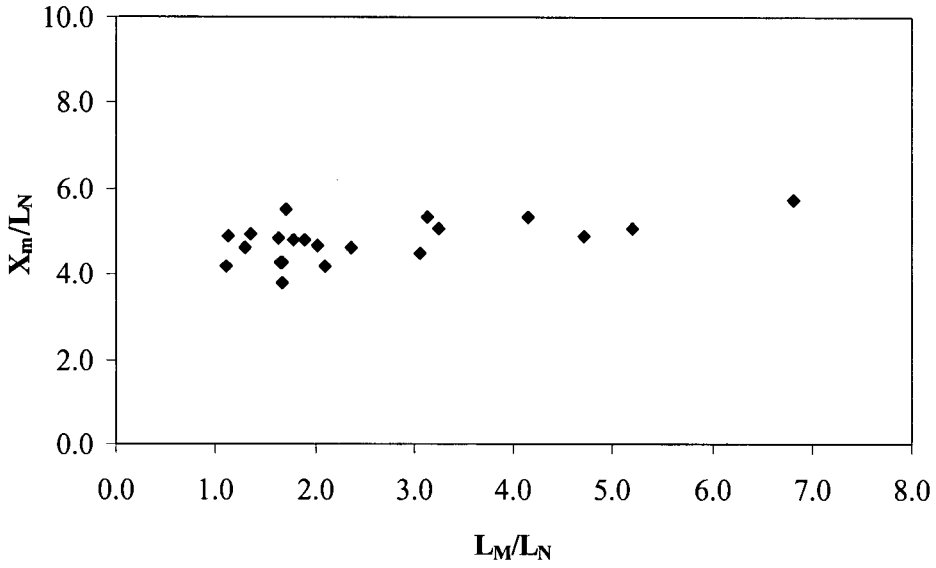

Figure A.5 Dimensionless location of maximum rise height in linearly stratified fluid

A.2.2 Top of spreading layer

The dimensionless top of the spreading layer after jet collapse (Z_t / ℓ_N) tends to decrease as ℓ_M / ℓ_N increases, regardless of the discharge angle shown in Figure A.6. Also, as the discharge angle decreases, Z_t / ℓ_N decreases. Jirka and Doneker (1991) suggested an equation relating the top of the spreading layer to the discharge angle:

$$Z_t = \left\{ \frac{\ell_b'^4}{\ell_M^3 \cos\theta^{3/4}} \right\}^{\alpha} \qquad \text{(A.2)}$$

where ℓ_b' is a characteristic length defined in section 2.2.4, θ a discharge angle and α a coefficient of $\alpha = 2.0 \pm 0.5$. For 3° downward discharge angle and $\ell_M / \ell_N > 1.5$, Z_t / ℓ_N for the present study is higher than that estimated using Eq. (A.2). On the other hand, 3° downward discharge results in a lower top of the spreading layer than that of the horizontal jet investigated by Wong (1984).

A.2.3 Spreading layer thickness

Figure A.7 also shows that T_f / ℓ_b' increases with ℓ_M / ℓ_b'. In addition, buoyant jets with a horizontal (Wong, 1984) resulted in a slightly larger spreading layer thickness than 3° downward discharge. It is because for the same source momentum the vertical momentum of downward jets is smaller than that of horizontal jets, causing slightly smaller entrainment in the vertical direction.

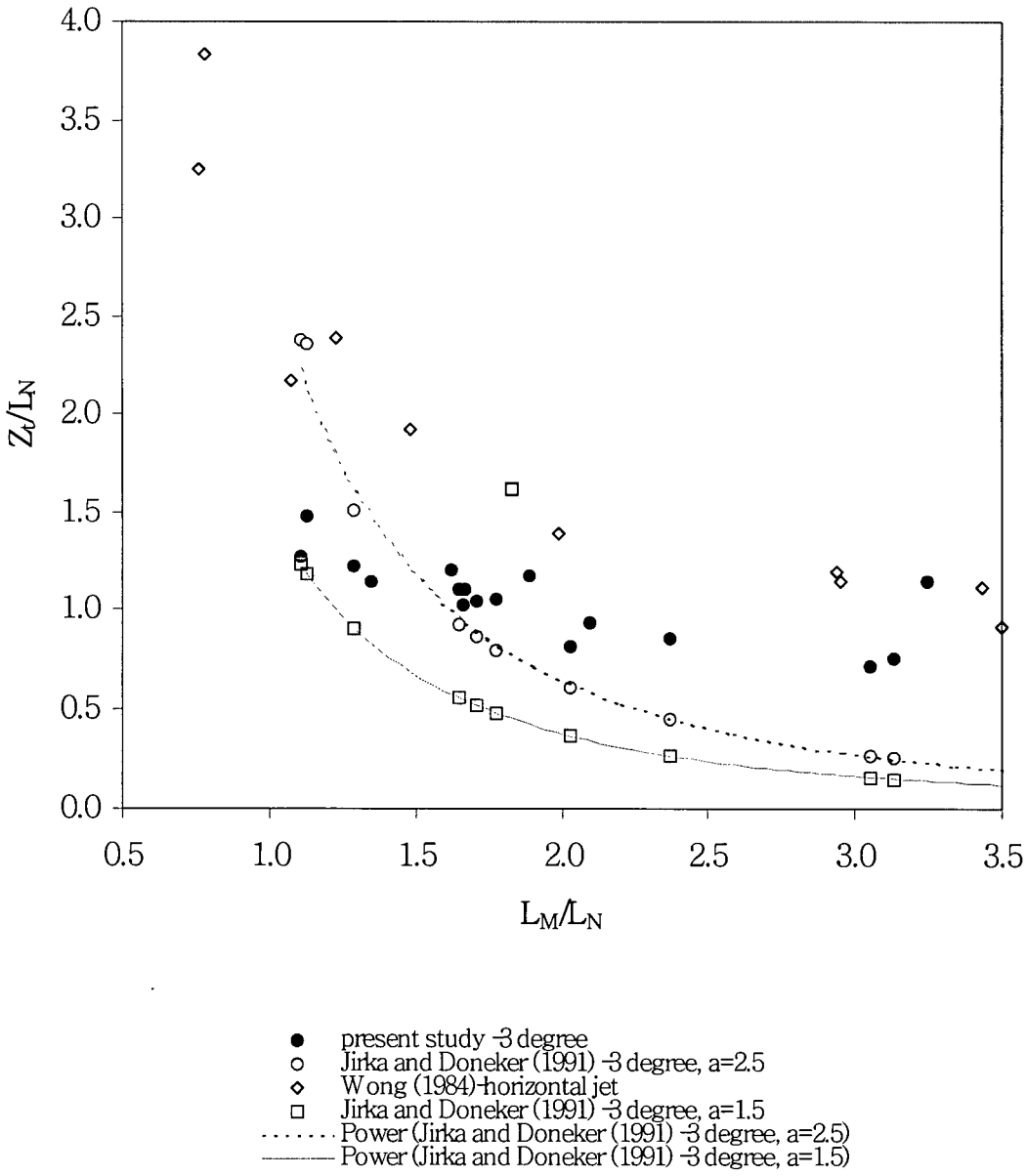

Figure A.6 Dimensionless top of the spreading layer in linearly stratified fluid

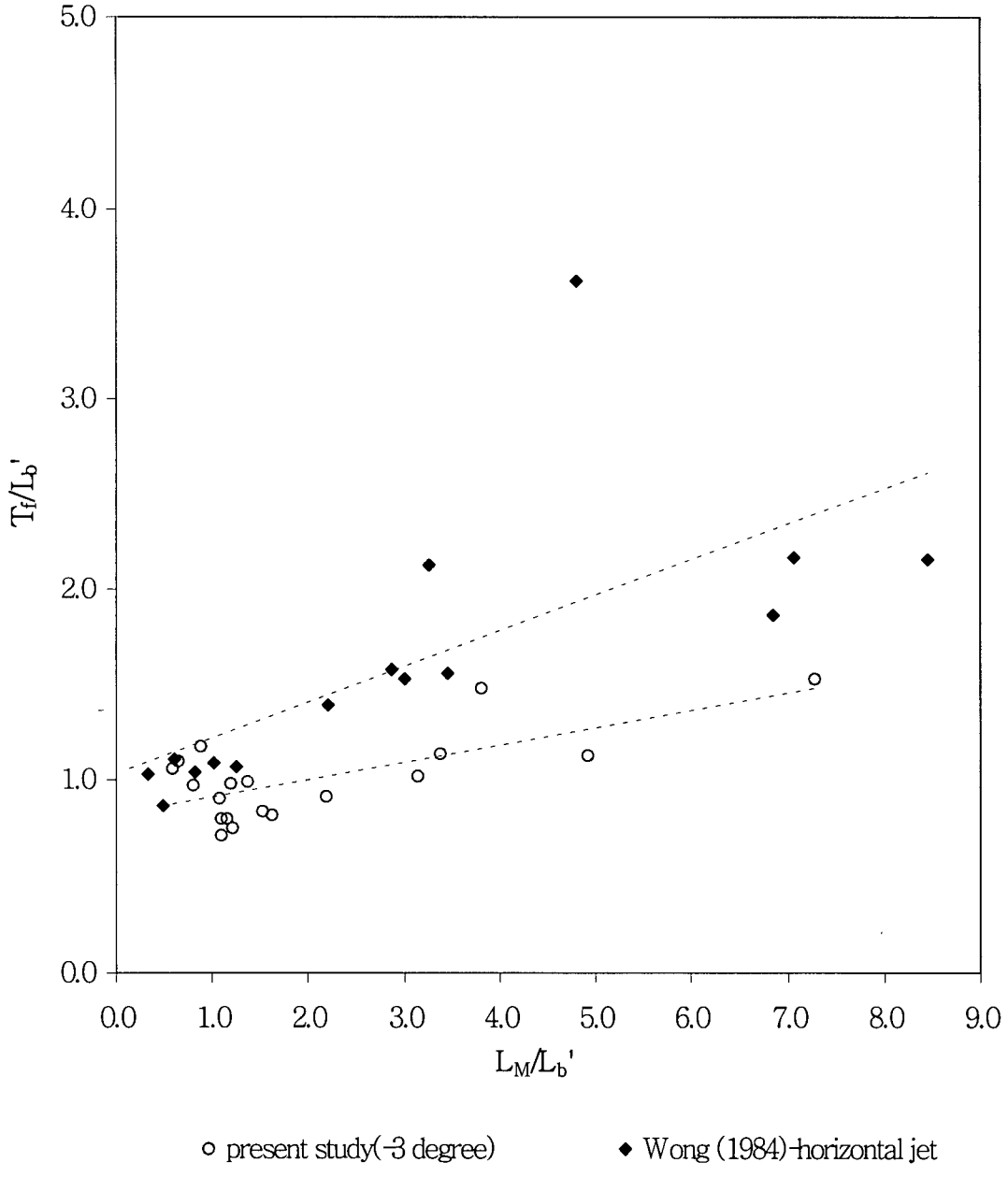

Figure A.7 Dimensionless spreading layer thickness in linearly stratified fluid

A.3 Summary of fluid jets in linearly stratified fluid

The experiments also suggested that in a linearly stratified ambient fluid, a buoyant jet grew linearly with distance near the jet exit. However, the jet collapsed abruptly as it reached the maximum rise height and advanced as a horizontal gravity current.

The dimensionless maximum rise height (Z_M/ℓ'_b) was found to be constant at 0.98 for the momentum-dominant region ($\ell_M/\ell'_b > 1$) and to decrease for $\ell_M/\ell'_b < 1$. The location of the maximum rise height was independent of ℓ_M/ℓ_N and found to be constant at a value of 4.8, which is significantly larger than that value of 3.5 found for non-buoyant horizontal jets by Roberts (2001). The top of the spreading layer (Z_t/ℓ'_b) tended to decrease as ℓ_M/ℓ_N increases. The spreading layer thickness (T_f/ℓ'_b) increased as ℓ_M/ℓ'_b and the discharge angle increases.

Appendix B

Particle-laden jets in linearly stratified ambient fluid

The gross characteristics of particle-laden jets in a linearly stratified fluid are analyzed quantitatively using the same methods as in the two-layer system.

B.1 Behavior of particle-laden jets

The gross flow characteristics of particle-laden jets in a linearly stratified fluid were found to be similar to that in a two-layer system. The linear density gradient resulted in a symmetric shape of the spreading layer compared with that in two-layer systems and no apparent maximum rise was observed, as illustrated in Figure B.1(a). For jets of low particle concentration, the linear stratification suppressed vertical spreading at the top while constant individual particle settling occurred. As the particle concentration increased, the flow exhibited a U-shaped bottom configuration resulting from group settling at the near field (Figure B.1(b)).

On the other hand, when a jet plunged down due to its large initial bulk density, it initially behaved like that in a two-layer system (Figure B.1(c)). A large amount of particles settled at some distance and the jet started to rise. As the head of the flow rose and mixed with heavy ambient fluid, the density of interstitial fluid increased. However, due to the constant discharge of buoyant interstitial fluid, the density of ambient fluid gradually decreased. As a result, the buoyancy of newly discharged fluid became smaller than that of previously discharged fluid. Eventually the individual separate spreading layers were formed at their neutral buoyancy as illustrated in Figure B.1(d) – this was also observed by Spark et al. (1993). This is the main difference between jet behavior in two-layer systems and linearly stratified ambient fluids.

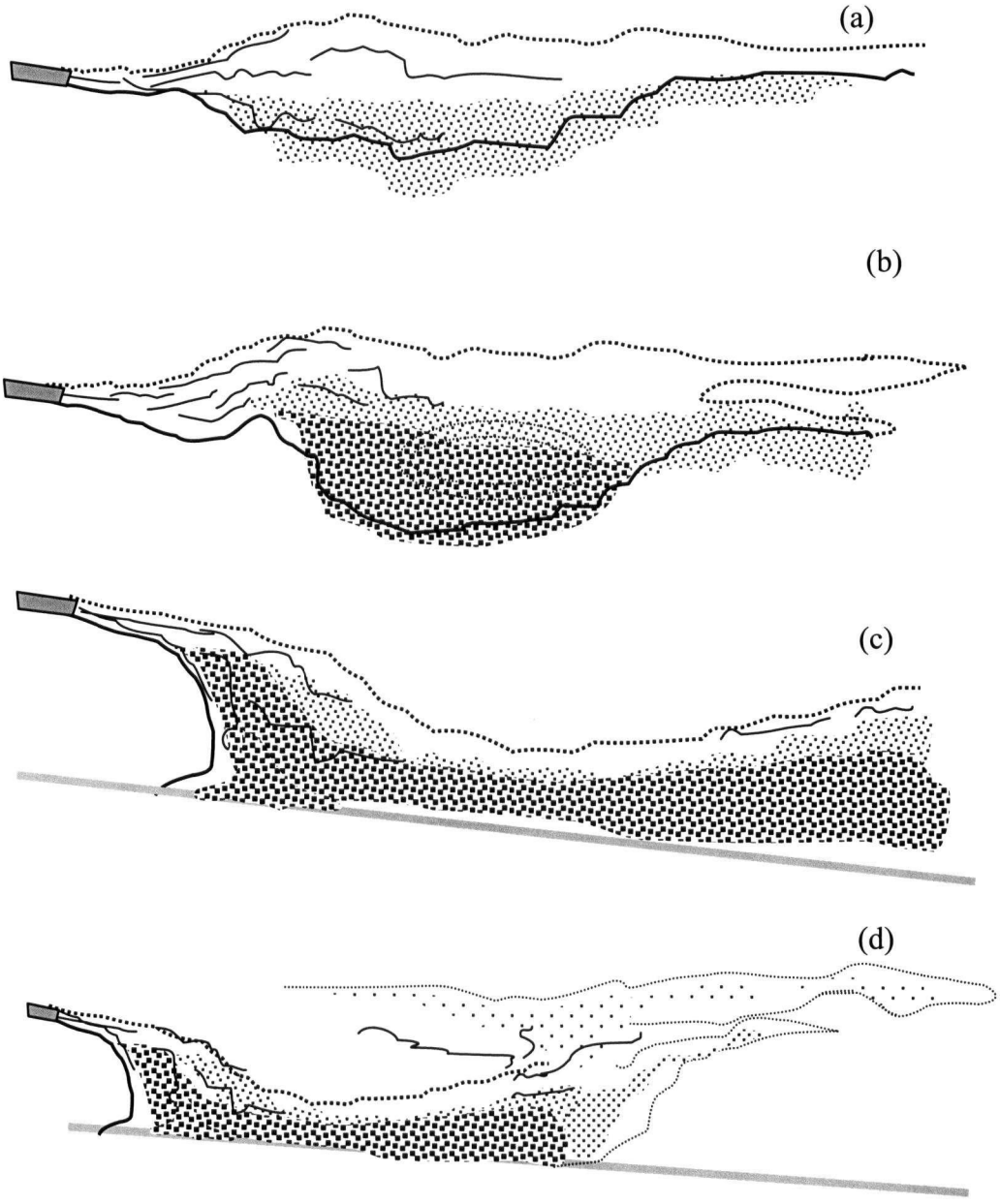

Figure B.1 Behavior of particle-laden jets in linearly stratified fluid (a) fluid jet like behavior, (b) intermediate (c) plunging in the near-field and (d) detrainment of interstitial fluid in the far field

B.2 Analysis of gross flow characteristics

The discharge height from the bed (h) and a characteristic length scale ℓ'_b are appropriate parameters for buoyant jets in linearly stratified fluid defined in section 2.3. These two parameters are combined to give the dimensionless form ℓ'_b/h and plotted against R. When $R < -2.0$ the jets plunged down to the bed, while when $-2.0 < R < 0$ jets formed a thick intermediate spreading layer but did not plunge.

Figure B.2 shows the dimensionless maximum rise height, the top of the spreading layer and the spreading layer thickness of particle-laden jets in linearly stratified ambient fluid. The parameters were normalized by the discharge height above the bed (h) and plotted against ℓ_M/ℓ'_b . The maximum rise height and the top of the spreading are slightly influenced by the dimensionless density (R). The results clearly show that Z_m and Z_t decrease as the concentration increases and jets of high concentration ($R < -2.0$) plunged to the bed. Also, the spreading layer thickness tends to increase with ℓ_M/ℓ'_b. These results are compared with fluid jets and previous studies in Chapter 6.

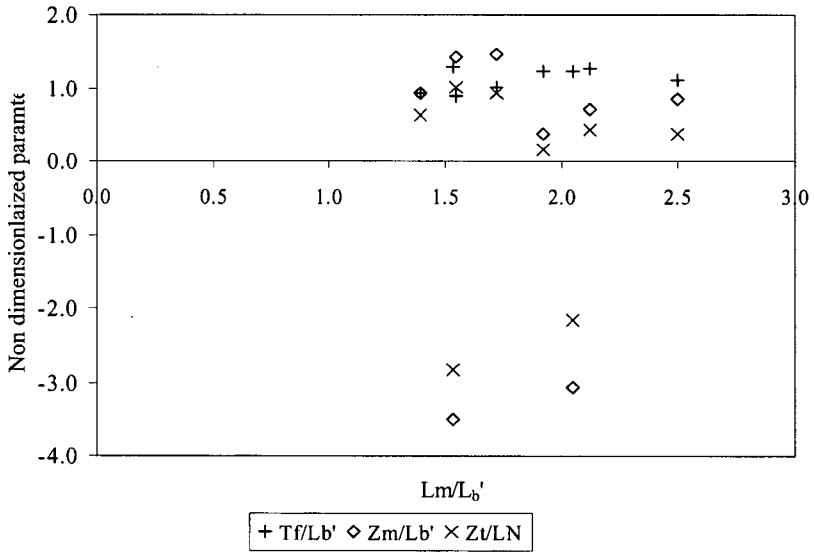

Figure B.2 Dimensionless parameters for particle-laden jets in linearly stratified fluid

Appendix C

Comparison of fluid jets and particle-laden jets in linearly stratified ambient fluid

C.1 Gross characteristics of jets

Figure C.1 presents the comparison of the maximum rise height of fluid jets and particle-laden jets in linearly stratified ambient fluid. There was no apparent difference in the maximum rise height for three cases except for the Strong Plunging Regime where the jets plunged down to the bed (P12 and P14) like in two-layer systems. The top of the spreading layer of particle-laden jets Z_t/ℓ_N is plotted against ℓ_M/ℓ_N in Figure C.2. The present results are also compared with those of 3° downward inclined fluid jets of Jirka and Doneker (1991). Z_t/ℓ_N of fluid jets from both present study and Jirka and Doneker (1991) are higher than that of particle-laden jets.

Figure C.3 shows the comparison of the dimensionless spreading layer thickness (T_f/ℓ'_b) for the two types of jet. The Strong Plunging Regime is excluded in the figure. It is shown that T_f/ℓ'_b slightly increases with ℓ_M/ℓ'_b and the thickness of particle-laden jets tends to be slightly larger than fluid jets and increases with the particle-concentration. This is because when particles settle interstitial fluid also descends and entrains heavy ambient fluid whereas linear stratification inhibits the vertical mixing of interstitial fluid. It also appears that particle-laden jets result in a slightly thinner spreading layer that the horizontal jets but the difference is negligible.

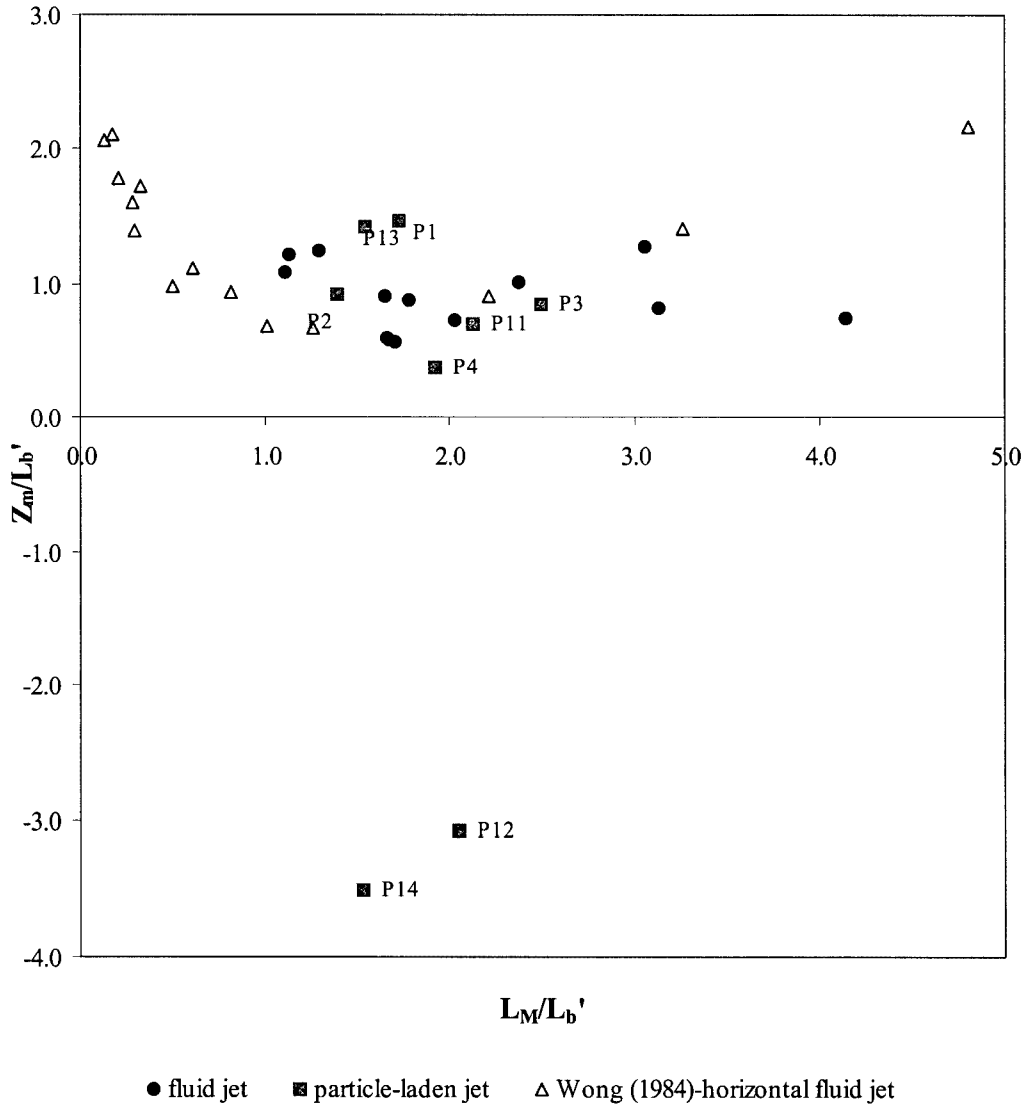

Figure C.1 Comparison of the dimensionless maximum rise height (Z_m / ℓ'_b) between fluid jets (Wong, 1984); present study) and particle-laden jets in linearly stratified fluids

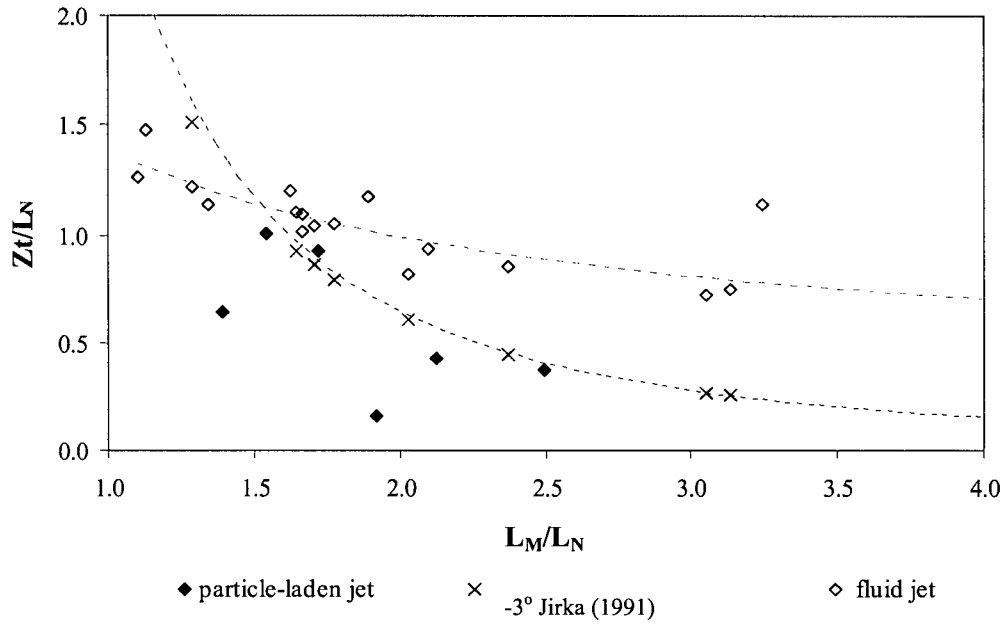

Figure C.2 Comparison of the dimensionless of top of the spreading layer (Z_t / ℓ_N) between fluid jets (Jirka, 1991; present study) and particle-laden jets

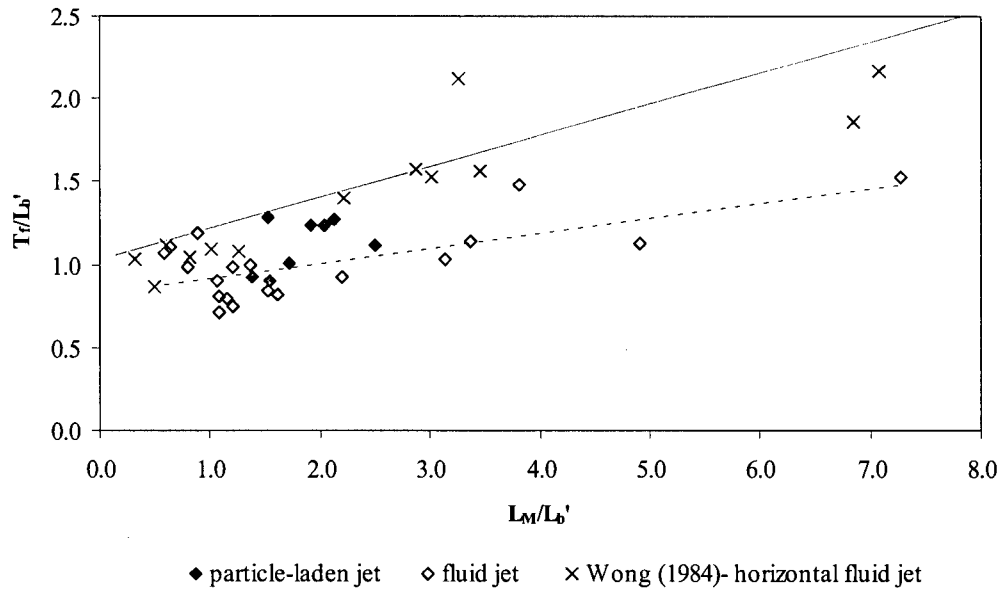

Figure C.3 Comparison of the dimensionless spreading layer thickness (T_f / ℓ'_b) between fluid jets and particle-laden jets in linearly stratified fluids

C.2 Conclusions

C.2.1 Buoyant fluid jets in linearly stratified fluid

Buoyant jets grew linearly near the jet exit as if in a homogenous ambient fluid. However, as a jet reached the maximum rise height, it collapsed abruptly and proceeded as a horizontal gravity current. The maximum rise height decreased for $\ell_M/\ell'_b < 1$ and was relatively constant for the momentum-dominant region ($\ell_M/\ell'_b > 1$). The spreading layer thickness appeared to be sensitive to the downward directed momentum and increased with ℓ_M/ℓ'_b and the discharge angle.

C.2.2 Particle-laden jets in linearly stratified fluid

The gross flow behavior of particle-laden jets in linearly stratified fluids was found to be similar to that in a two-layer system except for the symmetric shape of the spreading layer. After substantial particle settling, individual separate spreading layers formed. The ambient stratification had little influence on the flow behavior until a considerable amount of particles settled out of the flows. The higher the particle concentration, the lower the maximum rise height and top of the spreading layer.

Appendix D

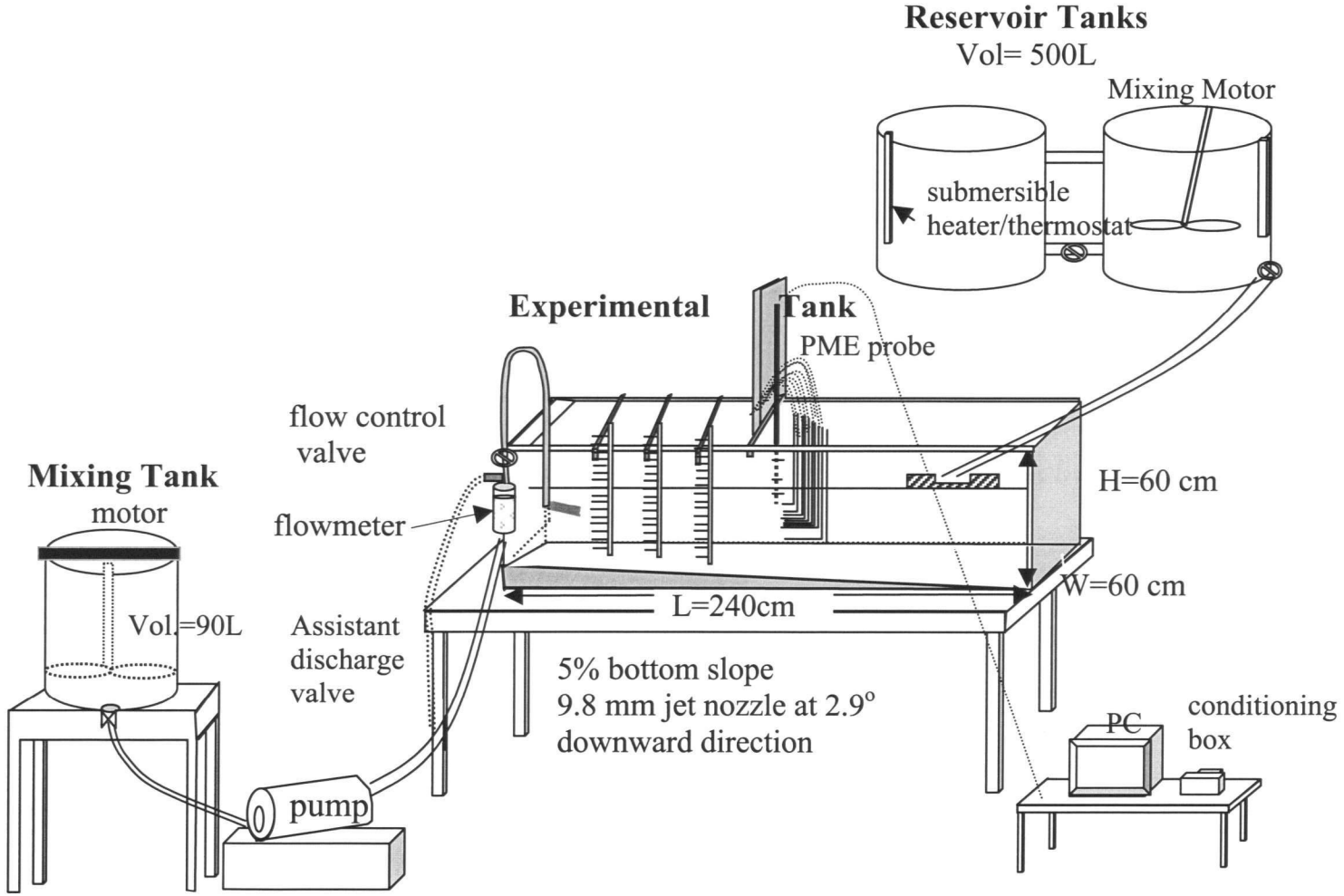

Figure D.1 Overview of the experimental set-up